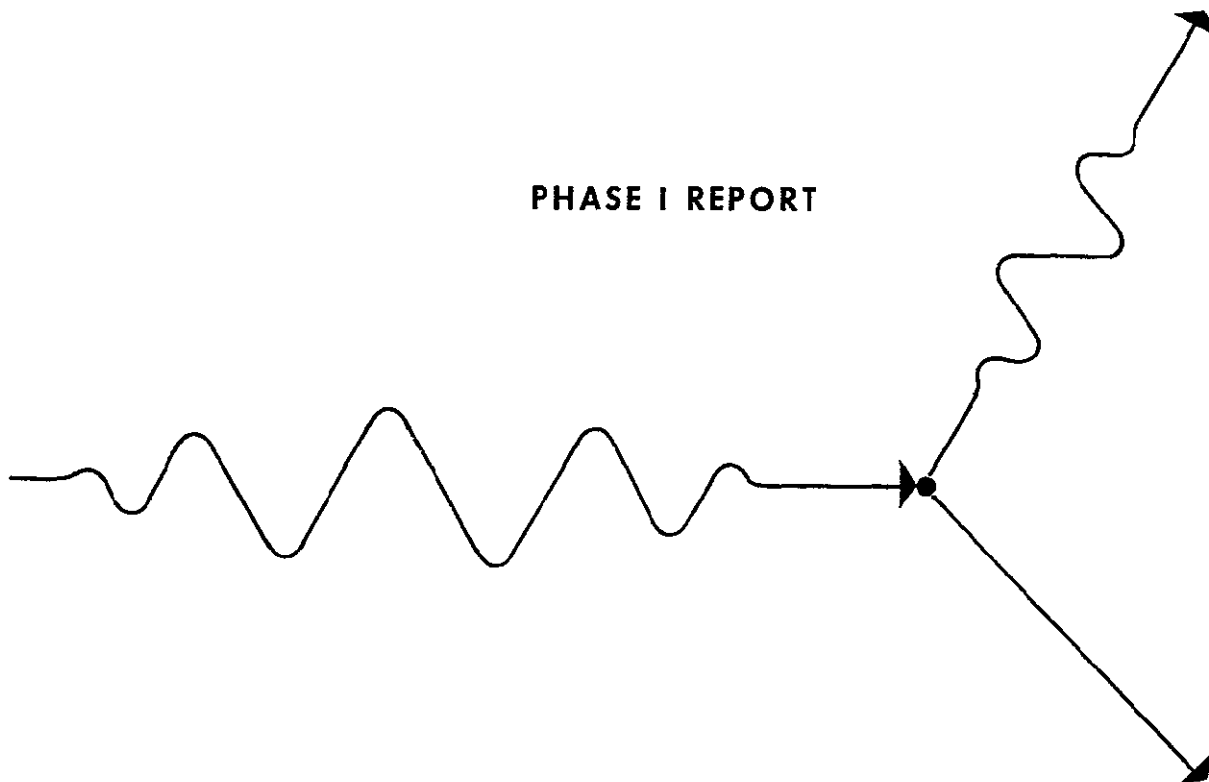2P

RTG/SCIENCE INSTRUMENT RADIATION INTERACTIONS STUDY FOR DEEP SPACE PROBES

PHASE I REPORT

PREPARED FOR **NASA AMES** RESEARCH CENTER

MOFFET FIELD, CALIFORNIA

CONTRACT NO. NAS 2–5222

TRW
SYSTEMS GROUP

PHASE I
FINAL TECHNICAL REPORT

RTG/SCIENCE INSTRUMENT RADIATION
INTERACTIONS FOR DEEP SPACE PROBES

NAS 2-5222

SUBMITTED TO·

NATIONAL AERONAUTICS AND SPACE ADMINISTRATION
AMES RESEARCH CENTER
MOFFETT FIELD, CALIFORNIA
31 JULY 1969

Prepared by:

R. A. Kaminskas
G. W. Ryan
C. A. Smith

APPROVED: ~~R. Kaminskas~~
for R. E. Loucks
Program Manager

APPROVED· ~~I. R. Jones~~
I. R. Jones, Manager
Nuclear Systems Department

TRW SYSTEMS GROUP
REDONDO BEACH, CALIFORNIA
90278

ABSTRACT

This document is the Phase I Report of a two-phase program to
investigate the interference effects of radiation emitted by a
plutonium-dioxide-fueled Radioisotope Thermoelectric Generator
(RTG) on scientific instruments carried onboard an RTG-powered
spacecraft. A review of scientific instruments commonly
carried in spacecraft was performed and the elements of the
instruments most suceptible to the RTG radiation were identified.
These elements, which included semiconductor detectors, plastic
scintillators, CsI scintillators and a number of other radiation
detectors were exposed to a SNAP-27 fuel capsule assembly The
resultant spectral response of each detector was determined along
with the effects of various separation distances, capsule
orientations, and different shielding materials and thicknesses
A detailed analysis of the nuclear radiation emitted from the
SNAP-27 fuel capsule was also performed, including the effect
of fuel form age on the source spectrum.

TABLE OF CONTENTS

i

CONTENTS (continued)

I. INTRODUCTION AND SUMMARY

This is the final report on Phase I of a study to investigate RTG Science Instrument Radiation Interaction for Deep Space Probes. The work was performed for the National Aeronautics and Space Administration under contract NAS 2-5222 during the period from 4 February to 30 June 1969.

During the decade of the 70's NASA is planning several scientific spacecraft missions into deep space to explore the outer planets and asteroid belts. These missions will be of long duration and encompass distances up to 30 astronomical units from the sun. At these distances the solar flux is greatly diminished. As a result, solar cell power supplies become heavy compared to the Radioisotope Thermoelectric Generators (RTG's) and, therefore, reduce the weight available for the scientific payload. RTG power sources are, therefore, being considered for deep space probes However, RTG's have a potential disadvantage because the radioisotope heat sources used to power the RTG's emit gamma and neutron radiation. This radiation may interfere with operation of some of the on-board radiation detection instruments.

A typical spacecraft for deep space missions includes a variety of radiation measuring instruments. These instruments cover a wide spectrum of radiation ranging from high energy solar and cosmic particles to low energy X-rays, ultra-violet rays, and infrared radiation. For some of these instruments, the radiation produced by the RTG provides a constant background which is superimposed on the measured signals. However, the extent of this interference is difficult to predict with confidence on a theoretical basis.

This program was designed to investigate the possible modes of RTG fuel capsule radiation interference with typical instrumentation found in deep space probes and experimentally measure the effects that the RTG will have on the radiation sensitive elements of the instruments. To accomplish this objective, a combined analytical and experimental

approach was adopted which included the acquisition and use of a SNAP-27 fuel capsule loaned to TRW by the AEC for radiation interference testing. The program was divided in two phases. The first phase was aimed at providing some of the most obvious and needed data required to evaluate the problem by studying the response of radiation sensitive elements of the spacecraft instruments individually. Phase II will extend the study to investigate the radiation effect on instrument systems and also includes the assessment of the radiation interference in terms of mission objectives.

The selection of radiation sensitive elements to be studied in Phase I was based on a survey of over a hundred previous spacecraft experiments. The radiation sensitive elements were identified and categorized, and the most commonly used detector types and sizes were selected This resulted in a set of 26 radiation detectors which were evaluated in the RTG radiation field.

To provide a basis for comparison between the data obtained with the SNAP-27 fuel capsule and other RTG's, a detailed study of SNAP-27 fuel capsule gamma and neutron radiation spectrum was performed along with an analysis of spectral changes as a function of fuel age. Also, radiation dose rates around the RTG and the possibility of radiation damage and neutron activitation of spacecraft components were considered.

The report is presented in six sections. Section 2.0 is a review of program objectives and summary of major tasks that were performed during Phase I. Section 3.0 describes the instrument survey and performance study and the selection of radiation sensitive elements for radiation interference tests. Section 4.0 gives the SNAP-27 fuel capsule radiation characteristics. Section 5.0 describes the experiments that were performed using the selected detectors, their response to SNAP-27 fuel capsule radiation, and the effects of countermeasures such as separation, shielding, and detector orientation in relation to the RTG. Section 6.0 gives several conclusions and recommendations for further studies.

The severity of RTG radiation interference will depend on the design and objectives of each instrument. However, in a general way, it is possible to make the following observations regarding the magnitude of the interference:

Type of Measurement	Effect of RTG Radiation
Cosmic ray and solar charged particles	
Energy > 100 Mev	Minor
Energy 10 to 100 Mev	Moderate, may require shielding (~1 lb)
Trapped Radiation	Significant during interplanetory flight, will require shielding (1 to 5 lbs). Moderate to minor in vicinity of planets.
Plasma and low energy electrons, energy < 1 Kev	Moderate, may require some shielding (~1 lb)
UV	Minor
IR	Minor

2. PROGRAM OBJECTIVES AND TASK SUMMARY

2.1 General

The RTG/Science Instrument Radiation Interaction Study was designed to provide the experimenters using scientific instruments onboard RTG powered spacecraft with basic data to assess the radiation interference caused by the radiation emanating from the RTG. The program had a dual purpose:

o To provide data for an immediate requirement concerning the RTG radiation interference with science instruments selected for the upcoming Pioneer F/G spacecraft missions.

o To provide data to assess RTG radiation interference with science instruments selected for future scientific spacecraft programs.

To satisfy these requirements, a two-phase program was initiated. Phase I, reported herein, was a five-month effort designed to study $^{238}PuO_2$ RTG fuel capsule radiation interference with a complement of radiation-sensitive detectors and elements. This part of the program consisted of identifying the most sensitive detectors and elements, defining RTG radiation characteristics, and empirically measuring the response of each sensitive element (primarily radiation detectors) to the $^{238}PuO_2$ radiation. In Phase II it is planned to extend these measurements to complete science subsystems and two other potentially radiation sensitive elements which were not included in Phase I. This phase also includes plans to set up a cooperative experimental program with experimenters that intend to fly instruments on RTG-powered spacecraft to test their prototype flight hardware with an RTG radiation field

To fulfill the requirements for a suitable RTG radiation heat source, TRW acquired, on loan from the AEC, a SNAP-27 fuel capsule. This source is roughly representative of the type and amount of radioisotopic fuel that would be used for a deep space probe mission employing an RTG. The source is fueled with 45 Kilocuries of $^{238}PuO_2$ (1500 thermal watts) contained in a superalloy capsule.

Pioneer F/G and Viking will use approximately twice this amount, whereas TOPS will be four or five times larger. However, the SNAP-27 can be used to simulate these sources by multiplying the results obtained with the SNAP-27 by appropriate factors because the neutron/gamma ratios and spectra will be nearly identical for all these fuel capsules

2.2 Task Summary

To satisfy the above requirements, the program was divided into several tasks which were accomplished sequentially. These tasks, a schedule, and other milestones are shown in Figure 2-1 and are summarized below.

- TASK I - Instrument Survey and Performance Study

    The primary purpose of this task was to review the scientific instrumentation used in spacecraft and identify the instruments and/or elements of instruments that showed the most susceptibility to interference by the radiation from the RTG. Since early in the program it became apparent that most problems will occur with instruments that are designed to measure space radiation itself, the majority of Phase I effort was concentrated on the study of RTG radiation effects on radiation detectors themselves. To select the radiation sensitive elements for a detailed study in Phase I, a general survey of instruments commonly used in spacecraft science payloads was performed. This survey included instruments that have been flown in the past as well as instrument designs proposed specifically for the Pioneer F/G spacecraft and consisted of a review of more than 100 experiments designed to perform radiation measurements in space. Tabulations of the detector types, sizes, and where possible, specific makes (manufacturer and part number) were made and the instrument configurations and the way they are used in the science subsystems were also noted. From this tabulation, the most frequently used detectors and detector sizes were identified.
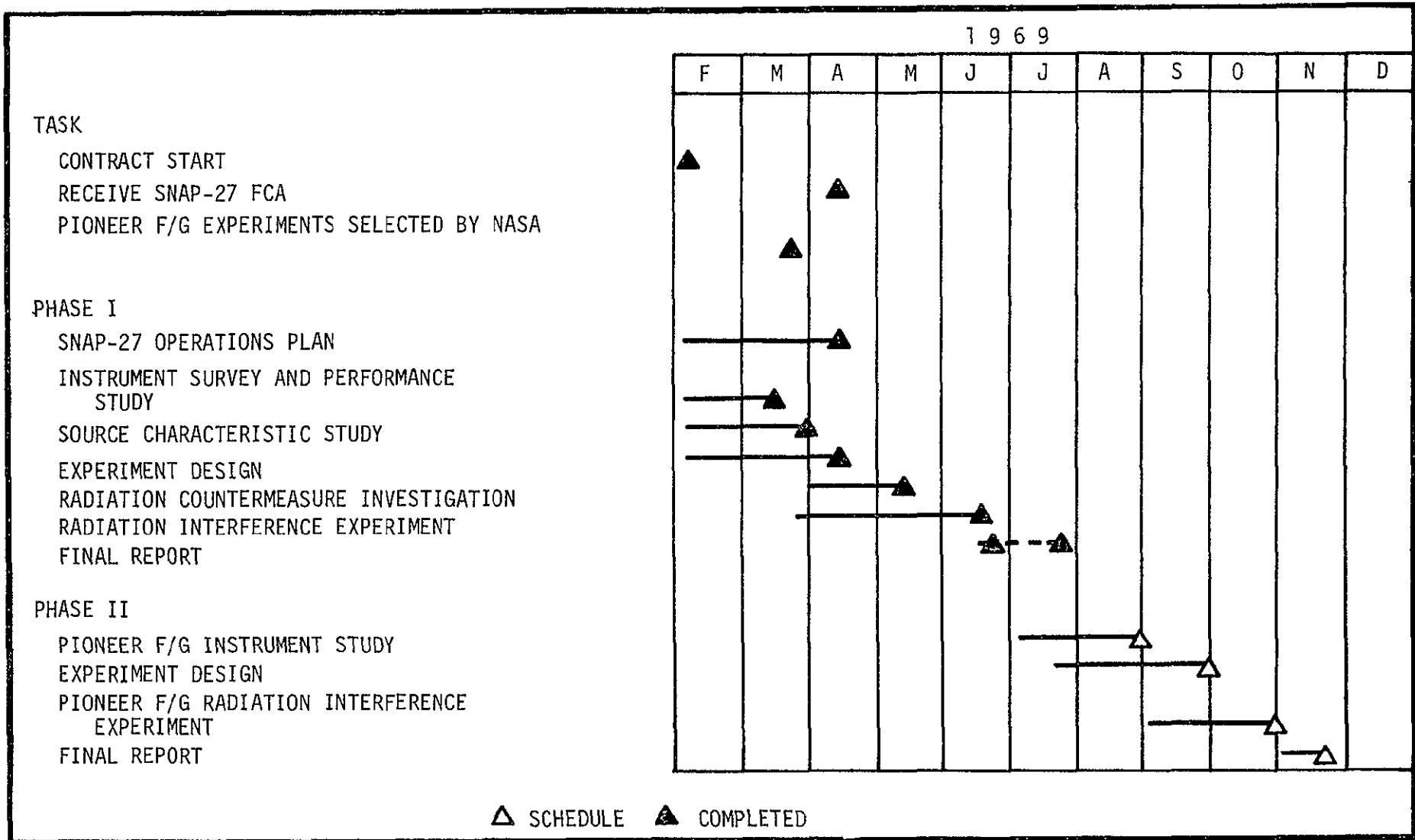
PROGRAM SCHEDULE

FIGURE 2-1

To complete the list, several detectors that are not necessarily commonly used in spacecraft but represent particular detector types which are of interest for closer study of the RTG fuel capsule radiation characteristics or else are anticipated to be used on future missions (e.g., NaI (Tℓ) scintillator and channeltrons) have been added. This effort resulted in the selection of 26 different radiation detectors tabulated in Table 2-1. All of these detectors were procured, exposed to the radiation from the SNAP-27 fuel capsule, and their spectral responses and detection efficiencies measured. The results gave differential spectra expressed in counts/sec-cm^2-Kev versus energy for each detector. Also, the effectiveness of various shielding materials and the effects of detector orientation in relation to the RTG heat source were measured. The detectors selected for the study included CsI scintillators, plastic scintillators, Cherenkov detectors, semiconductor detectors, gas detectors, NaI scintillators, a channeltron and several other detectors. This list of detectors includes the majority of detector types and sizes commonly found in spacecraft science payloads, including Pioneer F/G. The various thickness detectors allow interpolation to predict the spectral response and number of detected counts for virtually any detector size.

- TASK II - Source Characteristic Study

The objective of this task was to characterize the nuclear radiation environment produced by the SNAP-27 fuel capsule. The task included the assembly and cataloging of current data on the spectrum and field produced by a $^{238}PuO_2$ fueled SNAP-27 source (obtained from Oak Ridge National Laboratory). These data were compared with the characteristics of a bare $^{238}PuO_2$ source to determine the effect of the fuel encapsulation materials. Also, the characterization included the effects

DETECTORS SELECTED FOR RTG INTERFERENCE STUDY

ITEM	DESCRIPTION
PROPORTIONAL COUNTER	HARSHAW G-15
GEIGER TUBES	EON 6213
	EON 7302
PLASTIC SCINTILLATORS	1mm THICK, 1½" DIAMETER
	3mm " " "
	10mm " " "
	30mm " " "
CsI SCINTILLATORS	1mm THICK, 1½" DIAMETER
	3mm " " "
	10mm " " "
	1½" THICK, 1½" DIAMETER
NaI SCINTILLATORS	1½" THICK, 1½" DIAMETER
	1 mm THICK, 1¼" DIAMETER

TABLE 2-1

DETECTORS SELECTED FOR RTG INTERFERENCE STUDY
CONTINUED

ITEM	DESCRIPTION
CHERENKOV DETECTOR	1 mm THICK, 1½" DIAMETER
	3mm " " "
	10mm " " "
	30mm " " "
SEMICONDUCTOR DETECTORS	.050mm THICK, 1cm^2 AREA
	.200mm " " "
	.5 mm THICK, .8cm^2 AREA
	2. mm " " "
PHOSWICH	PLASTIC 2mm + CsI 5mm THICK
SEMICONDUCTOR TELESCOPE	2 SEMICONDUCTOR DETECTORS
PHOTOMULTIPLIER TUBES	RCA 6199
	RCA 4440
CHANNELTRON	BENDIX 4028

TABLE 2-1 CONTINUED

of different fuel impurities and age. The results of this
analysis were compared with the measured data obtained during
the Radiation Experiment Task using the SNAP-27 fuel capsule
and were found to be in agreement.

Additionally, the Source Characteristic Study task included a
study of the potential activation of the science instrument due
to long term exposure to the RTG radiation field environment.
This was found to be an insignificant problem.

● TASK III - Experiment Design

The task of experiment design consisted of the following
activities:

o Establishing test procedures.
o Design and construction of test fixtures, detector
   containers, shields, cables, etc.
o Selection, testing, and calibration of electronic
   components used for the tests.
o Assembly of radiation detectors.
o Detector check-out and calibration.

The equipment selected for the radiation interference testing
of each detector system is described in detail in Section 5.

● TASK IV - SNAP-27 Operations Plan

This task consisted of the majority of the documentation and
preparation of procedures which were required for the SNAP-27
fuel capsule acquisition and operations in the Radiation
Research Facility at TRW Systems, Redondo Beach, California.
Included in this task were a detailed Radiological Safety
Plan, Training Plan, and Emergency Procedures which were
subsequently presented to both the TRW Radiation Safety
Committee and the Operational Safety Division of the AEC.
They were approved by both bodies (copies of these documents
were transmitted to NASA/AMES).

An on-site inspection of TRW facilities by the AEC OSD/ALO was made on 12 March 1969. On 14 March 1969, a training course was arranged at Sandia Laboratories for TRW personnel responsible for SNAP-27 fuel capsule operations. The course included procedures for unloading and loading the fuel capsule from the Ground Shipping Cask (GSC) as well as the health physics and emergency procedures associated with this operation.

This task was completed by documenting and publishing a manual describing the detailed operational test procedures for operations with the SNAP-27 fuel capsule at TRW Systems.

o TASK V - Radiation Countermeasure Investigation

The radiation countermeasure investigation was performed primarily as part of the Radiation Interference Experiment described in Part VI and contained measurements of·

o Effects of various shielding materials.
o Effects of distance between fuel capsule and detector.
o Effect of detector orientation with respect to the fuel capsule.
o Effect of fuel capsule orientation with respect to detectors.
o Effect of coincidence shields.
o Measurements of fuel capsule spectrum as a function of detector thickness and type.

All results performed under this task are included together with other experimental data in Section 5.0.

o TASK VI - Radiation Interference Experiment

This task was designed to measure the direct interference of nuclear radiation from the SNAP-27 fuel capsule on the science detectors identified in Task I. The task commenced on 24 April 1969 and consisted of the following main areas of effort

- Detector Set-Up and Check-Out - The science detectors and support instrumentation were installed at TRW Systems Radiation Test Facility and all systems were checked out to verify proper operation and calibration.

- Radiation Mapping - The SNAP-27 fuel capsule was placed in the fuel capsule positioning fixture. The gamma radiation from the fuel capsule was measured and mapped as a function of direction in the plane parallel to the long axis of the fuel capsule.

- Interference Tests - The radiation detectors were exposed to radiation of various intensities utilizing the SNAP-27 fuel capsule and the radiation response characteristics of each detector was measured.

- Countermeasure Investigation - Tests were performed to evaluate the effectiveness of radiation interference countermeasure techniques. This task included the investigation of shielding and separation between the fuel capsule and radiation detectors

3. INSTRUMENT SURVEY AND PERFORMANCE STUDY

In order to study the effects of the RTG radiation on spacecraft equipment and instrumentation, it was necessary to survey the instruments commonly found in spacecraft and isolate the sensor elements that appeared to be most sensitive to the RTG radiation. The survey consisted of reviewing the operating principles of the instruments and assessing on a theoretical basis, by considering the possible modes of radiation interactions with each instrument, what effects the RTG may have on its performance. It was not unexpected that the systems most sensitive to RTG radiation are those designed to measure space radiation itself and thus, the majority of the Phase I effort was concentrated on these systems. Other scientific experiments involving measurements such as magnetic fields, plasma, detection of meteorites, radio wave propagation, UV, IR, and video TV transmission, appeared to be either totally unaffected or else fell into a "gray" area where some effects appeared possible; however, the exact magnitude could not be clearly established on a theoretical basis. Several of the experiments listed above, where a clear assessment of effects of RTG radiation could not be obtained during the Phase I study, have been included for a detailed experimental evaluation under Phase II.

3.1 Space Radiation Measurements

Radiation measurement instruments in spacecraft are most commonly designed to measure solar, cosmic and planetary trapped radiation fields. The radiation of interest consists of electrons, protons, alpha particles, and sometimes heavier ions with atomic weights ranging from 6 to 16.

Typical radiation measurements include the identification of particle type, particle flux, energy spectra, and direction of travel. The energy range of interest for the space radiation is from a few ev to several Bev. The instruments to measure these radiation fields also range in design from very simple detectors that detect only the total ionization caused by the space radiation to very sophisticated charged particle telescopes capable of determining particle type, energy

range, particle flux, and flux direction. For example, the Pioneer F&G spacecraft contains a wide range of radiation detection systems with the dual function of.

- Measuring solar and cosmic radiation during transit from Earth to Jupiter.

- Measuring trapped radiation belts in the vicinity of Jupiter.

Since very dense radiation fields in the Jovian trapped radiation belts are anticipated, the RTG radiation contribution to these measurements is very small and should not compromise the experimental objectives. However, for determination of belt periphery and during the time of spacecraft flight from Earth to Jupiter at the periphery of the trapped radiation belts, and after Jovian encounter, the spacecraft will operate primarily in a low radiation environment (~ 0.05 particles sec/cm^2) and will, therefore, suffer the most interference from the RTG radiation.

3.2   Instruments

For purposes of assessing the RTG radiation effects, the science instruments may be subdivided into two general categories: single detector systems and multi-detector systems.

The effects of RTG radiation on single detector systems are relatively easy to present. The RTG radiation spectrum detected by a single detector system is simply added to the spectrum the detector is designed to measure. The only means of reducing the RTG radiation is by shielding or increasing the lower discriminator setting, or reducing the window width, thus rejecting part of the counts contributed by the RTG.

Pioneer F&G has several of these single detector systems. Some of these are intended primarily to operate in the Jovian trapped radiation belts and thus are designed to handle very high particle fluxes. This report provides most of the data required to assess the radiation interference caused by the RTG for these detector systems, and at least

at present, there appears to be no problem in meeting most of their scientific objectives.

Multiple detector systems commonly consist of two or more detector elements stacked next to each other in a telescope configuration. The first detector is usually a thin semiconductor radiation detector. For proton, alpha, and other heavy charged particle counting it is used to detect low energy events when the charged particles have insufficient energy to completely penetrate the first detector. For particles that have sufficient energy, it provides dE/dx measurement for particle identification and also produces a gating signal to gate the detectors located behind it. Thus, only events that occur in coincidence with the first detector are accepted. If the instrument contains more than two detectors, the coincidence logic demands that the events occurring in the third detector be in coincidence with the first and the second detector, etc However, for detection of electrons, the second (and subsequent) detectors are frequently operated in anticoincidence with the first detector because the electrons do not leave enough energy in penetrating the first detector to register an event.

The entire telescope assembly is frequently surrounded by an anti-coincidence detector causing rejection of counts occurring simultaneously in the telescope elements and in the anticoincidence shield

Thus, it appears that the most significant effects of the RTG heat source radiation on typical multiple element radiation detector systems will be as follows

- Charged particle detection - background superimposed on the first detector element of the telescope.
- Electron detection - background superimposed on the second detector element of the telescope.
- Overall detection system capability - background due to accidental coincidence counts in first few elements of the telescope and dead counting time losses caused by various counts detected in all the system detector elements and the anticoincidence shield.

3.3   Detector Selection Criteria

The criteria for selection of radiation detectors for the RTG
Science Instrument Interference Study were

o   Commonality with spacecraft instrumentation detectors used
    in the past.

o   Inclusion of at least one detector of each type that is
    likely to be used in future spacecraft.

o   The probability that the detector would be used on Pioneer
    F&G spacecraft.

The above criteria were also used to select detector sizes, radia-
tion shields between the RTG and the detector, and the detector operating
modes.

In order to make the selection, spacecraft instrumentation consisting
of more than one hundred experiments concerned with radiation measurements
in space was reviewed and the detector types, sizes, and where possible,
specific makes as well as how they are used in the system, were
tabulated.   From the tabulation, the most frequently used detectors and
detector sizes were identified and included in the interference study.
To complete the list, several detectors that were not necessarily common,
but were useful for better determination of the RTG special characteristics
(for instance two NaI (Tl) scintillators) were added

The review also provided information for selection of radiation
shielding materials of various thicknesses which were used to provide a
set of known attenuation media between the fuel capsule and the detectors.

Additionally, the survey of spacecraft instruments indicated how the
radiation detectors should be instrumented so as to provide maximum
information on the effects of the RTG radiation on the detectors, as
well as provide a means of predicting the effect that the RTG radiation
will have on the complete scientific experiment.

Types of radiation detectors considered as a result of the survey are outlined below·

Ionization Chambers

Since no ionization chambers were contemplated for the upcoming missions of RTG powered spacecraft at the time the detector selection was made*, they have been excluded from the list of detectors to be tested

Proportional Counters

Although proportional counters are not commonly found in spacecraft instrumentation, one proportional counter was tested in the RTG/Science Instrument Interference Study primarily for the purpose of obtaining low energy gamma spectra and their variation as a function of shield type and thickness.

Geiger Tubes

Geiger tubes are very common in spacecraft instrumentation Among some thirty experiments reviewed that used geiger tubes, eighteen used either Anton 213 or Anton 302 (later known as EON 6213 and 7302, respectively). Thus, the two tubes identified above were selected for testing.

Scintillators

Most of the common scintillator types are used in spacecraft instrumentation. Out of some thirty-five experiments reviewed that incorporated some type of scintillator, CsI and plastic scintillators were used fourteen times each. NaI four times, and Cherenkov radiators (most frequently lucite) three times. For the sake of completeness, all the scintillator detectors named above were included in the study, in thicknesses of 1 mm, 3 mm, 10 mm, for plastic, CsI, and Cherenkov detectors, 030" and 1.5" for NaI and also one 1.5" thick CsI crystal. Most of these scintillators are 1-1/2" in diameter and are operated with RCA 6199 and/or 4440 photomultiplier tubes.

* (Verbal communication from NASA AMES.)

Semiconductor Detectors

Semiconductor radiation detectors are very commonly used in spacecraft instrumentation. Their sizes, types, and the way in which they are used vary widely with each experiment. To cover the majority of cases, four semiconductor detectors were selected for this study. The detectors are 50 and 200 micron thick 1 cm^2 area silicon surface barrier and 500 and 2,000 micron, 0.8 cm^2 area silicon lithium drift.

PM Tubes

Seventy-five percent of the photomultipliers that were identified in the spacecraft instrument survey were either RCA 6199 or 4440, or their equivalent. Thus, these two photomultipliers were selected for the experimental study and were used with most scintillators in the experiments To see if any significant signals were generated by direct interaction of the tube structure with the RTG heat source radiation, these tubes were also exposed to the RTG radiation without scintillators

Coincidence Systems

- **Phoswich**

   A phoswich is a scintillation radiation detector that is quite common in spacecraft instrumentation. It consists of a sandwich of fast (e.g., plastic) and slow (e.g., CsI) pulse-producing scintillating materials optically coupled together and viewed by a single photomultiplier tube. An electronic circuit separates the fast and the slow electronic pulses and thus can determine if the nuclear interaction took place in the first, the second, or both scintillators. This scheme is frequently used for coincidence counting and discrimination between charged particles and gammas. One such phoswich scintillator consisting of a 2 mm Pilot B plastic scintillator and a 5 mm thick CsI crystal was procured for tests in this study to determine the spectrum of RTG radiation that will be detected in coincidence between the two scintillators.

- Coincidence Counts Between Two Semiconductor Detectors

Semiconductor radiation detectors in spacecraft instrumentation are very frequently used in sets of two or more and operate in the coincidence mode for charged-particle spectroscopy RTG radiation will cause a certain amount of coincidence counts due to the statistical probability of nuclear interactions occurring simultaneously in the two detectors.

The coincidence counts due to this effect are statistically independent and could be predicted by knowing certain electronic parameters and the response of each detector to the RTG radiation separately. However, a certain amount of statistically dependent coincidence counts is also anticipated as a result of nuclear reactions like Compton scattering of gammas occurring in the detector and one component of radiation escaping from the first detector and entering the other, or protons produced by (n,p) reactions and penetrating both detectors, etc. To measure this statistically dependent component of coincidence counts, two semiconductor detectors were arranged in a charged particle telescope configuration and instrumented to measure the spectra of coincidence counts. The spectra of statistically independent components of radiation was measured by physically separating the two detectors with a shield. Both the statistically dependent and independent components were measured by removing the shield and placing the detectors next to each other

Channeltrons

Channeltrons are very small, reliable, light, and require little power. Therefore, they have become popular in spacecraft instrumentation. Channeltrons are customarily used as electron detectors in electrostatic or magnetic electron spectrometers or for detection of UV radiation.

Although it is anticipated that the RTG radiation will interfere very little with the channeltrons, one channeltron (Bendix CEM 4028) was selected for inclusion in this study. The channeltron was operated in the saturated mode, exposed to the RTG radiation and the channeltron output recorded with a pulse height analyzer.

4. NUCLEAR ENVIRONMENT AND SOURCE CHARACTERISTIC STUDY

4.1 General

The purpose of this task was to estimate the expected radiation fields from the radioisotope fuel capsule used in the radiation interference experiments. The information in the current literature was reviewed and the most reliable data selected for use in estimating the radiation fields. Discrepancies in the literature for the gamma radiation source have been found. A discussion of these discrepancies and the expected radiation field from the fuel capsule is presented in this section.

In addition, an estimate of the radiation field surrounding a SNAP-27 radioisotope fuel capsule two years after fuel encapsulation was made. Also, two effects that may alter the radiation field surrounding the fuel capsule were considered. These two effects are attenuation of emitted radiation by air, and neutron-induced activation of materials external to the fuel capsule.

A processing report from Mound Laboratory describing the history and characteristic of the fourth SNAP-27 fuel capsule used in this program is included as an appendix to this report.

4.2 Discussion

4.2.1 Radiation Source

The isotope used in the SNAP-27 fuel capsule is plutonium-238. The fuel product obtained from the separation process contains several other plutonium isotopes in fair abundance in addition to the plutonium-238. A typical distribution of isotopes obtained in the plutonium fuel product is given in Reference 1 and is presented in Table 4-1. The fuel form used in the fuel capsule is plutonium dioxide, PuO_2. As discussed later, references to gamma and alpha radiation outputs per gram of plutonium may be converted to radiation outputs per gram of PuO_2 fuel form with fair accuracy by using the ratio of the molecular weights of Pu to PuO_2 (0.8816). However, the neutron radiation outputs of Pu and PuO_2 differ by roughly a factor of ten due to the α, n reactions with O^{18} and other light elements in the oxide fuel form.

TABLE 4-1:   Typical Distribution of Isotopes
             In Plutonium-238 Isotopic Fuel
             (Metal)

ISOTOPE	PERCENT ABUNDANCE (%)
Pu-236	0.00012
Pu-238	.81.0
Pu-239	15.0
Pu-240	2.9
Pu-241	0.8
Pu-242	0.1
Np-237	0.5
Th	0.01
U	0.005
Others	0.3

Although Table 4-1 shows that plutonium-238 is the predominant isotope in the PuO_2 fuel form, Reference 1 also shows that a 2.6 Mev gamma in the complex plutonium-236 decay chain can result in a considerable gamma radiation field five years after encapsulation. Thus, the relatively small quantity of plutonium-236 in the fuel form is important and must be considered in the analysis of the gamma radiation fields.

4.2.2 Gamma Source

For times of less than one year after encapsulation, the gamma source associated with the plutonium-238 fuel results mainly from the alpha decay of plutonium-238. However, spontaneous fission,

fission products, and gamma rays from the alpha-neutron reaction with oxygen-18 also contribute to the gamma source. For longer times after encapsulation, the plutonium-236 and plutonium-241 impurities in the source may contribute significantly.

The alpha and beta activities of the plutonium-238 fuel product are presented in Table 4-2 (Reference 2).

TABLE 4-2· Alpha and Beta Activities of
Plutonium-238 Fuel Product*

Isotope	Abundance, %	Activity of Pure Isotope, d/sec-gm	Contribution to the Activity of 1 Gram of Fuel Product d/sec-gm
^{238}Pu	81	6.35×10^{11}	5.14×10^{11} (α)
^{239}Pu	15	2.27×10^{9}	3.41×10^{8} (α)
^{240}Pu	2.9	8.38×10^{9}	2.43×10^{8} (α)
^{241}Pu	0.8	4.12×10^{12}	3.30×10^{10} (β)
^{242}Pu	0.1	1.44×10^{8}	1.44×10^{5} (α)
^{236}Pu	0.00012	1.97×10^{13}	2.37×10^{7} (α)

* To convert to PuO_2, multiply by 0.8816

Table 4-2 indicates that the plutonium-238 isotope is the most important alpha source. The alpha emission is accompanied by gamma radiation whose source strength is found by combining the alpha activity with the yield fractions for the alpha decay process and the branching ratios for the concomitant gammas. The alpha activity reported above for plutonium-238 was based on an alpha-decay half-life of 87.404 to 0.41 years is measured

by Mound Laboratory (Reference 3). The half-lives of 86.7 and 89.6 years used by TRW (Reference 4) and Isotope Incorporated (Reference 5) respectively will give slightly different alpha activities.

In Table 4-3 are tabulated the gamma activities due to alpha decay of plutonium-238 as calculated by various sources. The activities are based on one gram of plutonium-238 fuel product (Table 4-1).

TABLE 4-3. Calculated Gamma Activities *
(gammas/gm-sec)

Gamma Energy (Mev)	LASL, 1967 (Ref. 2)	Mound Lab., 1967 (Ref. 3)	TRW, 1966 (Ref. 4)	Isotopes Inc., 1964 (Ref. 5)
0.017	6.7×10^{10}	----	----	----
0 043	2.0×10^{8}	1.93×10^{8}	1.49×10^{11}	1.92×10^{8}
0.099	4.6×10^{7}	4.60×10^{7}	5.30×10^{8}	4.02×10^{7}
0 150	5.2×10^{6}	5.10×10^{6}	2.66×10^{7}	5.03×10^{6}
0.203	2.0×10^{4}	2.04×10^{4}	2.12×10^{4}	$2 01 \times 10^{4}$
0.760	2.6×10^{5}	2.28×10^{5}	2.66×10^{5}	2.50×10^{5}
0.810	----	9.10×10^{4}	----	5.02×10^{4}
0.875	----	----	1.06×10^{5}	1.00×10^{5}

*Based on 1 gram Pu-238 fuel product with 81% Pu-238. Multiply by 0.8816 to convert to grams of PuO_2.

The data concerning the yield fractions for some of the alpha decay processes and the branching ratios for the concomitant gammas are rather scarce. The decay mode which produces the 0.76, 0.810, and 0.875 Mev gammas is the most poorly defined. Earlier experimental data (Ref. 6) indicated that the yield fractions were 5×10^{-5}, 0, and 2×10^{-5}, respectively. Reference 3 (1967) reports values of 5×10^{-7}, 2×10^{-7}, and 0 respectively for the yield fractions.

However, private communication with Mound Laboratory (Ref. 7) revealed that the recently measured gamma spectra from a SNAP-27 fuel capsule showed little contribution to the gamma spectra at 0.810 and 0.875 Mev. In contrast the measured spectra showed a large contribution at 0.760 Mev. Recently, Matlack, Bubernak, and Metz at Los Alamos Scientific Laboratory (Ref. 8) measured the gamma spectra emitted by plutonium-238 metal. Their results are presented in Table 4-4. The activities agree well with the calculated activities for the 0.099, 0.15, and 0.203 Mev gammas. Additionally, the higher energy gammas are clearly defined in energy and activity, clarifying the previously ambiguous values for these gamma energies

TABLE 4-4: Measured Gamma Activities of Pu-238
in Pu-238 Fuel Product* by LASL, 1968

Gamma Energy (Mev)	Activity (gammas/gm-sec) **
0 0996	3.82×10^7
0.1525	3.50×10^6
0.201	2.06×10^4
0 7424	2.32×10^4
0 7658	1.03×10^5
0.7858	1.445×10^4
0 8076	3.09×10^3
0 8513	6.20×10^3
0.8829	3.82×10^3
0 9265	2.58×10^3
0.9418	3.10×10^3
1.0011	4.4×10^3
1 0418	7.03×10^3
1 0851	5.16×10^2

*Measured 1-1/2 months after fuel purification

**Based on 1 gram Pu-238 fuel product with 81% Pu-238
Multiply by 0.8816 to convert to PuO_2

Good agreement exists between the calculated gamma activities (Table 4-3) for 0.760 Mev and lower energy gammas except for the 1966 TRW calculated values. The yield fractions and branching ratios selected by TRW in 1966 for the 0.043, 0.099, and 0.150 Mev gammas were based on older and sparse data which has since been updated. As discussed in the previous paragraph, the 0.810 and 0.875 Mev gammas show up experimentally with small yield fractions. In light of the previous discussion, the gamma activites measured by LASL (Table 4-4) (Ref. 8) for the alpha decay of plutonium-238 are the best to date.

Also, LASL (Ref. 2) calculated the gamma activities of the other plutonium isotopes. These activities are presented in Table 4-5.

TABLE 4-5: Gamma Activities of Plutonium Isotopes

Isotope	Energy, Mev	Photons/gm-sec*
^{239}Pu	0 017 (L x-ray)	3.4×10^7
	0.052	2.4×10^4
^{240}Pu		Negligible
^{241}Pu	0.145	$\leq 4 \times 10^4$
^{236}Pu	0.048	$\leq 7 \times 10^7$

*Based on 1 gram Pu-238 fuel product with 81% Pu-238.
Multiply by 0.8816 to convert to grams PuO_2.

The gamma activities of the plutonium isotopes other than plutonium-238 contribute little to the total gamma activity as can be seen by comparing the values in Table 4-5 to those in Table 4-3.

An additional source of gamma rays results from the spontaneous fission of plutonium-238 and the concomitant fission products. Both prompt fission and fission product gammas are emitted in a spectrum of energies.

The spectrum and yield fractions for uranium-235 fission gammas were obtained from Reference 8 and are presented in Table 4-6. The spectrum of fission gammas should not vary significantly for plutonium-238 fission so that the fission gamma characteristics presented in Table 4-6 are considered valid for plutonium.

A third source of gamma radiation results from the (α, n) reaction with the oxygen-18 isotope of the PuO_2 fuel form which produces an excited state of Neon-21 that decays by prompt gamma emission. Table 4-7 obtained from Reference 1, shows the gamma rays from the alpha particle interaction with oxygen-18. A comparison of results presented in this table with the gamma ray source associated with spontaneous fission presented in Table 4-6 shows that the gamma source from the (α, n) reaction is about a factor of two greater than the fission gamma source.

However, the alpha-neutron gamma ray source is still a factor of about 40 smaller than the gamma ray source from the alpha decay of plutonium-238 and, thus, the alpha decay gamma ray source is usually the most important to consider from a radiation hazards standpoint.

Table 4-4, Table 4-5, Table 4-7 and Figure 4-1 give the entire effective gamma ray source for PuO_2 fuel form for times of less than one year after fuel separation. For times greater than one year after separation, the decay gammas from the plutonium-236 and plutonium-241 impurities represent an increasingly significant gamma source. Gamma rays will result from the radioactive decay of daughter nuclides of plutonium-238 and plutonium-241

TABLE 4-6:   238Pu Fission Gamma Spectrum Derived From
Measured 235U Fission Gamma Spectrum

Energy Band (Mev)	Median Energy (Mev)	Gammas Per Disintegration	Gammas per Second Per Gram of Pu-238 Fuel Product
Prompt Fission Gammas			
0 - 0.75	0.5	3.1	2.76×10^3
0 75 - 1.25	1.0	1.9	1.69×10^3
1 25 - 1.75	1.5	0.84	7.48×10^2
1.75 - 2 25	2.0	0.55	4.90×10^2
2.25 ÷ 2.75	2.5	0.29	2.58×10^2
2.75 - 3.25	3.0	0 15	1.34×10^2
3.25 - 3.75	3 5	0.062	5.51×10^1
3.75 - 4.25	4 0	0.065	5.79×10^1
4.25 - 4.75	4.5	0.024	2.14×10^1
4.75 - 5.25	5.0	0.019	1.69×10^1
5.25 - 5.75	5.5	0.017	1.51×10^1
5.75 - 6.25	6.0	0.007	6.2
6 25 - 6.75	6.5	0.004	3.5
Fission Product Gammas			
0 - 0.60	0.4	1.61	1.43×10^3
0 60 - 1.05	0.8	4.84	4.30×10^3
1 05 - 1.50	1.3	0.496	4.41×10^2
1.50 - 1.94	1.7	0.624	5.55×10^2
1.94 - 2.34	2.18	0 311	2.77×10^2
2.34 - 2.65	2.5	0.01142	1.02×10^1
2.65 - 3 0	2.8	0.01142	1.02×10^1

TABLE 4-7·   Gamma Rays from the (α, n) Reaction in PuO_2

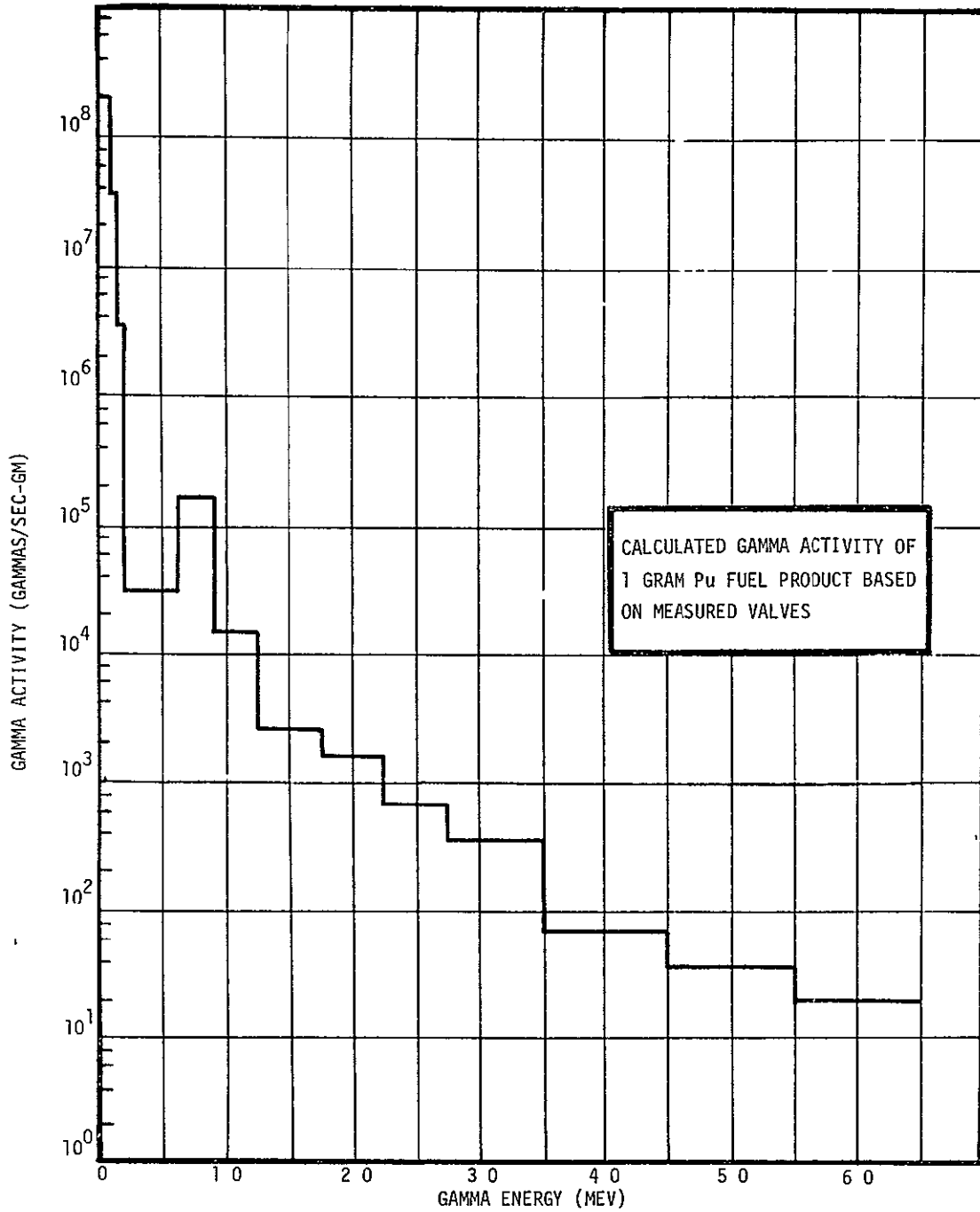| Energy (Mev)	Gammas per Second per Gram of Pu-238 Fuel Product
0 0 - 0.5	8.5×10^3
0.5 - 1.0	0.0
1.0 - 2.0	2.59×10^3
2 0 - 3.0	7.7×10^2

FIGURE 4-1   TOTAL GAMMA SOURCE ACTIVITY FROM Pu FUEL PRODUCT FOR
              TIMES LESS THAN ONE YEAR - MULTIPLY BY 0.8816 TO
              CONVERT TO GRAMS EQUIVALENT PuO_2

4-9

The decay chain for plutonium-236 obtained from Reference 2 is shown below in Figure 4-2

$$^{236}Pu \xrightarrow[\alpha]{2.85\ Y} {}^{232}U \xrightarrow[\alpha]{72\ Y} {}^{228}Th \xrightarrow[\alpha]{1\ 91\ Y}$$

$$^{224}Ra \xrightarrow[\alpha]{3.64\ d} {}^{220}Rn \xrightarrow[\alpha]{52\ s} {}^{216}Po \xrightarrow[\alpha]{0.16\ s}$$

$$^{212}Pb \xrightarrow[\beta]{10\ 6\ h} {}^{212}Bi \xrightarrow[\alpha\ (34\%)]{60\ m} {}^{208}Tl$$

$$\beta\ (66\%)\ \big\downarrow\ 60\ m \qquad \beta\ \big\downarrow\ 3\ m$$

$$^{212}Po \xrightarrow[\alpha]{0.3\ us} {}^{208}Pb\ (Stable)$$

Figure 4-2. Plutonium-236 Decay Chain

The rate-controlling step in the sequence, as far as the formation of gamma-emitting daughters is concerned, is the growth of 1.91 year Th- 228 The amount of gamma activity from lead, bismuth, and thallium daughters increases with time after purification of the plutonium fuel product, reaching a maximum in 18 years.

The principal gamma rays of these three elements and their abundances are shown in Table 4-8 (obtained from Reference 2) based on Th- 228 disintegration. This convention is used since these short-lived daughters are nearly always seen in equilibrium with Th-228, and because of the branching decay of Bi-212

4-10

The neutron source from PuO_2 fuel has been calculated and measured
by several organizations. Presented in Table 4-11 are the values
reported in the literature. The values for the total neutron source
are in fair agreement. The low value reported by LASL is based on a
reduced content of oxygen-18 in the oxygen of the PuO_2. The two
measured values are direct measurements reflecting source self-
absorption and shielding by cladding materials. The SNAP-27 measure-
ment of 2.2×10^4 n/gm-sec is then in good agreement with the source
values of 2.6×10^4 and 2.8×10^4 n/gm-sec calculated by References
4 and 1, respectively Presented in Figure 4-3 is the neutron spec-
trum measured by Reference 7 for the SNAP-27 fuel capsule.

TABLE 4-11: Neutron Source from Plutonium Oxide
(Neutrons/sec-gm)*

Source of Data	Reference	Spontaneous Fission	Alpha-Neutron Reactions With Oxygen	Neutron Induced Fission	Total Neutron Source
Isotopes Incorporated	5 (1964)	2.64×10^3			3.33×10^4
TRW	4 (1966)	$2 6 \times 10^3$	1.7×10^4	$6 46 \times 10^3$	2.6×10^4
Savannah River Laboratories	1 (1965)	1.9×10^3	1.9×10^4	6.9×10^3	2.8×10^4 2.1×10^4**
Mound Laboratory	3 (1967)	3×10^3			1.9×10^4
Mound Laboratory	7 (1968)	$2 75 \times 10^3$			2.22×10^4***
LASL	2 (1967)	2.1×10^3			1.13×10^4

*Based on 1 gram fuel product Pu-238   **Measured Value.   ***Measured Value of SNAP-27 Fuel Capsule

4.2.4 Gamma Radiation Fields

In the calculation of gamma radiation fields by various sources,
differences have arisen in the calculated values. The causes of the
differences may be attributed to two areas: (1) the selection of
gamma source activities and (2) the calculated transport of the gammas
through materials.

4-13
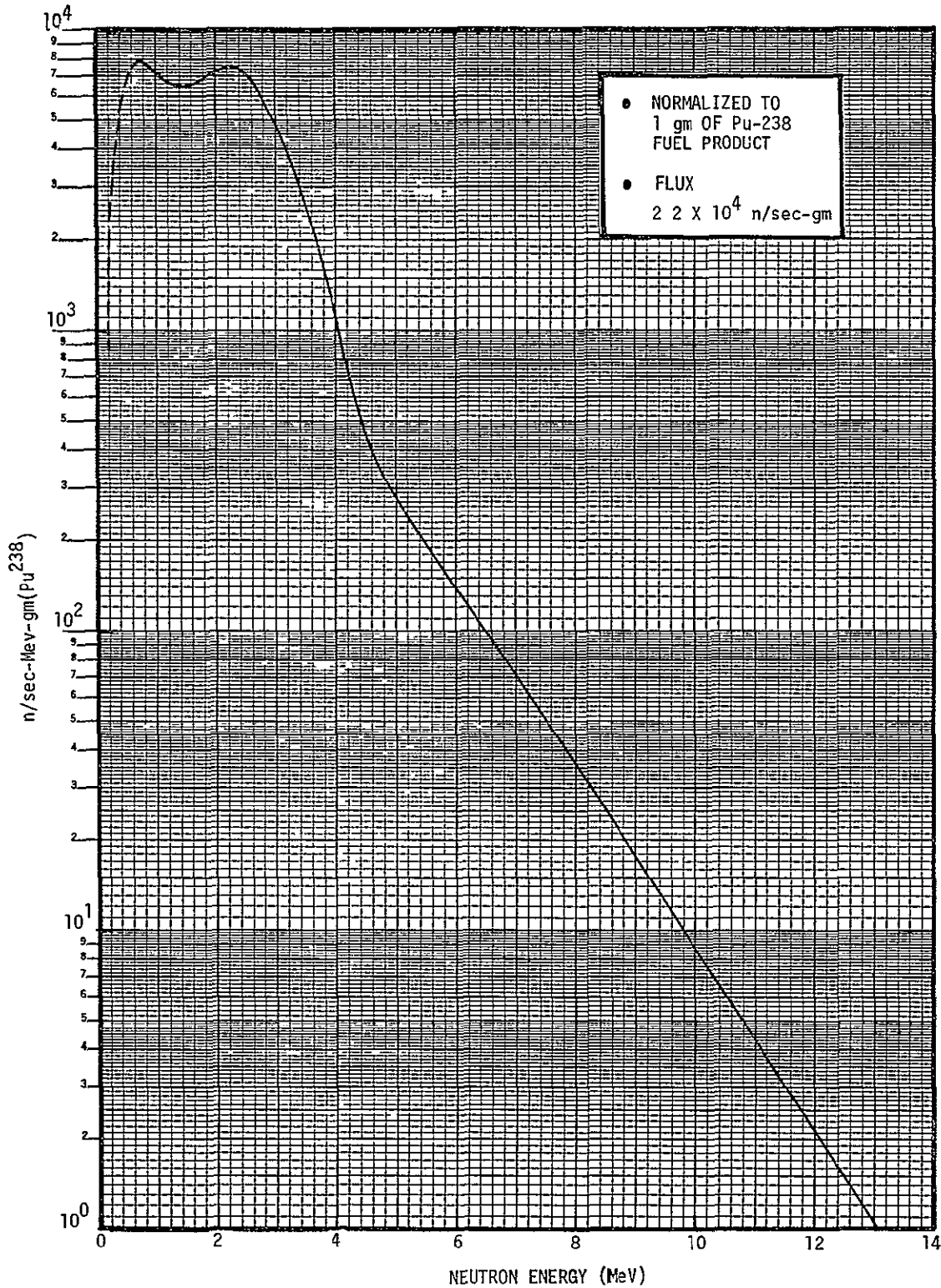
FIGURE 4-3. SNAP 27-1 NEUTRON SPECTRUM MEASURED BY MOUND LABORATORY

Differences in the gamma source activities result mainly from the scarcity of data for some of the gamma yield fractions and branching ratios Additionally, different half-life values for the decay modes have been used in determining the gamma activities resulting in small differences. It can be seen in Table 4-3 that disagreement exists over the yield fractions for the 0.810 and 0.875 Mev gamma. As discussed in Section 4.2.2, recent experimental data indicate that the yield fractions for these two gamma rays is small. Inclusion of the small yield fractions in place of the previously used larger yield fractions for the 0.810 and/or 0.875 Mev gammas in the gamma source will cause an appreciable change in any calculated gamma field.

Differences in the source values for the lowest energy gammas will not change calculated gamma fields since these gammas are almost completely attenuated by self-absorption of the source and the shielding of the fuel cladding materials. Hence inclusion or exclusion of the high intensity low-energy "L" X-ray reported by LASL will not affect calculated gamma fields. Also, the high values of gamma activities used by TRW for low energy gammas should not significantly affect calculated gamma fields.

At first glance the gamma activities reported in the literature may seem in disagreement. The activities are reported on the bases of 1 gram pure plutonium-238, 1 gram plutonium fuel product (81% plutonium-238) and on 1 watt of power. Confusion may exist when the activity basis is stated as 1 gram Pu-238. A 19% difference exists between the pure Pu-238 and Pu-238 fuel product basis.

Another difference in gamma source activities may result from the time dependence of the gamma source. The plutonium-236 and plutonium-241 impurities in the plutonium-238 fuel product cause the gamma activity of the source to increase with time after encapsulation of the fuel. Depending on the time after encapsulation, the calculated gamma field will have different values.

The gamma field calculated using the same gamma source will vary due to differences in cross-section values, buildup factors, and self-absorption values used in transport calculations. Characteristically, the differences in these values will cause calculated values to differ by a factor of 2 or more. The standard deviation of the cross-section values may alone cause a factor of 2 difference in transported gamma values.

The source geometry model used for the transport of the gamma rays may affect calculated results. However, for gamma fields calculated for distances far from the gamma source, all source models will act as a point source with $1/R^2$ behavior.

4.2.5 SNAP-27 Fuel Capsule Radiation Fields

The radioisotope fuel used in the SNAP-27 fuel capsule is plutonium-238 in the form of plutonium dioxide microspheres. The fuel is contained in a cylindrical annulus as shown in Figure 4-4. The capsule produces 1480 watts of thermal power. Utilizing the dimensions given in Figure 4-4 and the fact that one gram of plutonium-238 produces 0.55 watts, the density of the fuel was found to be 5 92 gm/cm^3

For purposes of computing the gamma ray fields around the fuel capsule the radiation source was assumed to consist of two line sources as shown in Figure 4-5. The line source intensities were scaled by the volume fractions of each of the two sections of the fuel annulus denoted by the dotted lines in Figure 4-5 (Sections A and B). The methods outlined by Case & Zweifel (Ref. 10) for the treatment of source self-attenuation were used. The gamma mass absorption coefficients for the source region and cladding material are shown in Table 4-12. The values were obtained from Reference 11 Gamma ray buildup factors to account for scattered radiations in all calculations were taken from Reference 9. The gamma source used in the gamma field calculations is shown in Table 4-13 and Figure 4-1. These values were derived by utilizing the data presented in Table 4-4, Table 4-6, and Table 4-7, corredsponding to the best gamma source values available to date.
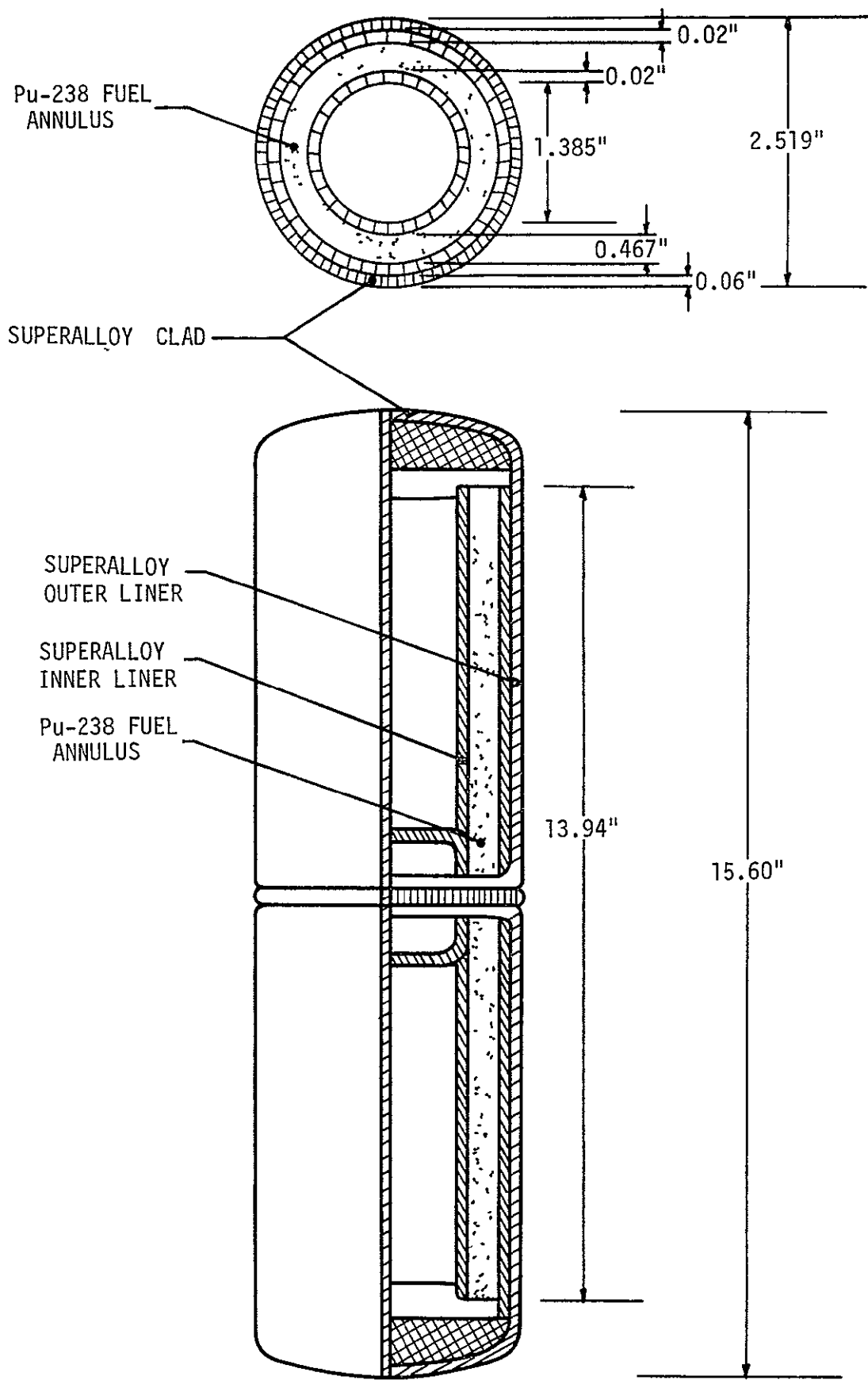
FIGURE 4-4. SNAP-27 FUEL CAPSULE
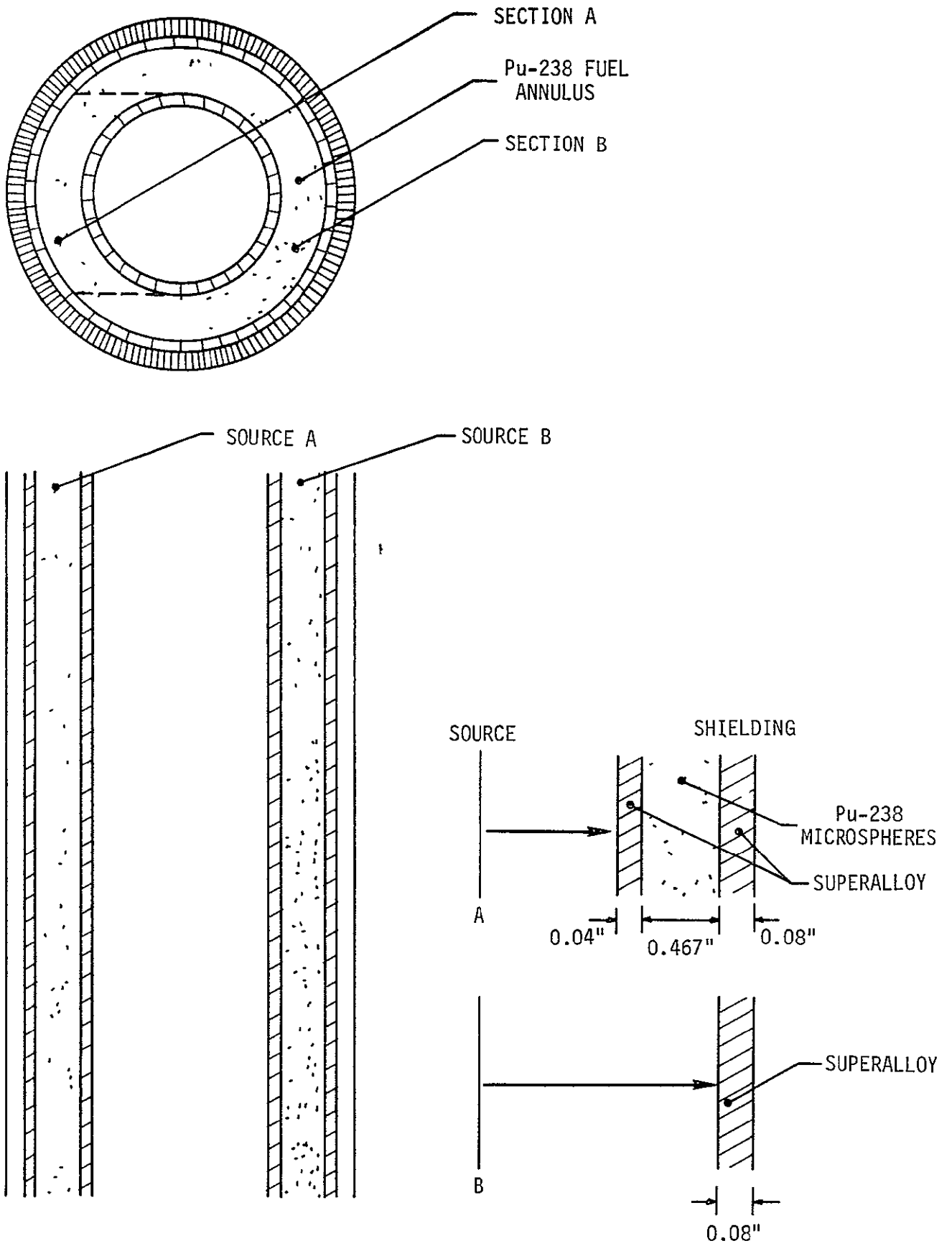
FIGURE 4-5. RADIATION SOURCE MODEL AND SHIELDING

4-18

TABLE 4-12· Mass Absorption Coefficients

Energy Group	Median Energy (Mev)	PuO$_2$ Mass Absorption Coefficients (cm^2/gm)	Superalloy Mass Absorption Coefficients (cm^2/gm)
1	0.05	9.902	2.289
2	0.10	1.591	0.9077
3	0.15	2.296	0.3760
4	0.20	1.148	0.2257
5	0.80	0.0953	0.0682
6	1.0	0.0756	0.0600
7	1.5	0.0553	0 0487
8	2.0	0.0480	0.0426
9	2.5	0.0458	0.0396
10	3.0	0.0437	0.0366
11	4.0	0.0427	0.0341
12	5.0	0.0432	0.0329
13	6.0	0.0436	0.0321

TABLE 4-13· Gamma Source From PuO$_2$ Fuel for Times Less Than One Year

Energy Group	Median Energy (Mev)*	Activity** (gammas/sec-gm)
1	0.05	2.00×10^8
2	0.10	3.82×10^7
3	0.15	3.50×10^6
4	0.20	3.05×10^4
5	0.80	1.60×10^5
6	1.0	1.34×10^4
7	1.5	2.60×10^3
8	2.0	1.61×10^3
9	2.5	6.53×10^2
10	3.0	3.64×10^2
11	4.0	6.86×10^1
12	5.0	3.51×10^1
13	6.0	1.72×10^1

*Median energy is adjusted in some cases to agree with most abundant gamma in group.
**Based on 1 gram of Pu-238 fuel product.

The results of the gamma field calculations are presented in Figure 4-6 and Table 4-14, showing the gamma ray spectrum and intensity at one meter from the capsule centerline. The gamma intensity at other distances can be found by assuming the field falls off as $1/R^2$. This is a good assumption for distance greater than 100 cm. The spectrum shown in Figure 4-6 will be somewhat harder than the actual measured spectrum due to the use of the buildup factor approximation.

TABLE 4-14: Calculated Gamma Radiation Field of
the SNAP-27 Fuel Capsule at One Meter

Group	Median Energy (Mev)	Gamma Flux (gammas/sec-cm^2)	Dose Rate (Roentgens/hr)
1	0.05	4.36×10^3	$5\ 72 \times 10^{-4}$
2	0.10	2.04×10^4	$3\ 16 \times 10^{-3}$
3	0 15	1.60×10^3	4.21×10^{-4}
4	0 20	2.92×10^1	1.095×10^{-5}
5	0.80	1.55×10^3	2.48×10^{-3}
6	1.0	$1\ 54 \times 10^2$	2.96×10^{-4}
7	1.5	$3\ 39 \times 10^1$	8.92×10^{-5}
8	2.0	$2\ 27 \times 10^1$	7.33×10^{-5}
9	2.5	9.31×10^0	3.54×10^{-5}
10	3 0	5.23×10^0	2.22×10^{-5}
11	4.0	9.96×10^{-1}	5.11×10^{-6}
12	5.0	5.03×10^{-1}	3.17×10^{-6}
13	6.0	2.44×10^{-1}	1.75×10^{-6}
TOTAL		2.82×10^4	7.17×10^{-3}
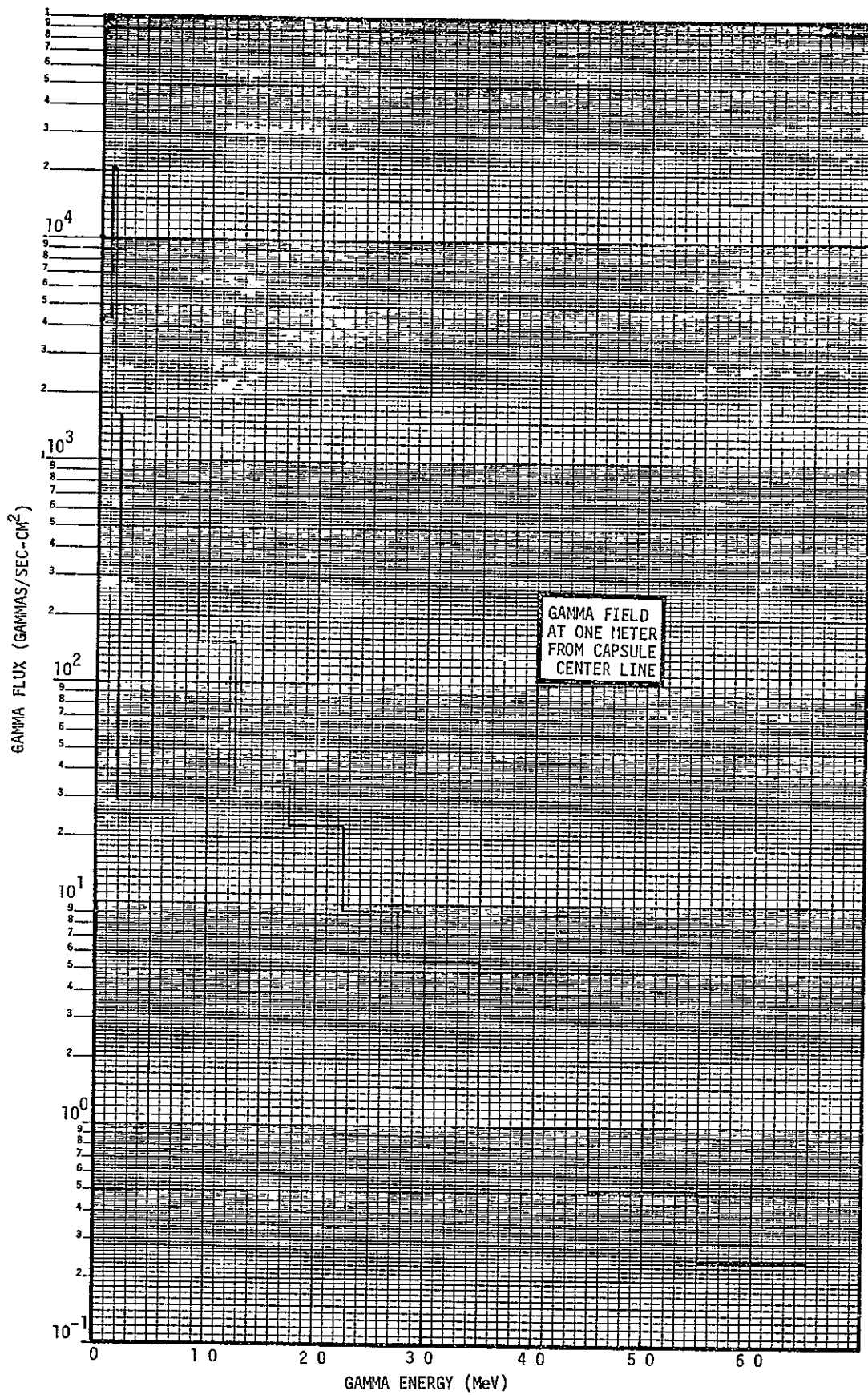
FIGURE 4-6. CALCULATED GAMMA FIELD AT ONE METER FROM SNAP-27 FUEL CAPSULE

4-27

Since the neutron radiation field generated by the SNAP-27 fuel capsule was directly measured by Mount Laboratory (Ref. 7, 1968), the field was not calculated here. The measured neutron spectrum per gram of plutonium-238 fuel product is shown in Figure 4-3. The neutron intensity of 2.2×10^4 n/gm-sec is in agreement with other reported values (Table 4-9) For the 1480 watt (thermal) SNAP-27 capsule, the corresponding neutron intensity is 5.92×10^7 n/sec This value can be used as an effective point source. Then the neutron flux at radial distance R from the center at the capsule can be found from Equation 1

$$FL\ (R) = \frac{5\ 92 \times 10^7\ n/sec}{4\pi R^2}$$

where.

$FL\ (R)$ = Neutron flux at radial distance R (n/sec-cm^2)

R = Radial distance from source (cm)

At one meter from the SNAP-27 fuel capsule the neutron flux is 471 n/sec-cm^2.

4 3   SNAP-27 Fuel Capsule Radiation Fields As A Function of Age

The SNAP-27 fuel capsule of interest was assumed to have aged 2 years since fuel encapsulation. Given in Section 4.2 is the radiation source for times of less than one year. At two years after fuel encapsulation, there is an added source of gamma radiation from the growth of daughter nuclides in the Pu-236 and Pu-241 decay chains. Presented in Table 4-15 is the gamma source at times less than one year and at two years (from data presented in Section 4.2)

TABLE 4-15   AGE EFFECT ON SNAP-27 FUEL CAPSULE
GAMMA ACTIVITY

Group	Median Energy (Mev)	Activity (gammas/sec-gm) *	
		<1 yr.	2 yrs.
1	0.05	2.00×10^8	2.38×10^8
2	0.10	3.82×10^7	3.82×10^7
3	0.15	3.50×10^6	3.50×10^6
4	0.20	3.05×10^4	1.205×10^5
5	0.80	1.60×10^5	1.92×10^5
6	1.0	1.34×10^4	$1 34 \times 10^4$
7	1.5	2.60×10^3	2.60×10^3
8	2.0	1.61×10^3	1.61×10^3
9	2.5	6.53×10^2	$3 78 \times 10^4$
10	3.0	3.64×10^2	3.64×10^2
11	4.0	6.86×10^1	6.86×10^1
12	5.0	3.51×10^1	3.51×10^1
13	6.0	$1 72 \times 10^1$	1.72×10^1

* Based on 1 gram of Pu-238 fuel product

Using the source model and methods given in Section 4.2, and the gamma source spectrum at two years (4-15), the gamma field was calculated at one-half, one, three, and ten meters from the fuel capsule centerline. The effect of air attenuation was calculated by using exponential attenuation without buildup or scattering. This is a valid assumption as even 10 meters of air is equivalent to less than 1/2 a mean free path for the lowest energy gammas. It was found that the air attenuation reduced the dose rate at one-half meter by 1.6%, at one meter by 3%, at three

meters by 8.8%, and at ten meters by 26.6%. Presented in Figure 4-7 is the calculated gamma dose rate profile around the SNAP-27 fuel capsule. In Figure 4-8 the gamma dose rate is plotted as a function of radial distance.

A check of the exponential attenuation of neutrons by air for the neutron spectrum of the fuel capsule indicated that the air attenuation is negligible for the neutrons. Thus, the neutron field results given in Section 4.2 can be used. Presented in Figure 4-9 is the calculated neutron dose rate profile around the SNAP-27 fuel capsule. In Figure 4-8 the neutron dose rate is plotted as a function of radial distance along with the gamma dose rate. The necessary dose rate conversion factors were obtained from Reference 9. The total radiation fields (neutron and gamma fields) at one-half, one, three, and ten meters are presented in Tables 4-16, 4-17, 4-18 and 4-19, respectively.

4.4 Neutron Induced Activation

The gamma ray field resulting from neutron induced activation of materials external to the fuel capsule may be significant compared to the gamma ray field generated by the fuel capsule itself. Presented here is an estimate of the relative values of these two components of the gamma field at a selected flux point external to the capsule. The methods and data in Reference 12 were utilized to calculate neutron activitation of several materials. Of specific interest are materials used in construction of scientific instruments. The materials considered here are aluminum, stainless steel, iron alloys, copper, beryllium, and titanium.
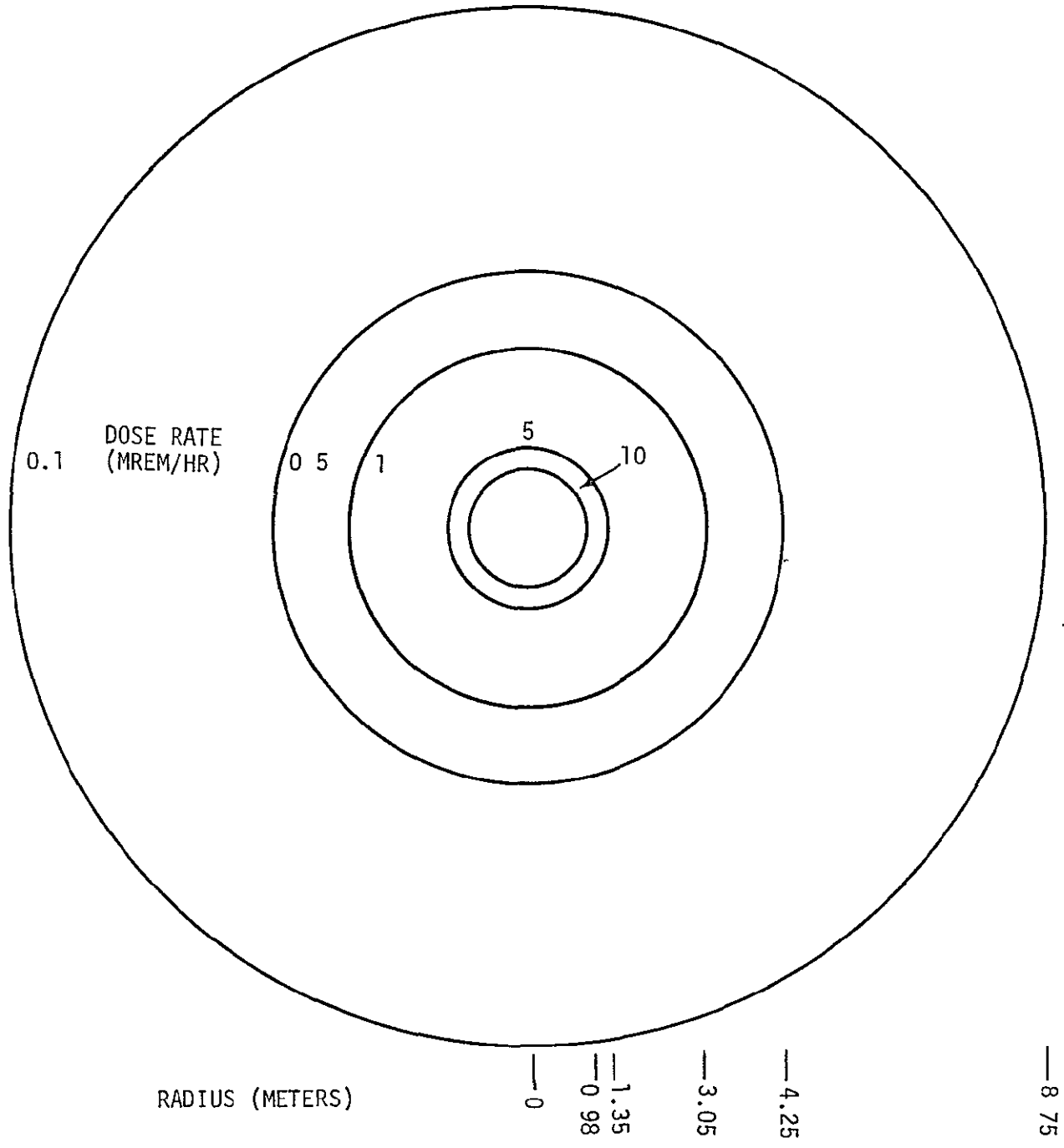
FIGURE 4-7 GAMMA ISODOSE-RATE PROFILE AROUND A SNAP-27
RADIOISOTOPE FUEL CAPSULE
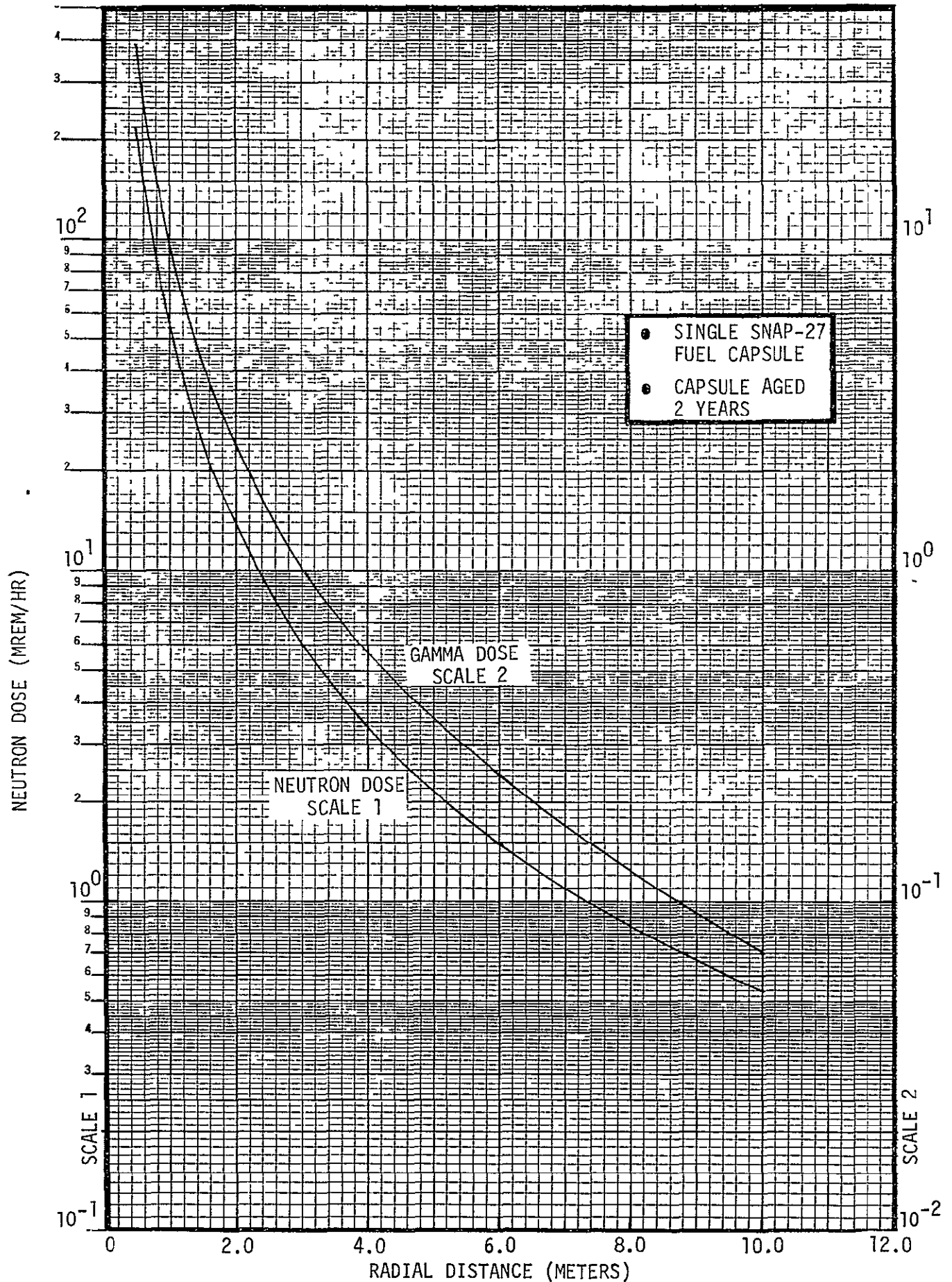
FIGURE 4-8: NEUTRON AND GAMMA DOSE RATE AS FUNCTION OF
RADIAL DISTANCE FROM THE SNAP-27 FUEL CAPSULE
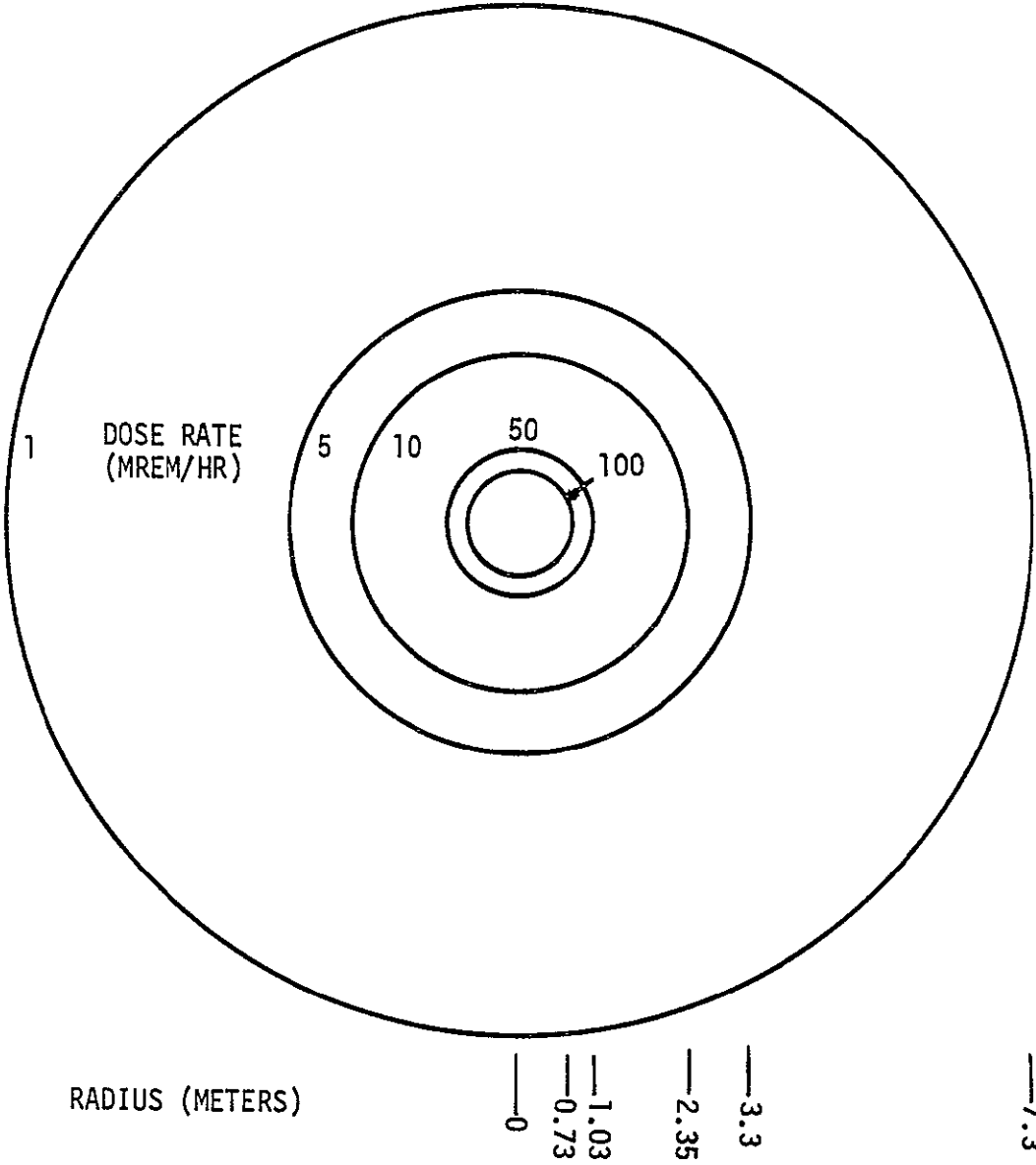
FIGURE 4-9· NEUTRON ISODOSE-RATE PROFILE AROUND A SNAP-27
RADISOTOPE FUEL CAPSULE

TABLE 4-16:- CALCULATED RADIAL RADIATION FIELD AT ONE-HALF
METER FOR A SNAP-27 FUEL CAPSULE[*]

GAMMA FIELD			NEUTRON FIELD		
Energy Interval (Mev)	Gamma Flux (gammas/sec-cm^2)	Gamma Dose Rate (MREM/HR)	Energy Interval (Mev)	Neutron Flux (N/sec-cm^2)	Neutron Dose Rate (MREM/HR)
0 - 0 075	1.915×10^4	2.508×10^0	0.2 - 0.6	159.6	9.68
0.075 - 0.125	$7\ 779 \times 10^4$	1.205×10^1	0.6 - 1.0	256 8	24.92
0.125 - 0.175	$6\ 334 \times 10^3$	1.678×10^0	1.0 - 1.4	226.8	26 80
0.175 - 0.50	4.544×10^2	1.704×10^{-1}	1.4 - 1.8	225.2	26 40
0.50 - 0.90	7.517×10^3	1.202×10^1	1 8 - 2.2	244.0	28.80
0.90 - 1.25	6.17×10^2	1.184×10^0	2.2 - 2.6	245.2	29 00
1.25 - 1 75	1.351×10^2	3.563×10^{-1}	2.6 - 3 0	195.2	23.64
1.75 - 2 25	$9\ 07 \times 10^1$	2.929×10^{-1}	3.0 - 3.4	163.2	20.72
2.25 - 2 75	2.146×10^3	8.049×10^0	3.4 - 3.8	75.6	10 00
2.75 - 3.5	2.087×10^1	8.871×10^{-2}	3.8 - 4 6	56.0	7.84
3.5 - 4.5	4.017×10^0	2.129×10^{-2}	4.6 - 6.6	33.0	5.28
4.5 - 5.5	2.034×10^0	1.281×10^{-2}	6.6 -13.0	10 9	2.18
5 5 - 6.5	9.89×10^{-1}	7.124×10^{-3}	-------	------	-----
TOTAL	1.142×10^5	$3\ 845 \times 10^1$	-------	1891.48	215.26

* Fuel has been encapsuled for 2 years

TABLE 4-17   CALCULATED RADIAL RADIATION FIELD AT ONE METER
FOR A SNAP-27 FUEL CAPSULE*

GAMMA FIELD			NEUTRON FIFLD		
Energy Interval (Mev)	Gamma Flux (gammas/sec-cm^2)	Gamma Dose Rate (MREM/HR)	Energy Interval (Mev)	Neutron Flux (N/sec-cm^2)	Neutron Dose Rate (MREM/HR)
0 - 0 075	$4 184 \times 10^3$	5.481×10^{-1}	0.2 - 0.6	39 9	2 42
0 075 - 0.125	1.978×10^4	3.066×10^0	0.6 - 1.0	64.2	6.23
0.125 - 0.175	$1 557 \times 10^3$	4.127×10^{-1}	1.0 - 1 4	56.7	6 70
0.175 - 0.50	1.122×10^2	4.208×10^{-2}	1.4 - 1.8	56 3	6.60
0.50 - 0 90	$1 844 \times 10^3$	$2 950 \times 10^0$	1.8 - 2.2	61.0	7.20
0.90 - 1.25	1.520×10^2	2.919×10^{-1}	2.2 - 2.6	61.3	7 25
1.25 - 1.75	3.355×10^1	8.825×10^{-2}	2.6 - 3.0	48.8	5 91
1.75 - 2.25	2.250×10^1	7.268×10^{-2}	3.0 - 3.4	40.8	5.18
2.25 - 2 75	5.338×10^2	$2 001 \times 10^0$	3 4 - 3.8	18.9	2.50
2.75 - 3 5	5.193×10^0	$2 207 \times 10^{-2}$	3.8 - 4.6	14.0	1.96
3.5 - 4 5	9.890×10^{-1}	5.246×10^{-3}	4.6 - 6.6	8.25	1.32
4.5 - 5 5	5.000×10^{-1}	3.151×10^{-3}	6.6 -13.0	2.72	0 545
5.5 - 6.5	$2 420 \times 10^{-1}$	1.748×10^{-3}	------	-----	-----
TOTAL	2.823×10^4	9.506×10^0	------	472.87	53.815

*   Fuel has been encapsuled for 2 years

TABLE 4-18· CALCULATED RADIAL RADIATION FIELD AT THREE METERS
FOR A SNAP-27 FUEL CAPSULE*

GAMMA FIELD			NEUTRON FIELD		
Energy Interval (Mev)	Gamma Flux (gammas/sec-cm^2)	Gamma Dose Rate (MREM/HR)	Energy Interval (Mev)	Neutron Flux (N/sec-cm^2)	Neutron Dose Rate (MREM/HR)
0 - 0.075	4.284×10^2	5.613×10^{-2}	0.2 - 0.6	4.43	0.268
0.075 - 0.125	$2 070 \times 10^3$	3.209×10^{-1}	0.6 - 1.0	7.13	0.692
0.125 - 0.175	1.642×10^2	4.352×10^{-2}	1.0 - 1.4	6.30	0.744
0.175 - 0.50	1.189×10^1	4.461×10^{-3}	1.4 - 1.8	6.25	0.733
0 50 - 0.90	1.994×10^2	3.191×10^{-1}	1.8 - 2.2	6.77	0.800
0.90 - 1.25	1.646×10^1	$3 161 \times 10^{-2}$	2.2 - 2.6	6.81	0.805
1.25 - 1.75	3.656×10^0	$9 615 \times 10^{-3}$	2.6 - 3.0	5.42	0.656
1.75 - 2.25	2.464×10^0	7.959×10^{-3}	3.0 - 3.4	4.53	0.575
2.25 - 2.75	5.840×10^1	2.190×10^{-1}	3.4 - 3.8	2.10	0.277
2 75 - 3 5	5.687×10^{-1}	2.416×10^{-3}	3.8 - 4.6	1.55	0.217
3.5 - 4.5	1.089×10^{-1}	5.771×10^{-4}	4.6 - 6.6	0.916	0.146
4.5 - 5.5	5.499×10^{-2}	3.464×10^{-4}	6.6 -13.0	0.302	0.0605
5.5 - 6.5	2.669×10^{-2}	1.921×10^{-4}	--------	-----	-----
TOTAL	2.956×10^3	1.0159×10^0	--------	52.541	5.979

* Fuel has been encapsuled for 2 years

TABLE 4-19.   CALCULATED RADIAL RADIATION FIELD AT TEN METERS
FOR A SNAP-27 FUEL CAPSULE*

GAMMA FIELD			NEUTRON FIELD		
Energy Interval (Mev)	Gamma Flux (gammas/sec-cm^2)	Gamma Dose Rate (MREM/HR)	Energy Interval (Mev)	Neutron Flux (N/sec-cm^2)	Neutron Dose Rate (MREM/HR)
0 - 0.075	4.15×10^1	5.436×10^{-3}	0.2 - 0.6	3.99×10^{-1}	2.42×10^{-2}
0.075 - 0.125	1.819×10^2	2.819×10^{-2}	0.6 - 1.0	6.42×10^{-1}	6.23×10^{-2}
0.125 - 0 175	1.224×10^1	3.243×10^{-3}	1.0 - 1 4	5.67×10^{-1}	6.70×10^{-2}
0.175 - 0.50	9.010×10^0	3.381×10^{-4}	1.4 - 1.8	5.63×10^{-1}	6.60×10^{-2}
0.50 - 0.90	1.626×10^1	2.603×10^{-2}	1.8 - 2.2	6.10×10^{-1}	7.20×10^{-2}
0.90 - 1.25	1.361×10^0	2.613×10^{-3}	2.2 - 2.6	6.13×10^{-2}	7.25×10^{-2}
1.25 - 1 75	3.061×10^{-1}	8.050×10^{-4}	2.6 - 3.0	4.88×10^{-1}	5.91×10^{-2}
1.75 - 2.25	2.079×10^{-1}	6.715×10^{-4}	3 0 - 3.4	4.08×10^{-1}	5.18×10^{-2}
2.25 - 2.75	4.970×10^0	1.863×10^{-3}	3.4 - 3.8	1.89×10^{-1}	2.50×10^{-2}
2.75 - 3.5	4.872×10^{-2}	2.070×10^{-4}	3.8 - 4.6	1.40×10^{-1}	1.96×10^{-2}
3.5 - 4.5	9.372×10^{-3}	4.967×10^{-5}	4.6 - 6.6	8.25×10^{-2}	1.32×10^{-2}
4.5 - 5.5	4.763×10^{-3}	3.000×10^{-5}	6.6 -13.0	2.72×10^{-2}	5.45×10^{-3}
5.5 - 6.5	2.322×10^{-3}	1.671×10^{-5}	--------	--------	--------
TOTAL	2.601×10^2	6.950×10^{-2}	--------	4.73×10^0	$5 382 \times 10^{-1}$

*   Fuel has been encapsuled for 2 years

The activation flux point of interest was chosen at 2 cm from a 5 pound sample of material (a typical weight for a spacecraft instrument). The material sample was assumed for convenience to be located 100 cm from the fuel capsule. For any radial distance from the fuel capsule at which the material sample may be located, the relative contributions of the fuel capsule primary gammas and the neutron induced gammas to the total gamma flux (at 2 cm from the material sample) is approximately constant. This result is due to the $1/R^2$ geometrical attenuation of both the primary capsule generated fields; i.e., the gamma field, and the neutron field which controls the activation gamma source strength.

The neutron induced activation in the materials was calculated using the effective activation cross-sections given in Reference 12. These effective "cross sections" were measured with the ORNL reactor spectrum. The reactor spectrum is largely low-energy while the capsule neutron spectrum is relatively high-energy with little low-energy neutron contribution. The higher energy spectrum will induce relatively more (n, p) and (n, n', γ) reactions, with concomitant gammas, but will induce relatively fewer (n, γ) reactions. Hence, the effective "cross-sections" for the higher energy capsule spectrum is conservatively estimated to be of the same order of magnitude as the effective "cross-sections" for the reactor spectrum.

Using the effective activation cross-sections given in Reference 12 and assuming a point source model for the neutron induced gammas, the neutron induced gamma flux was calculated. Presented in Table 4-20 are the contributions to the gamma field from the activated materials at 2 cm from the activated materials and 100 cm from the fuel capsule. It can be seen from Table 4-20 that for the materials considered here, the neutron induced gamma field is two to five orders of magnitude smaller than the primary fuel capsule gamma field (2.8×10^4 gammas/s-cm^2). Self attenuation effects, which were not included in the calculation, would reduce the flux still further. Hence, the effect of neutron induced activation can be neglected when estimating the SNAP-27 fuel capsule gamma radiation field.

TABLE 4-20: NEUTRON INDUCED GAMMA FLUX AT 2 CM FROM
A FIVE POUND SAMPLE OF VARIOUS MATERIALS
LOCATED ONE METER RADIALLY FROM SNAP-27
FUEL CAPSULE*

MATERIAL	Gamma Flux $(gammas/cm^2-sec)$
Aluminum .	25.5
Iron (1030 alloy)	30.9
Stainless Steel (316)	80.4
Copper	174
Beryllium	0.2
Titanium	1.1

* Flux contribution from the fuel capsule at the same flux point
is 2.8×10^4 gammas/sec-cm^2.

4.5 Summary of Results

In Section 4.2, a good estimate of the neutron and gamma radiation fields emitted by a SNAP-27 fuel capsule was obtained by utilizing the information available from recent measurements of plutonium-238 sources. The neutron field is well defined by the direct measurement performed on a SNAP-27 capsule reported in Reference 7. The recent measurements in Reference 8 of the gamma rays emitted by plutonium-238 have resolved the differences found in previous estimates of Pu-238 gamma ray source. Of specific importance, the measurements reveal that the yield fractions for the 0.810 and 0.875 Mev gammas are very small and that the 0.760 Mev gamma yield fraction is roughly a factor of 2 less than previously reported.

Differences in the calculated gamma field exterior to the SNAP-27 fuel capsule will arise depending on the model assumed for the source, the mass attenuation cross sections used for the materials, the buildup factors used for scattering effects, and the method used to account for self-absorption of the source. The source model used is not overly important as any source model chosen will appear as a point source at a sufficient distance.

In Section 4.3 the radiation fields at one-half, one, three, and ten meters for a two year old SNAP-27 radioisotope fuel capsule were calculated utilizing the data presented in Section 4.2. It was found that the effect of air attenuation reduced the gamma dose rate at one-half meter by 1 6%, at one meter by 3%, at three meters by 8 8%, and at ten meters by 26.6%. The neutron dose rate was unaffected by air attenuation. In Section 4.4 it was found that neutron induced gamma activation in materials (materials typically found in scientific instruments) external to the fuel capsule produced a negligible perturbation of the field surrounding the fuel capsule.

REFERENCES

1   Stoddard, D H., and Albenesius, "Radiation Properties of Pu-238 Produced for Isotopic Power Generators," Savannah River Laboratory, DP-984, July 1965.

2   Matlack, G. M., and Metz, C. F., "Radiation Characteristics of Plutonium-238," Los Alamos Scientific Laboratory, LA-3696, September 1967.

3. Grove, G. R., Data Sheets: Plutonium-238 Fuels, Monsanto Research Corporation, Mound Laboratory, Miamisburg, Ohio, July 1, 1967.

4   King, M., et al, "Application of Radioisotope Thermoelectric Generators to Advanced Scientific Spacecraft," TRW Systems, Report No. 9990-6129-T500 (CRD), December 31, 1966.

5. Spamer, A. M , and Davenport, K. G., "SNAP 19 Program Generator Radiation Analysis," Martin, MND-3169-15, August 1964.

6. Strominger, D., et al., "Table of Isotopes," Review of Modern Physics," Vol. 30, No. 2, Part 2, April 1958.

7. Private Communication with M E. Anderson, Mound Laboratory.

8. Matlack, G. M., Bubernak, J., and Metz, C. F., "Neutron and Gamma Radiations from Pu-238," A talk presented at the 1968 Winter Meeting of the American Nuclear Society, Washington, D. C., November 10-15, 1968.

9. Rockwell, T., Reactor Shielding Design Manual, McGraw Hill, 1956.

10. Case, K.M., and Zweifel, P. F., Linear Transport Theory, Addison-Wesley, 1967.

11. Storm, E., and Israel, H I., "Photon Cross Sections from 0.001 to 100 Mev for Elements 1 through 100," LA-3753, 1967.

12. Bopp, C. D., and O. Sisman, "How to Calculate Gamma Radiation Induced in Reactor Materials," Nucleonics, Vol. 14, No. 1, January 1956.

5. RADIATION INTERFERENCE EXPERIMENTS

5.1 General

The radiation interference experiments were carried out in a large 40' x 40' room with 20' ceiling and a 20' x 20' by 10' deep well in the center of the room covered with a low mass aluminum floor. The fuel capsule and the detectors were located near the center of the well to minimize radiation scattering from the surrounding walls and floor.

A typical experimental set-up used during the majority of the testing is illustrated schematically in Figure 5.1-1. Several photographs of the set-up are shown in Figures 5.1-2 and 5.1-3 Before each test, the SNAP-27 fuel capsule was taken out of its storage cask and mounted in a specially designed fuel capsule positioning fixture so it could be moved, by remote means, either up or down or in the horizontal plane. The radiation detectors were installed on a low mass supporting structure and the fuel capsule was moved to the desired distance from the detector. The distance measurements were performed using either a theodolite or a tape measure depending on which was more convenient for the particular set-up. Provisions were made on the detector supporting rack to mount absorber materials or heat shields between the fuel capsule and detector. The heat shields were made out of aluminum foil and were used to avoid overheating the detectors when they were operated in close proximity to the heat source.

The general test procedure for testing the detectors was as follows·

- Set up one detector in the test rack.
- Adjust the high voltage and/or amplifier gains to give the desired output.
- Check system gain using one or more calibration sources.
- Move the fuel capsule to desired distance from the detector.
- Record detector response to the fuel capsule spectrum.
- Insert various absorbers between the fuel capsule and the detector, and record detector response (usually without moving either the detector or the fuel capsule)

SNAP 27
FUEL CAPSULE

RADIATION
SHIELD

DETECTOR

H.V. POWER
SUPPLY

AMPLIFIER

PULSE
HEIGHT
ANALYZER

ANALYZER PRINTOUT
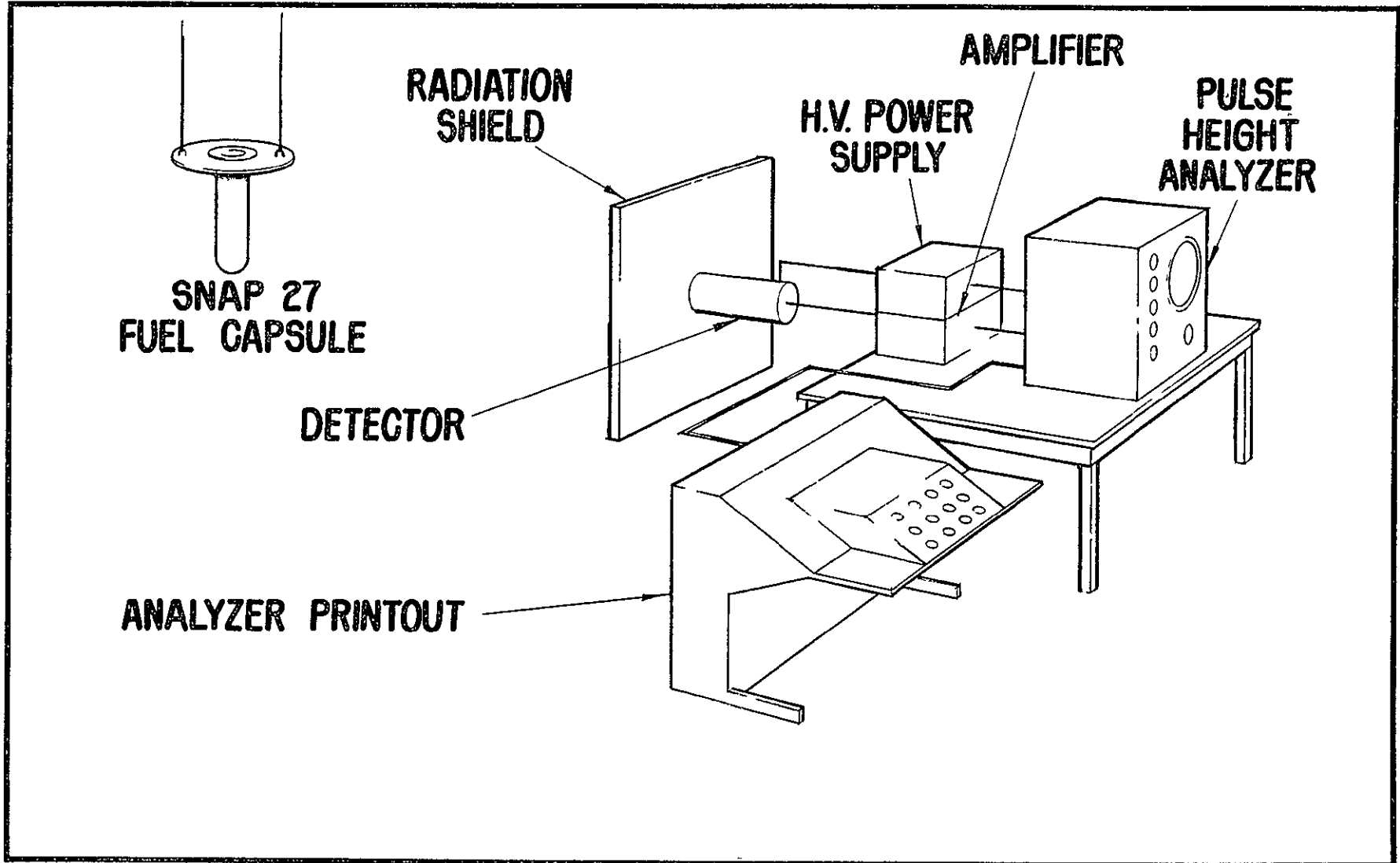
FIGURE 5.1-1 EXPERIMENTAL SETUP
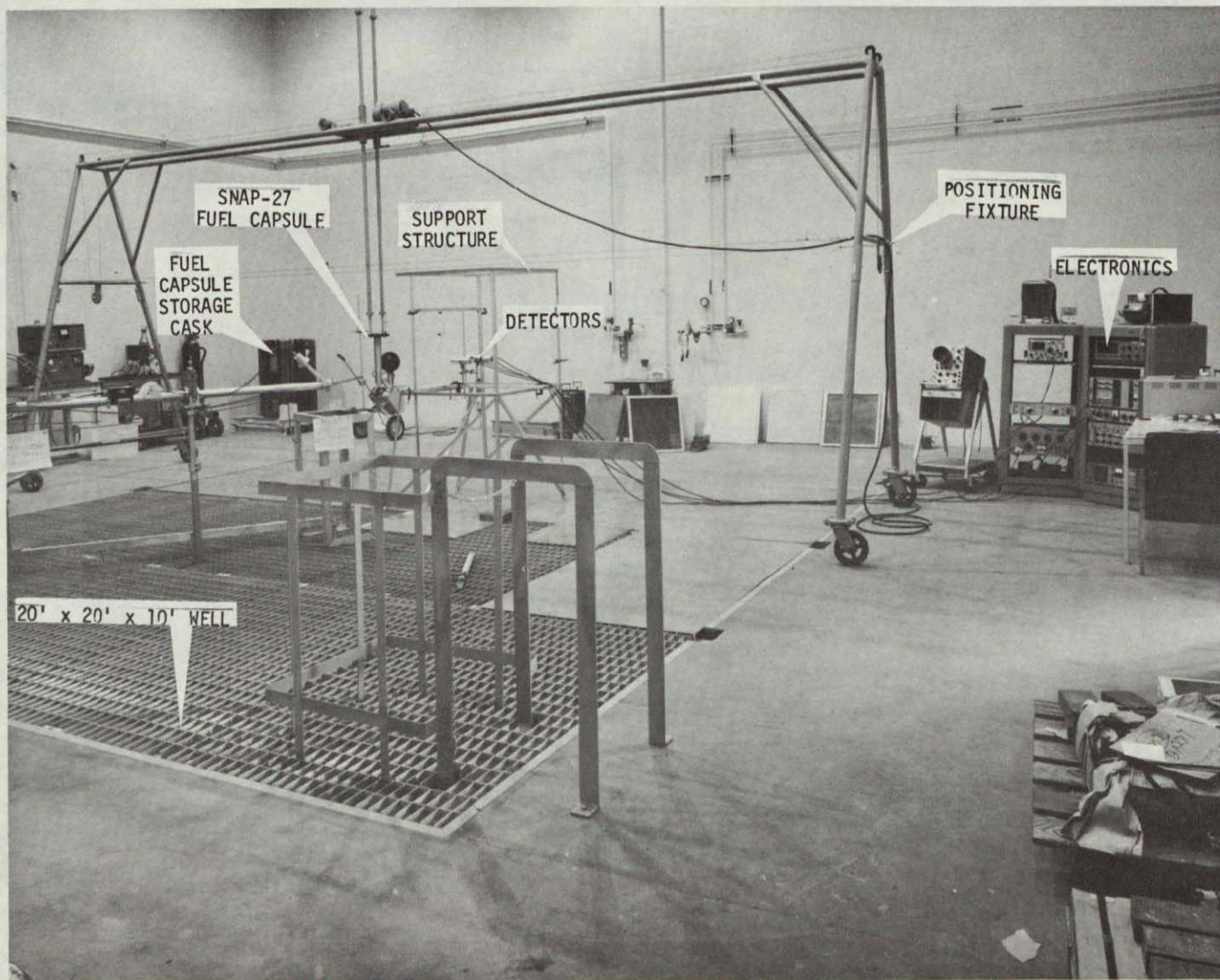
FIGURE 5.1-2 EXPERIMENTAL SETUP IN RADIATION RESEARCH FACILITY,
TRW SYSTEMS
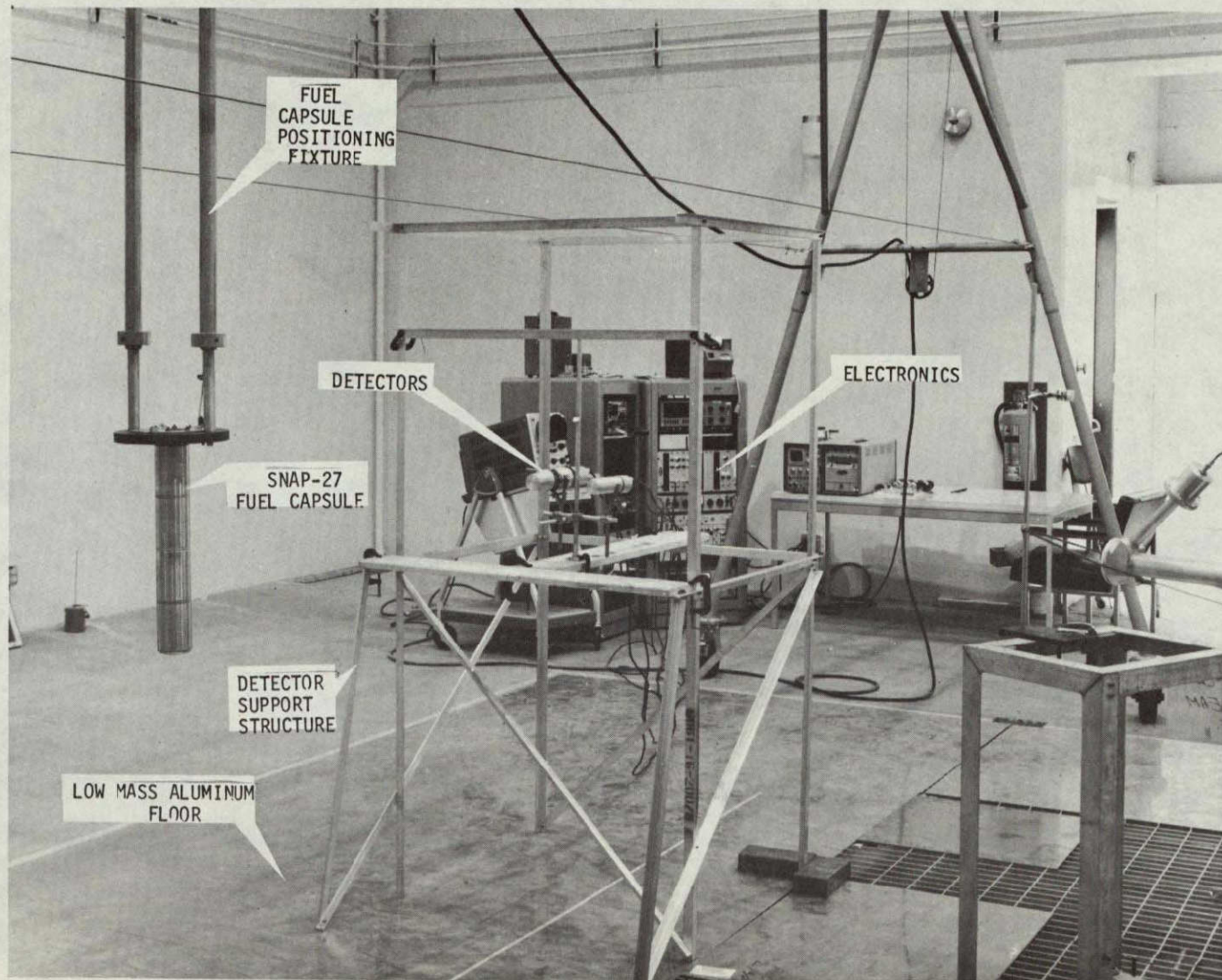
FIGURE 5.1-3 EXPERIMENTAL SETUP IN RADIATION RESEARCH FACILITY,
TRW SYSTEMS

• Change fuel capsule-to-detector distance and record the
detector response.

• Change detector orientation with respect to the fuel capsule
(by turning the detector 45° and 90° to the fuel capsule)
and record detector response.

• Check detector calibration to ensure that system has not
drifted during test.

5 2   Fuel Capsule to Detector Distance

Most of the testing was performed with the fuel capsule positioned
vertically and the detectors in the same horizontal plane as the center
of the fuel capsule.

The distance between the fuel capsule and the radiation detectors
was adjusted to suit the count rate of each particular detector system to
achieve good statistical data in reasonable counting times.   Then the
data were adjusted to correspond to a common distance of 36 inches.
Figure 5 2-1 illustrates how the theoretical count rate varies with
distance from the fuel capsule.   Experimental data taken during the
program verified that this count rate versus distance relationship was
in good agreement for each of the detectors used.

5.3   Shields

To measure the effectiveness of various shielding materials, a
set of standard shields was selected and used with each detector.

The standard shields consisted of:

Lead (0.031, 0.062, 0.125, 0.025, 0.5 inch thick or
0.90, 1.81, 3.62, 7.25, 14.5 gms/cm^2 respectively)

Aluminum (0.031, 0.062, 0.125, 0.25, 0.5 inch thick or
0.22, 0.43, 0.86, 1.71, 3.43 gms/cm^2 respectively)

Polyethylene (0.25, 0.50, 1.0, 2.5 inch thick or
0.675, 1.35, 2.70, 6.75 gms/cm^2 respectively)

Boron loaded polyethylene (with 5% boron) (1.0 inch thick,
∿2.6 gms/cm^2)
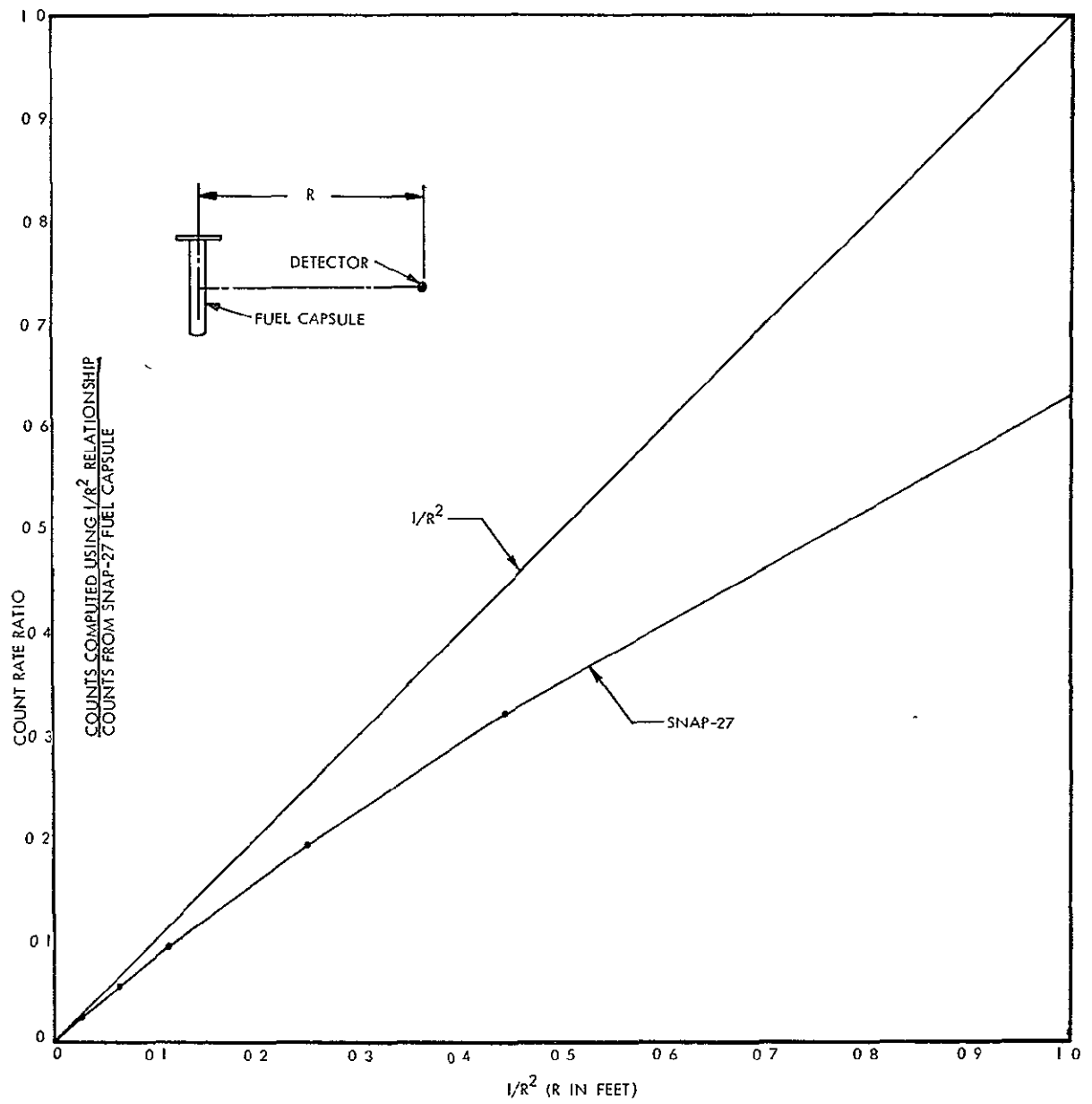
FIGURE 5.2-1 THEORETICAL COUNT RATE VARIATION
WITH DISTANCE FROM THE FUEL CAPSULE

5-6

All shields were of the same size, 24" x 24", and were positioned between the fuel capsule and detectors so that the detector was in the center of the shield and 4 to 6 inches behind it. The choice of these large area shields was made on the basis of the best compromise between convenience and experimental objectives. In practice for spacecraft applications only small shields just covering the area of the detector or the fuel capsule would be used. However, manufacturing of such shields for each detector used in the tests was beyond the scope of this program and it was chosen to approximate an "infinite" shield using 24" x 24" absorbers The use of this large size shield results in additional scattering and dose build-up seen by the detectors. In fact, in some cases, the count rate at the lower energies (several hundred kev) actually increased above the no-absorber level when a thin polyethylene sheet was inserted between the fuel capsule and detector. However, there is a relation between the measured absorption with the simulated infinite shields and absorbers just large enough to cover the detector. To measure this absorption relationship between small and large area absorbers, a set of small absorbers 3" x 3" was constructed and absorption data for several scintillator detectors was measured and compared with absorption data obtained with the large absorbers. SNAP-27 fuel capsule spectra taken with 1-1/2 x 1-1/2 NaI scintillator, are illustrated in Figure 5.3-1. Figure 5.3-2 shows spectra taken with small and large absorbers. Also, a correction curve, shown in Figure 5.3-3, was generated and can be used to obtain an approximate correction for the data obtained with large absorbers to what would be seen if small area absorbers were used. As would be expected, the deviation increases with decreasing gamma energy. However, in all cases neglect of this correction factor will result in conservative values of the shielding thickness required to reduce the RTG radiation to the desired level.

5.4 Radiation Around the RTG

A majority of the data on detector response to the fuel capsule radiation was taken with the fuel capsule positioned with its long axis vertically and the radiation detectors positioned in the horizontal plane
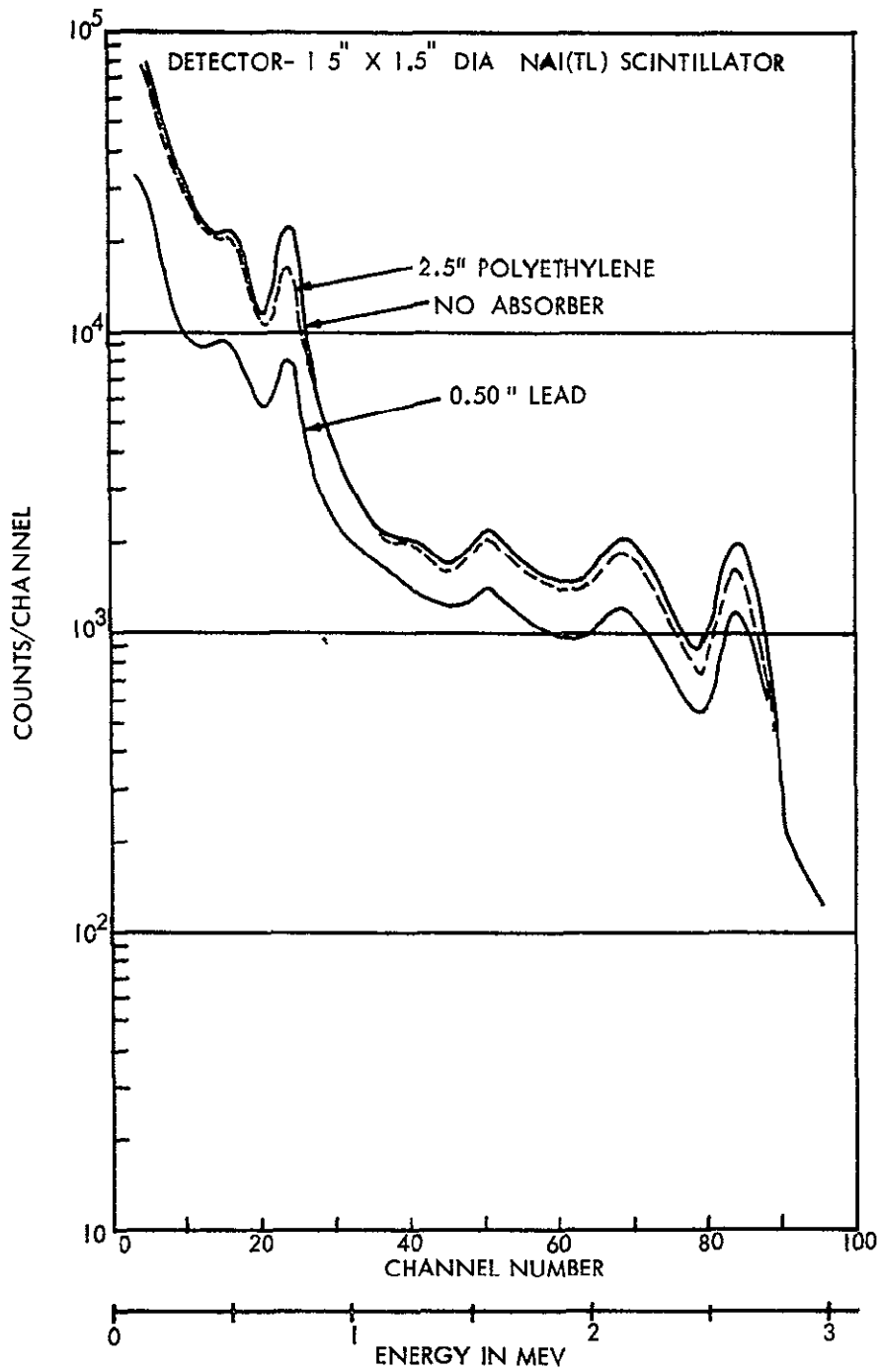
FIGURE 5.3-1 EFFECT OF ABSORBERS ON SNAP-27 FUEL
CAPSULE SPECTRA TAKEN WITH 1.5" x 1.5" DIA NaI(Tl) SCINTILLATOR
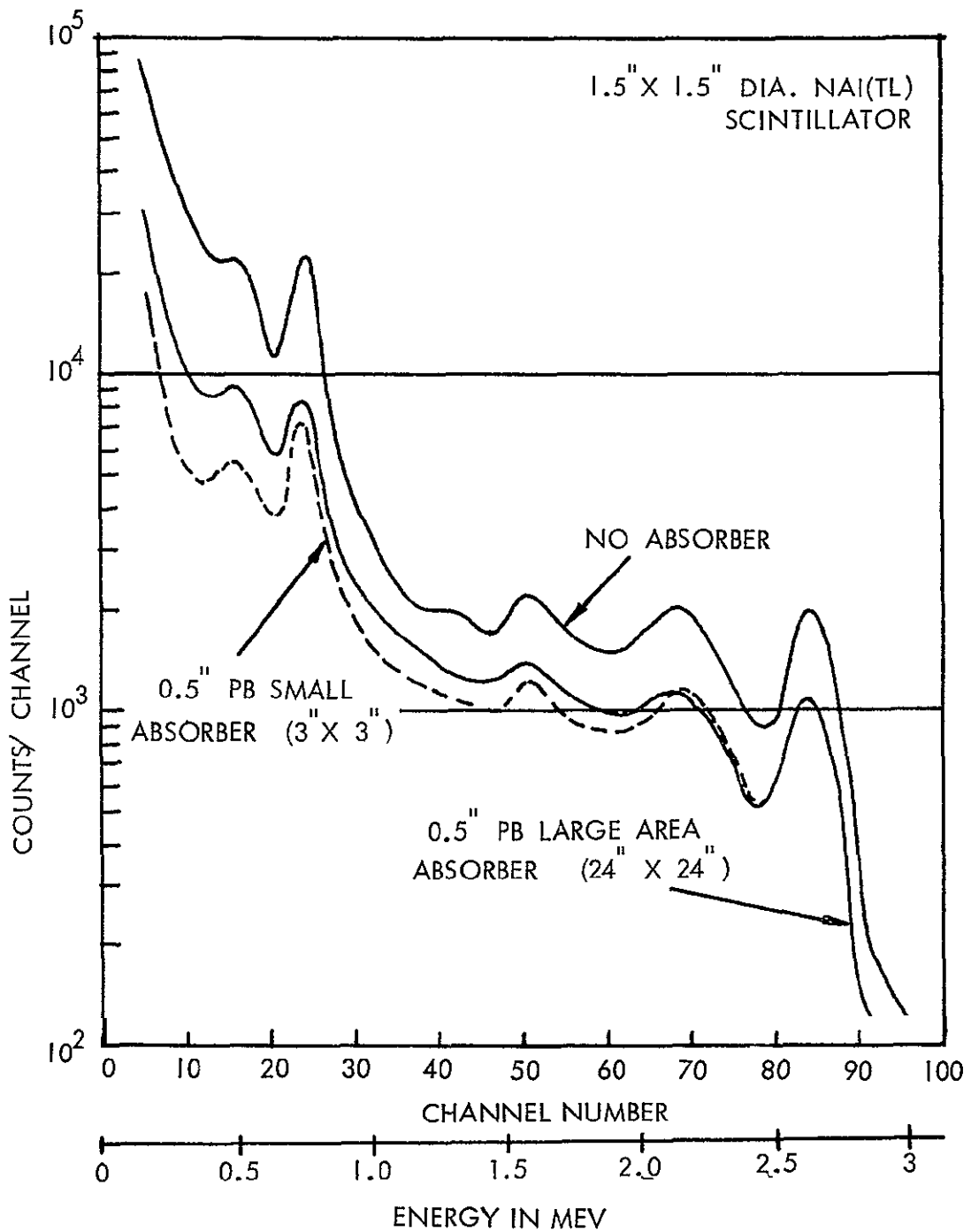
FIGURE 5.3-2   SNAP-27 HEAT SOURCE SPECTRA TAKEN WITH
SMALL & LARGE AREA ABSORBERS
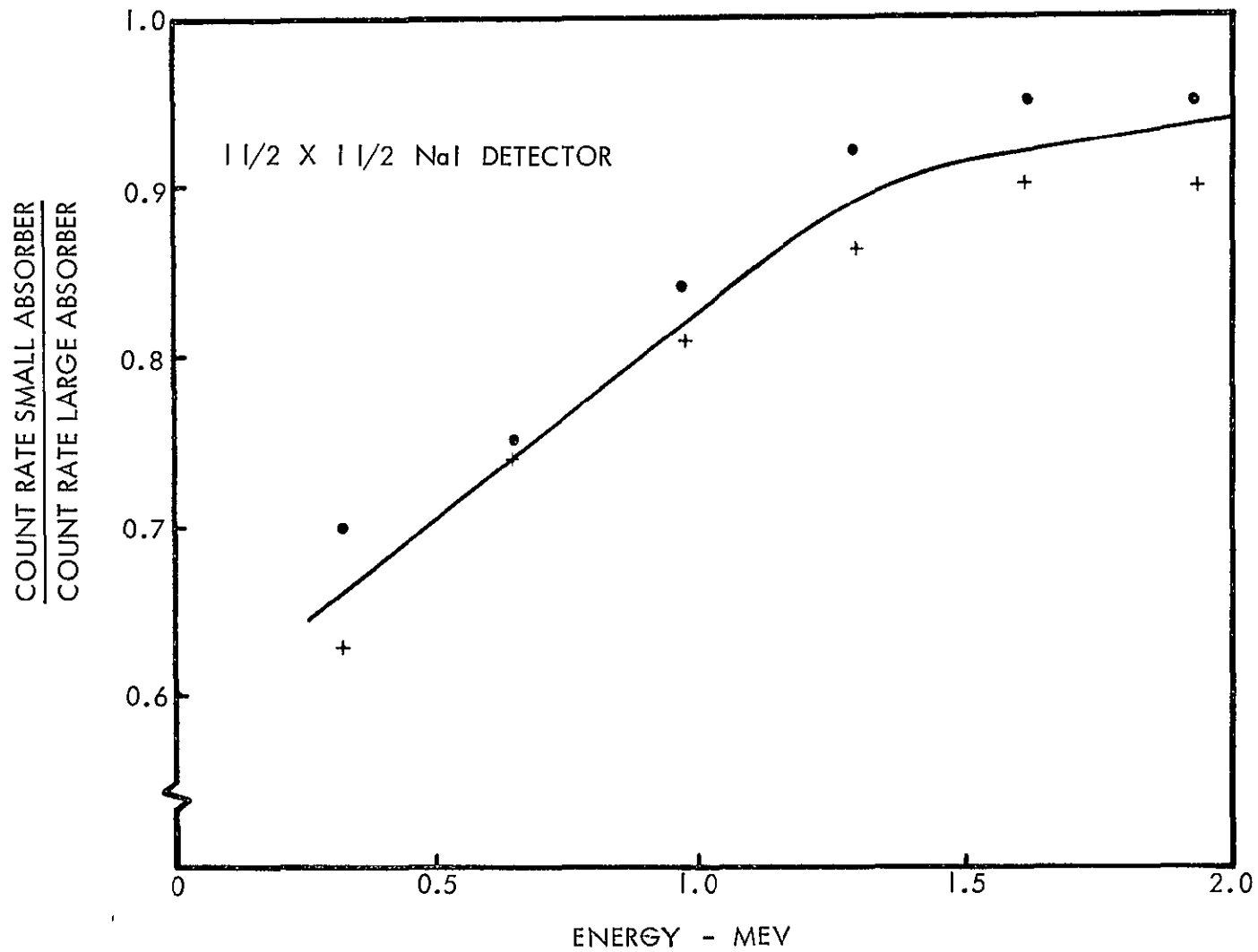
FIGURE 5.3-3 MEASURED RELATION BETWEEN ABSORPTION
OBSERVED WITH 24" x 24" ABSORBERS AND 3" x 3" SMALL ABSORBERS

coincident with the center of the fuel capsule In practice, the RTG's on a spacecraft would be oriented in such a way as to minimize the radiation level at the spacecraft instrument section However, the fuel configurations vary considerably among different RTG designs, as does the axial radiation intensity. To make the study as general as possible, the detectors were positioned broadside to the fuel capsule. This represents the worst case because self-shielding of a cylindrical-shaped fuel capsule in the direction of the long axis of the fuel element considerably reduced radiation levels.

Tests were performed to measure the SNAP-27 fuel capsule spectra as a function of detector position around the fuel capsule in the plane passing through its longitudinal axis. The test geometry used is illustrated in Figure 5.4-1. Fuel capsule spectra were taken with 1.5 x 1 5 inch and 0 03 inch thick x 1 25 dia inch NaI scintillators. The resultant spectra in the range of 0-600 kev and 0-3 Mev for various angles are illustrated in Figures 5.4-2 and 5.4-3, respectively. As can be seen from the figures, the spectra remain reasonably constant in the range θ = 0 to 60 degrees but changes markedly in shape and radiation intensity when it approaches 90 degrees. This change, as anticipated, is especially pronounced at the lower energies (0-1 Mev range) where fuel self-absorption is most significant.

Plots showing the detected number of counts as a function of angle θ between the detector and longitudinal axis of the fuel capsule, at constant distances, and for average energies of 90 kev, 200 kev, 400 kev, 1.6 Mev, and 2.55 Mev, are shown in Figures 5.4-4, 5.4-5, 5.4-6, 5.4-7, and 5.4-8, respectively.

In the range of θ from 45 to 90 degrees where the most variation in gamma flux exists, additional data were taken with a Geiger tube (EON 7302) by placing it on the low-mass aluminum flooring first directly below the fuel capsule and then moving it along the floor a few inches at a time. The data were corrected for the variation in distance for each position and are given in Figure 5.4-9.
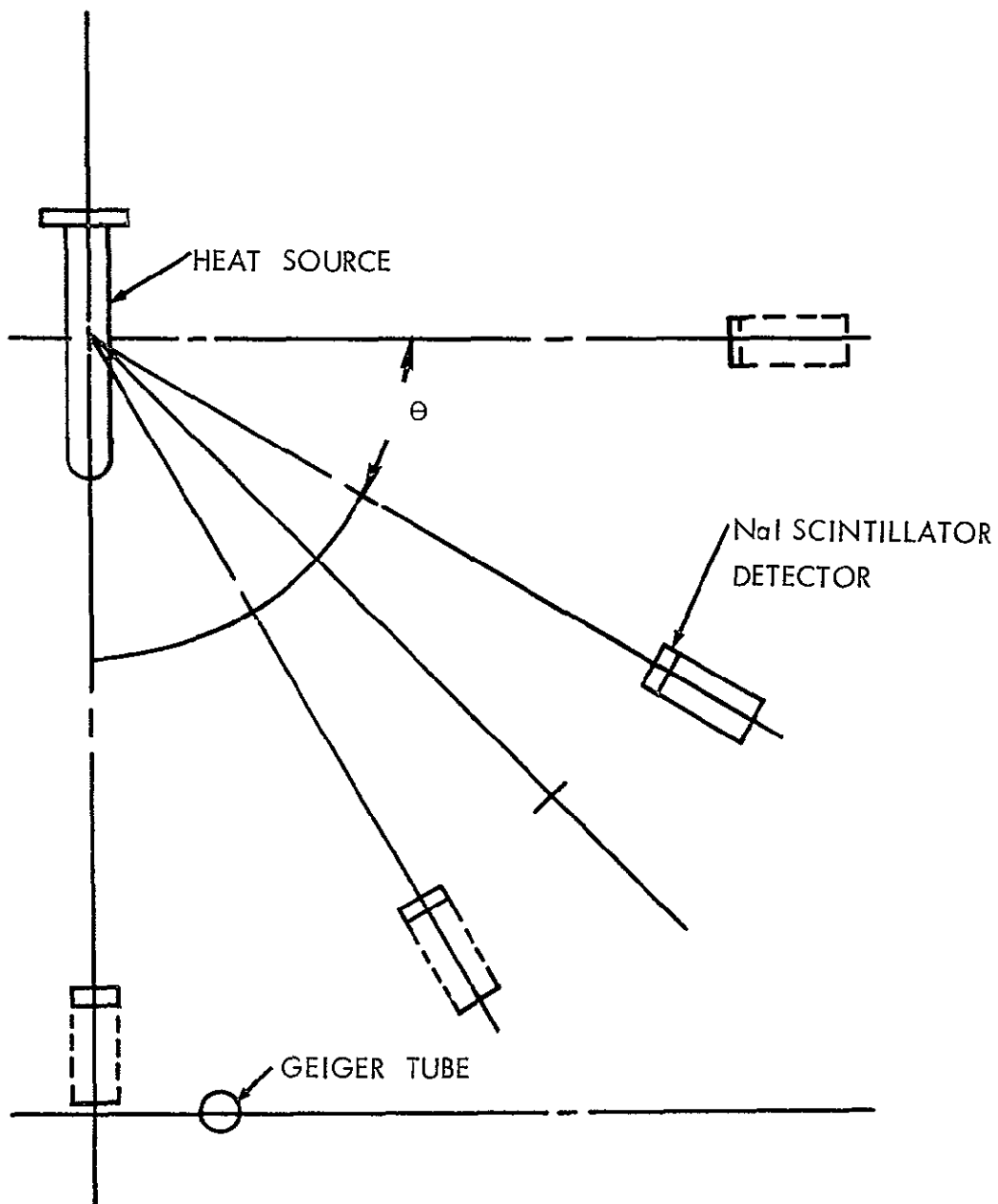
FIGURE 5.4-1 MEASUREMENTS OF SNAP-27 HEAT SOURCE RADIATION
AS A FUNCTION OF ANGULAR ORIENTATION (θ)
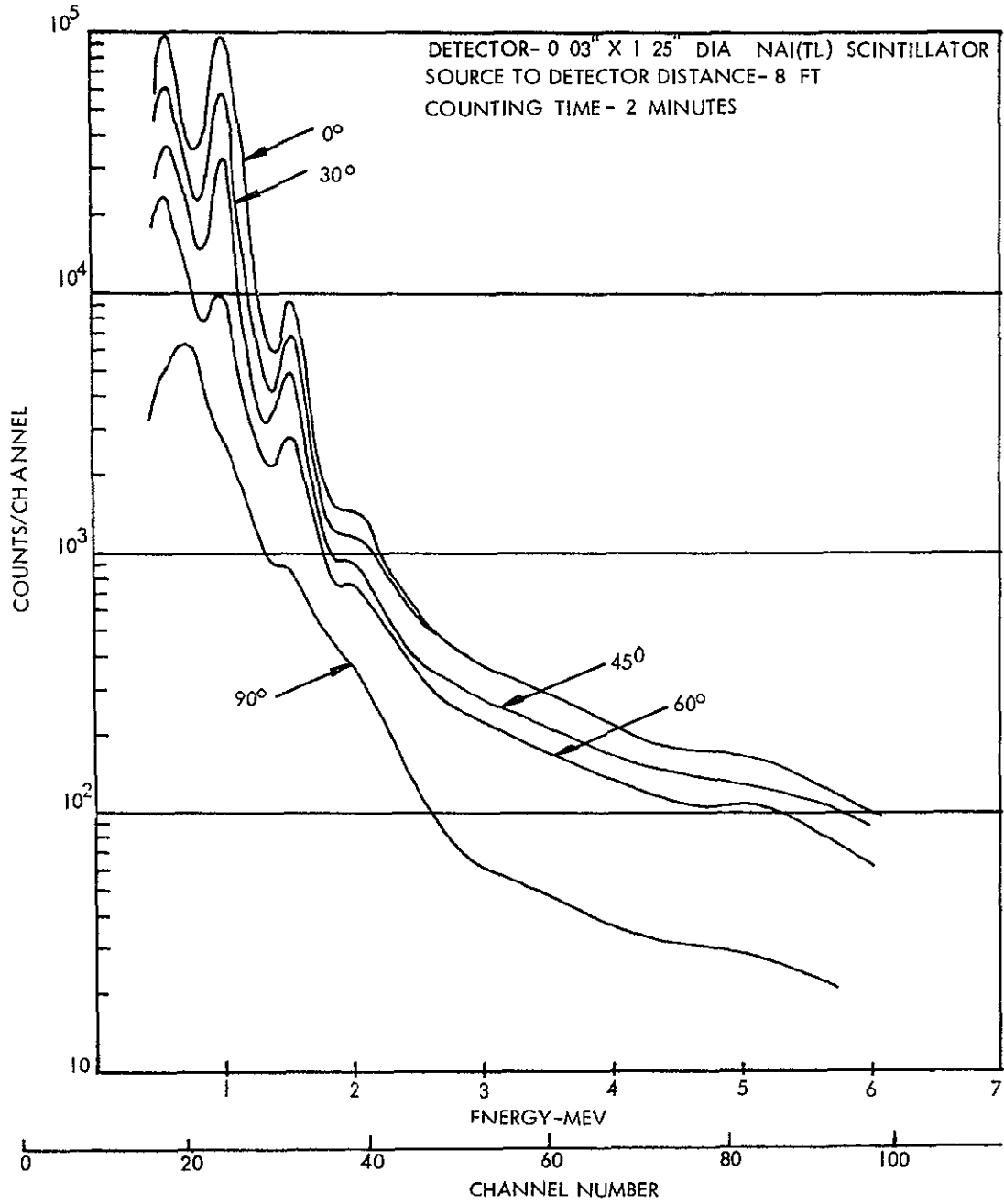
FIGURE 5.4-2 SPECTRA TAKEN AT VARIOUS ANGLES TO THE HEAT SOURCE
LONGITUDINAL AXIS

DETECTOR- 1 5" X 1.5" DIA. NAI(TL) SCINTILLATOR
COUNTING TIME- 1 MIN
SOURCE TO DETECTOR DISTANCE- 5 FEET

10⁴

10³

10²

10

1

NORMALIZED COUNT RATE

0°
45°
60°
90°

0   20   40   60   80   100
CHANNEL NUMBER

0   1 0   2 0   3 0
ENERGY- MEV
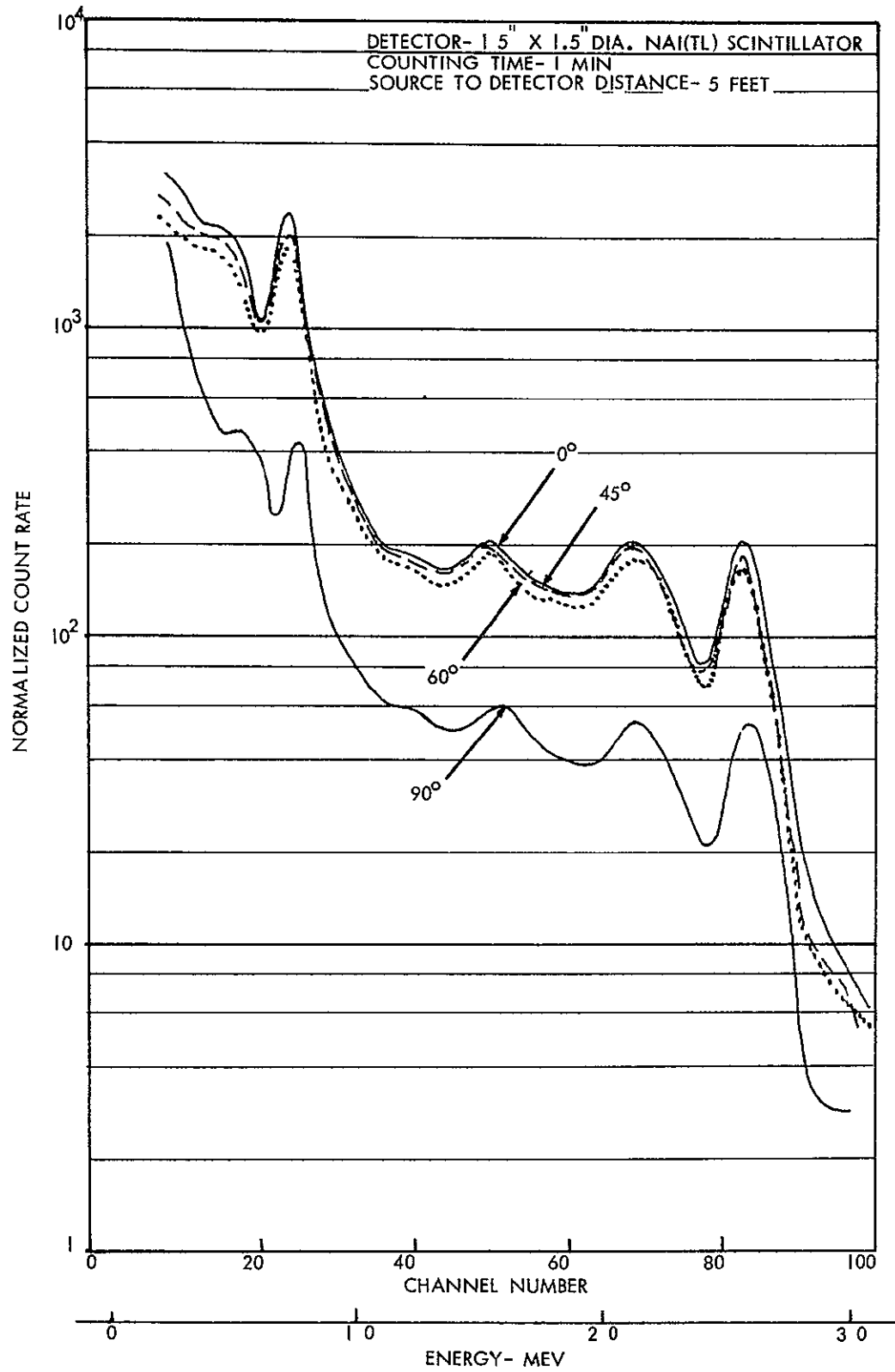
FIGURE 5.4-3   SPECTRA TAKEN AT VARIOUS ANGLES TO HEAT
SOURCE LONGITUDINAL AXIS

5-14
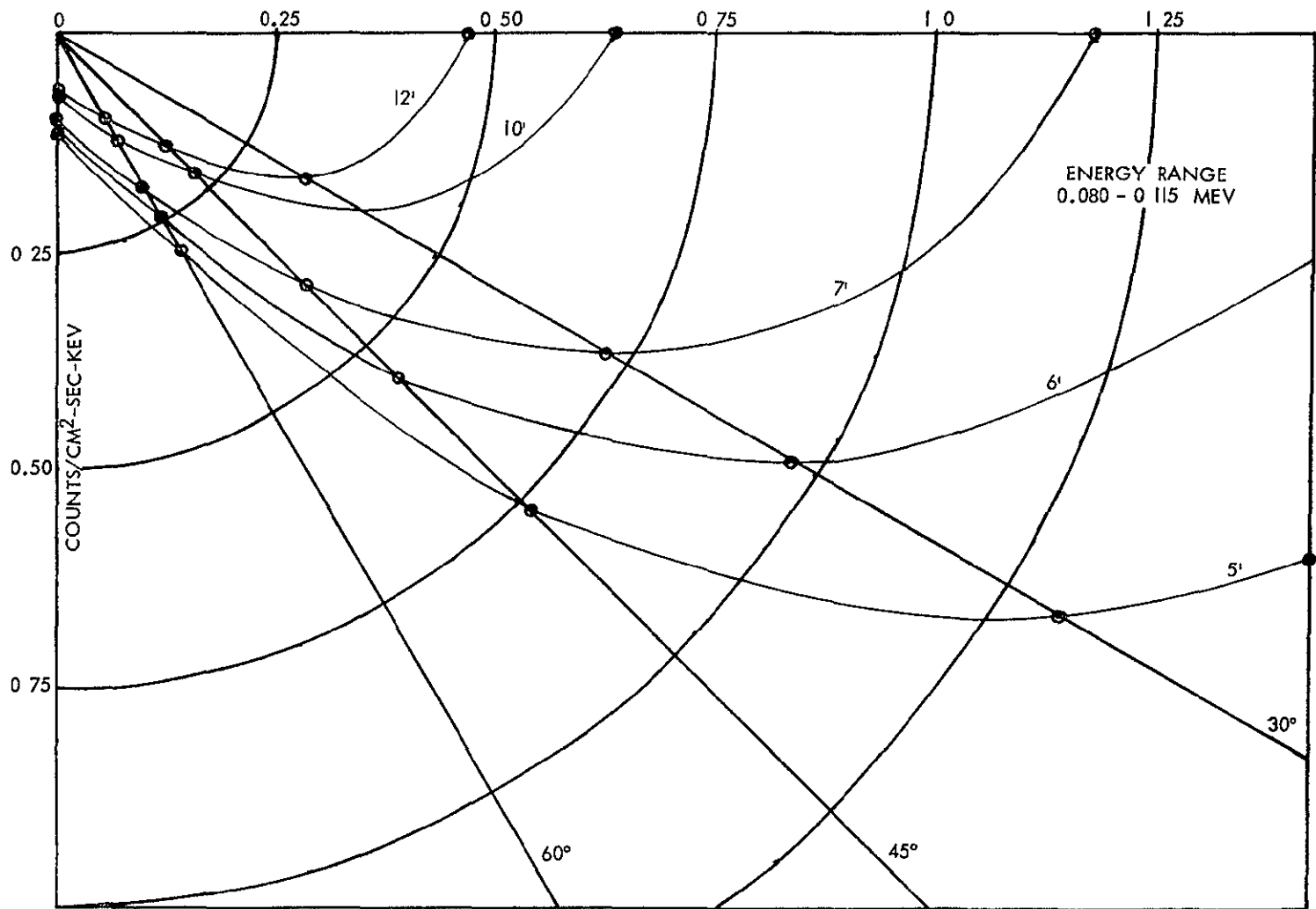
FIGURE 5.4-4 POLAR PLOT OF SNAP-27 FUEL CAPSULE RADIATION FLUX
AT CONSTANT DISTANCES IN THE ENERGY RANGE OF .080 to 115 Mev
0.030" THICK X 1.25" DIA NaI DETECTOR
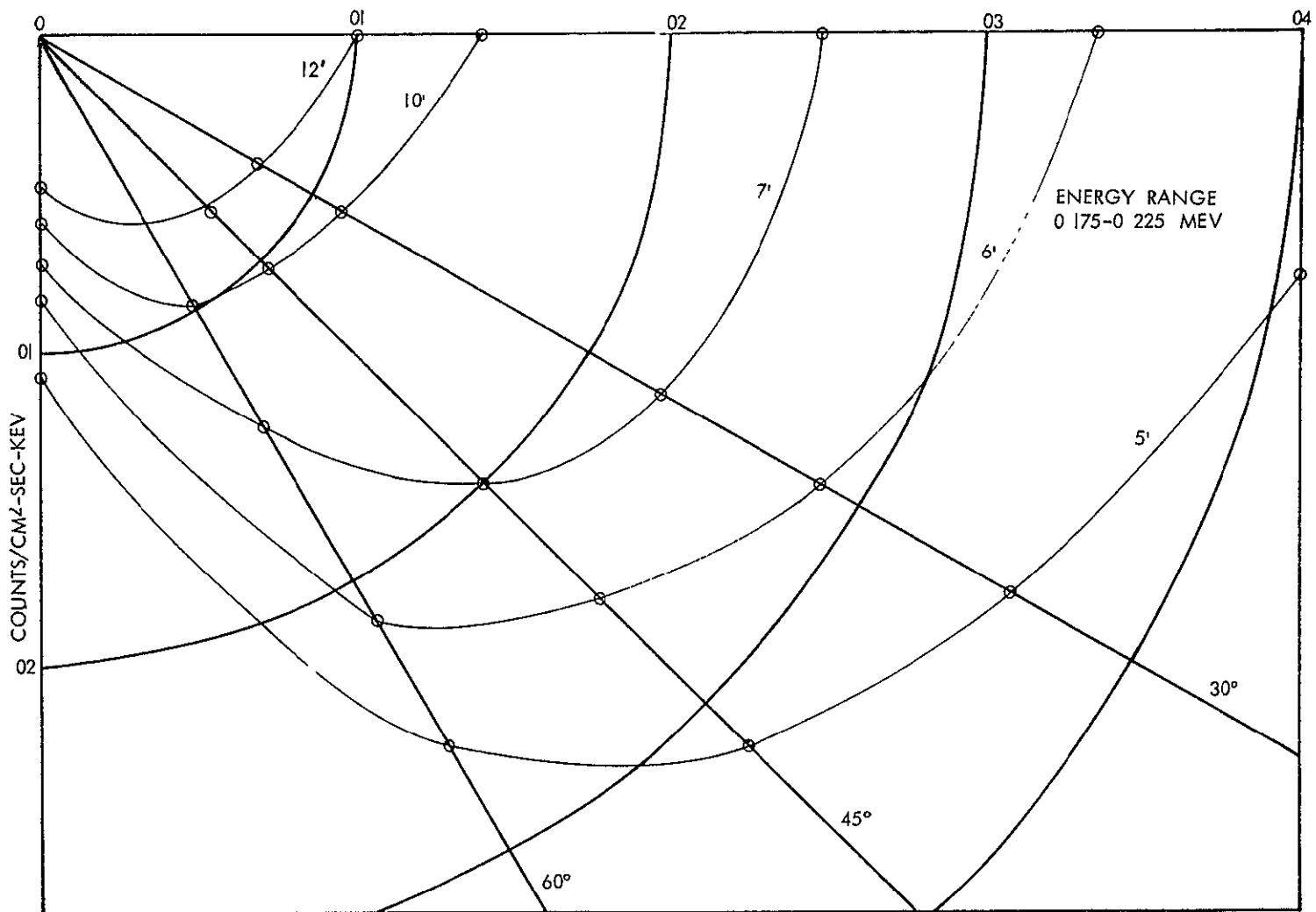
FIGURE 5 4-5   POLAR PLOT OF SNAP-27 FUEL CAPSULE RADIATION FLUX
AT CONSTANT DISTANCES IN THE ENERGY RANGE OF .175 TO .225 Mev
1.5" THICK X 1.5" DIA NaI DETECTOR
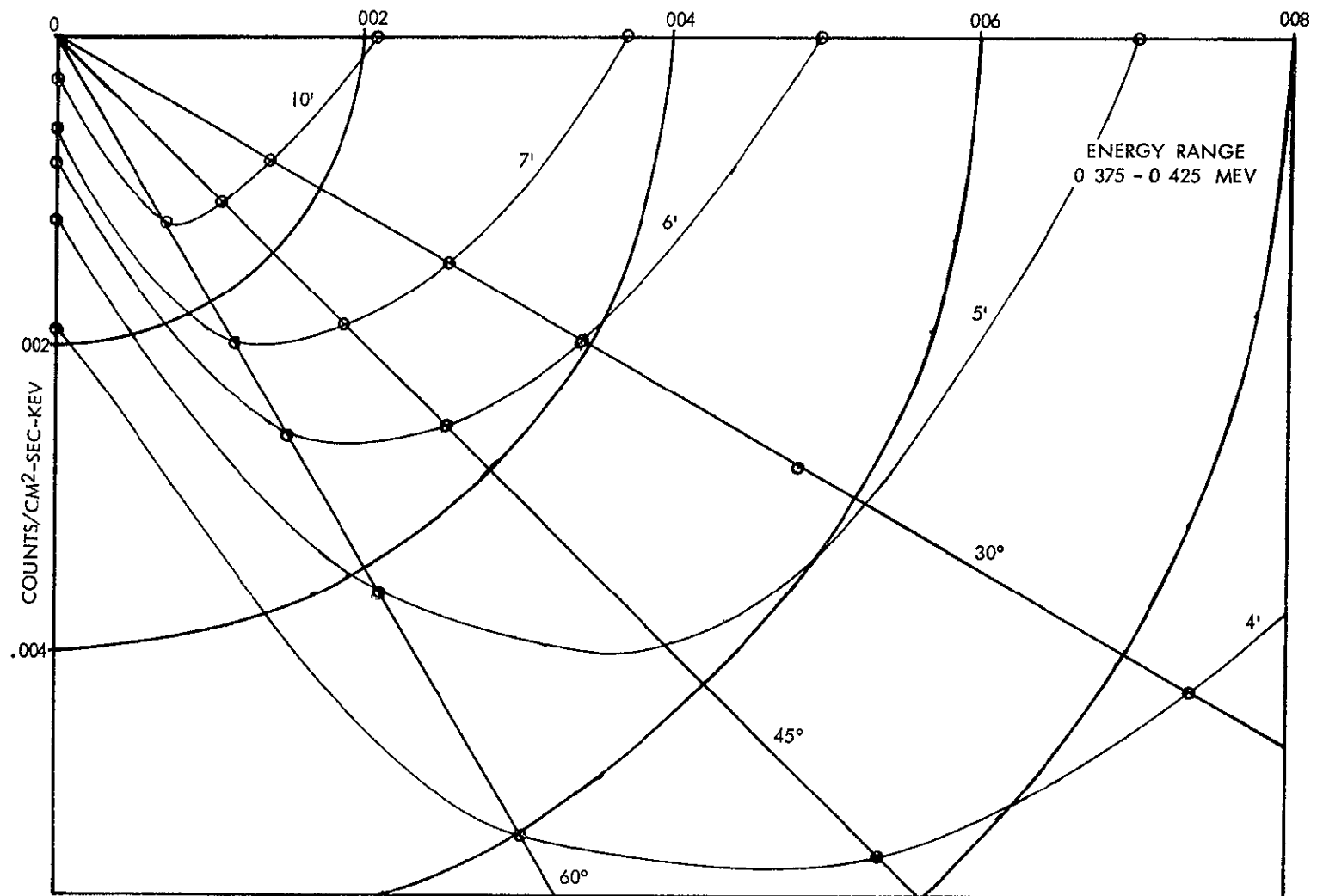
FIGURE 5.4-6 POLAR PLOT OF SNAP-27 FUEL CAPSULE RADIATION FLUX
AT CONSTANT DISTANCES IN THE ENERGY RANGE OF .375 TO .425 Mev
1.5" THICK X 1.5" DIA NaI DETECTOR
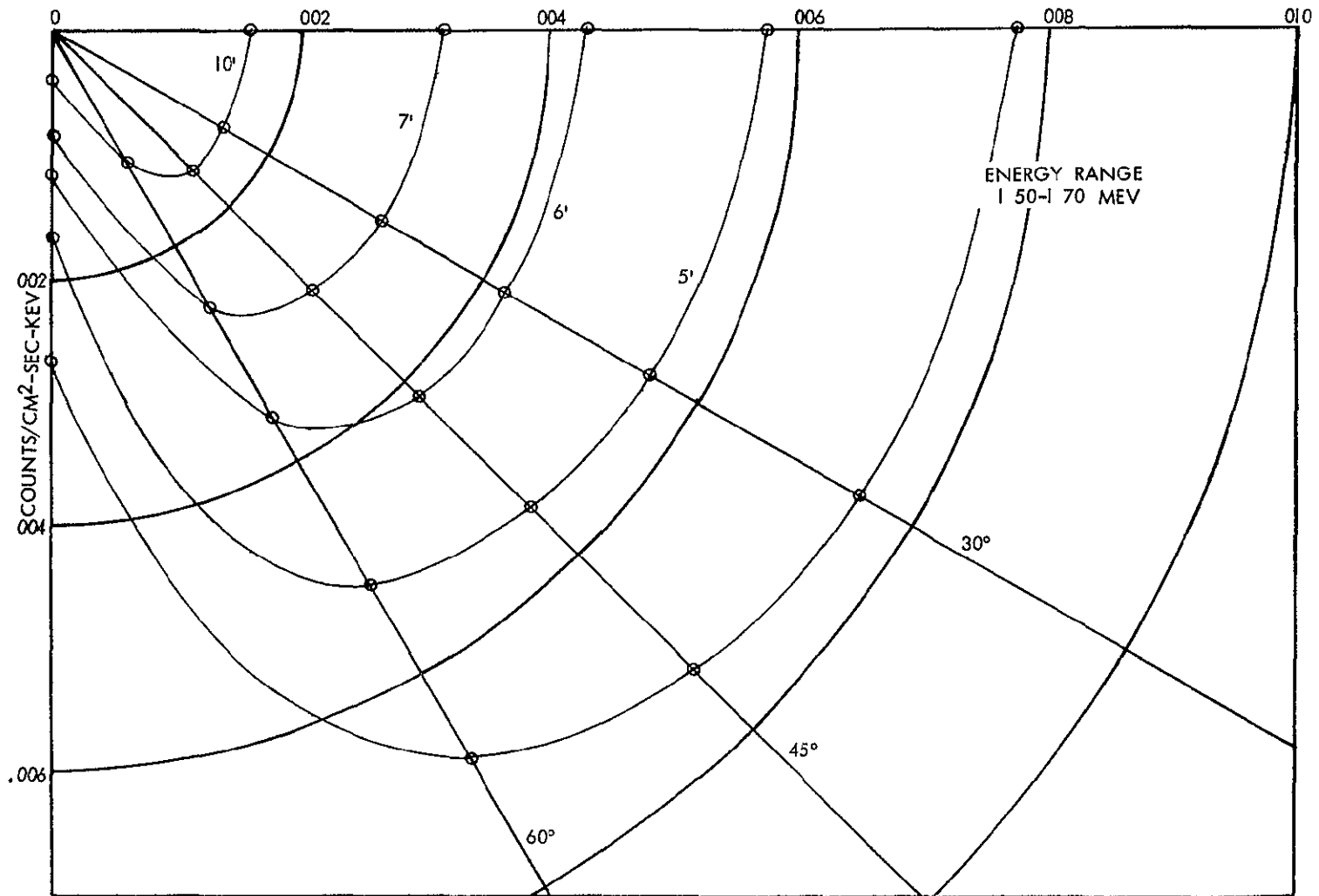
FIGURE 5.4-7   POLAR PLOT OF SNAP-27 FUEL CAPSULE RADIATION FLUX
AT CONSTANT DISTANCES IN THE ENERGY RANGE OF 1.50 TO 1.70 Mev
1.5" THICK X 1.5" DIA NaI DETECTOR
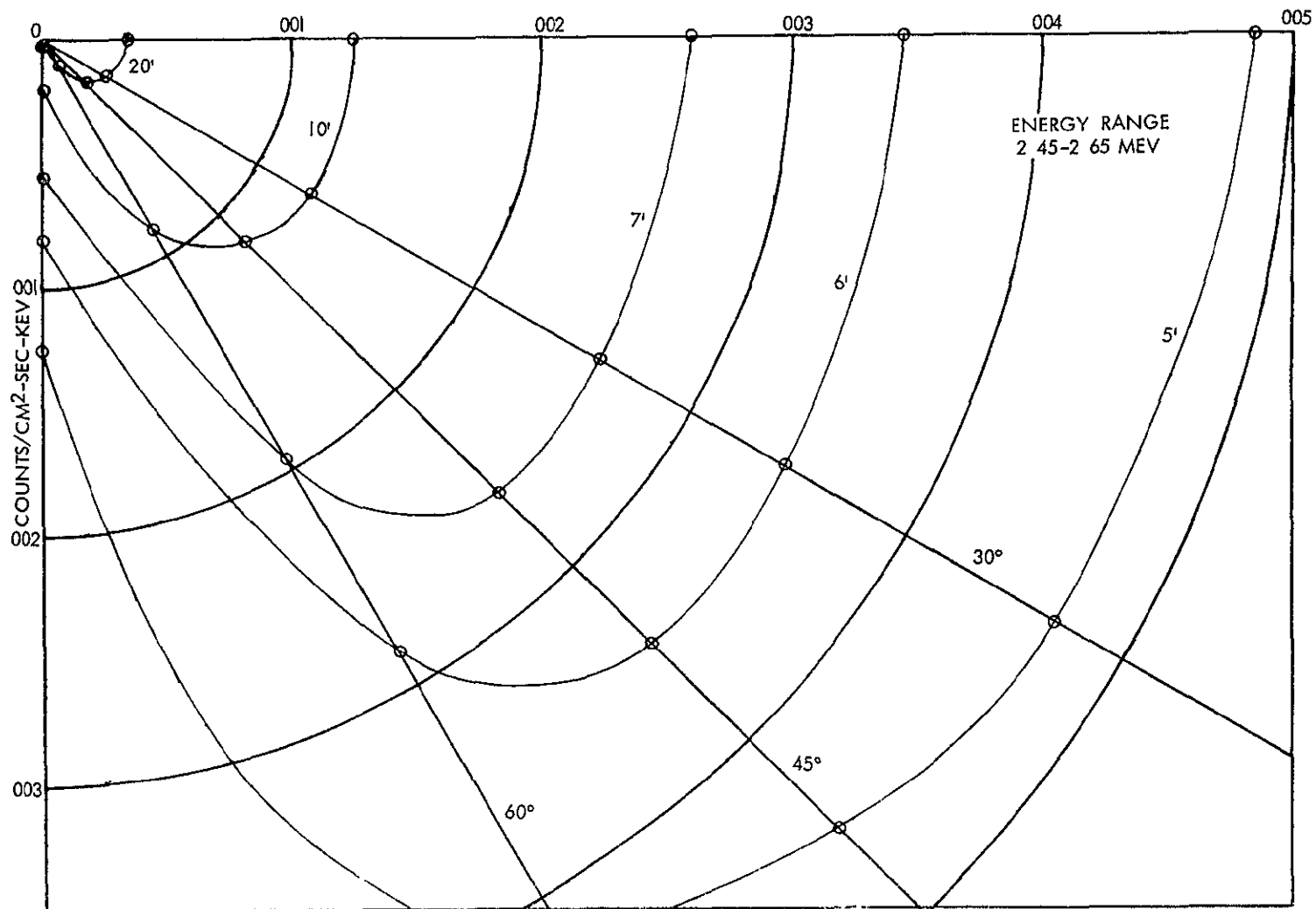
FIGURE 5.4-8   POLAR PLOT OF SNAP-27 FUEL CAPSULE RADIATION FLUX
AT CONSTANT DISTANCES IN THE ENERGY RANGE OF 2.45 TO 2.65 Mev
1.5" THICK X 1 5" DIA NaI DETECTOR
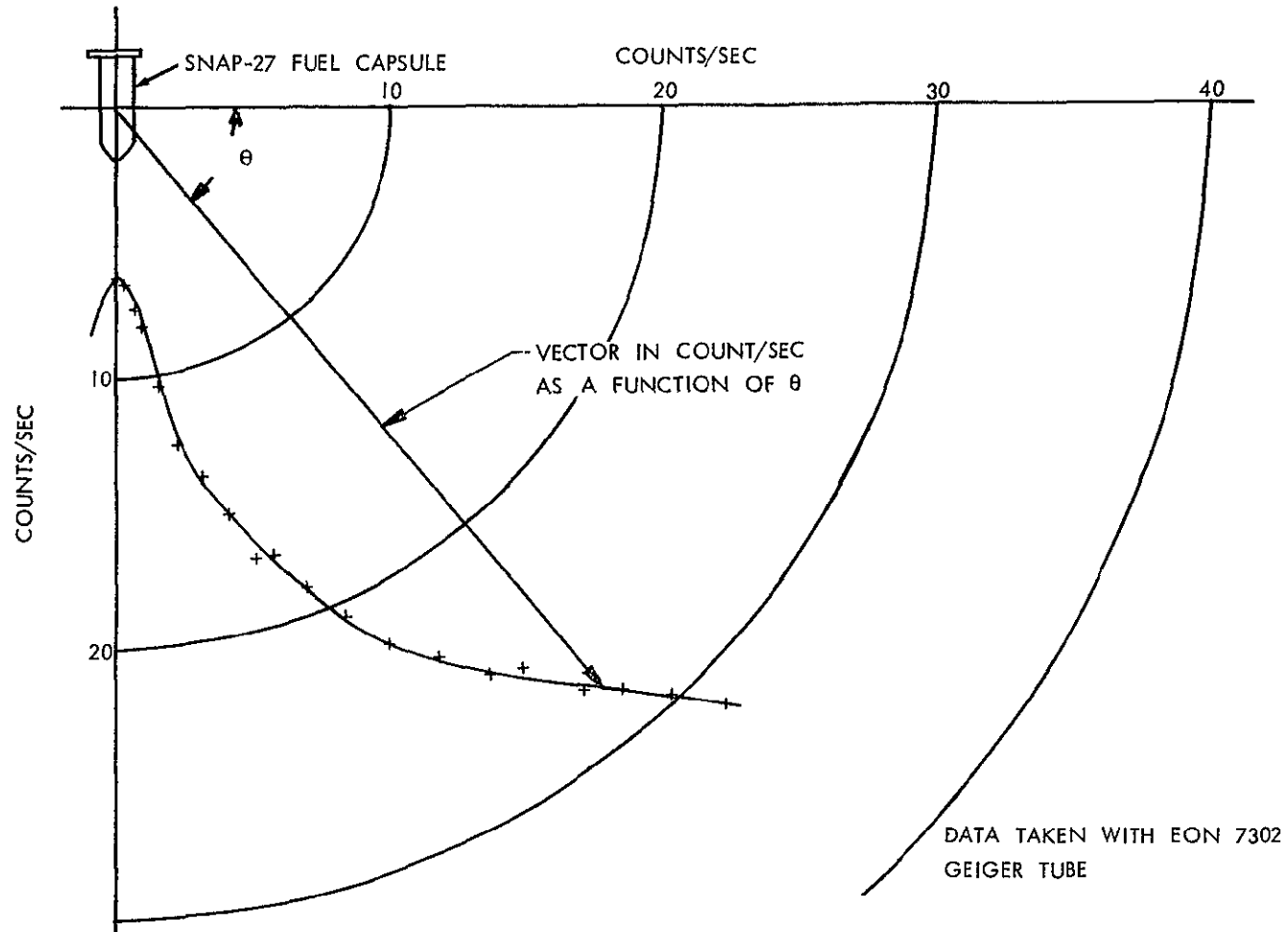
FIGURE 5.4-9   POLAR PLOT OF COUNT RATE VARIATION AROUND
THE SNAP-27 FCA

5.5 Semiconductor Detectors

Four silicon semiconductor detectors were selected for testing with the fuel capsule radiation. These detectors were as follows:

o KEVEX totally-depleted lithium-drift type C80-1/2, 0.5 mm thick, 0.8 cm^2 area, 13 kev FWHM resolution for beta particles.

o Nuclear Diodes totally depleted surface barrier detector mounted in a dE/dX mount, type MRde-200-100-25, 200 microns thick, 1 cm^2 area, 24 kev FWHM resolution for alpha particles.

o Nuclear Diodes totally-depleted surface barrier detector mounted in a dE/dX mount, type MRde-50-100-40, 0.053 micron thick, 1 cm^2 area, 35 kev FWHM resolution for alpha particles.

Also included in the tests were two semiconductor detectors that belonged to NASA/Goddard Space Flight Center and were of the type to be used in a Cosmic Ray Detector System in the Pioneer F&G spacecraft. These detectors were:

o 5 cm^2 area, 3 mm thick totally depleted lithium drift detector (manufactured by KEVEX).

o 0.25 cm^2 area, 50 mm thick surface barrier detector (manufactured by ORTEC).

The detectors were operated with a Tennelec TC-130 preamplifier and Tennelec TC-200 amplifier. Signal integration and differentiation time constants of 0.8 microseconds were used during all the tests. The Tennelec TC-200 amplifier output was connected directly to a pulse height analyzer.

The spectral response of these detectors to the SNAP-27 fuel capsule in units of counts/sec-cm^2-kev are given for the energy ranges of 0-1 Mev and 0-5 Mev in Figures 5.5-1 and 5.5-2, respectively.
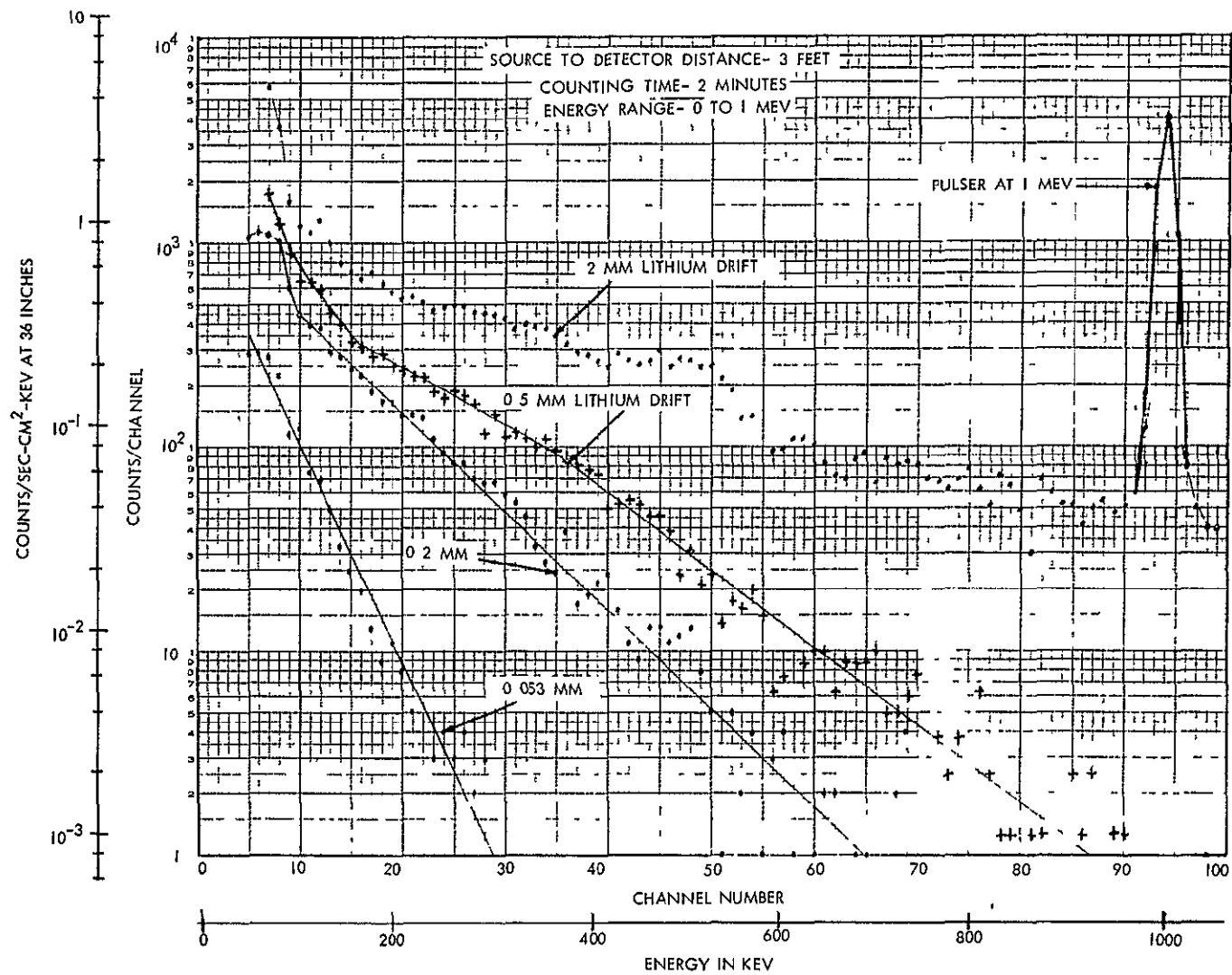
FIGURE 5.5-1   RESPONSE OF SEMICONDUCTOR DETECTORS TO SNAP-27 FUEL CAPSULE RADIATION
ENERGY RANGE 0 TO 1 Mev
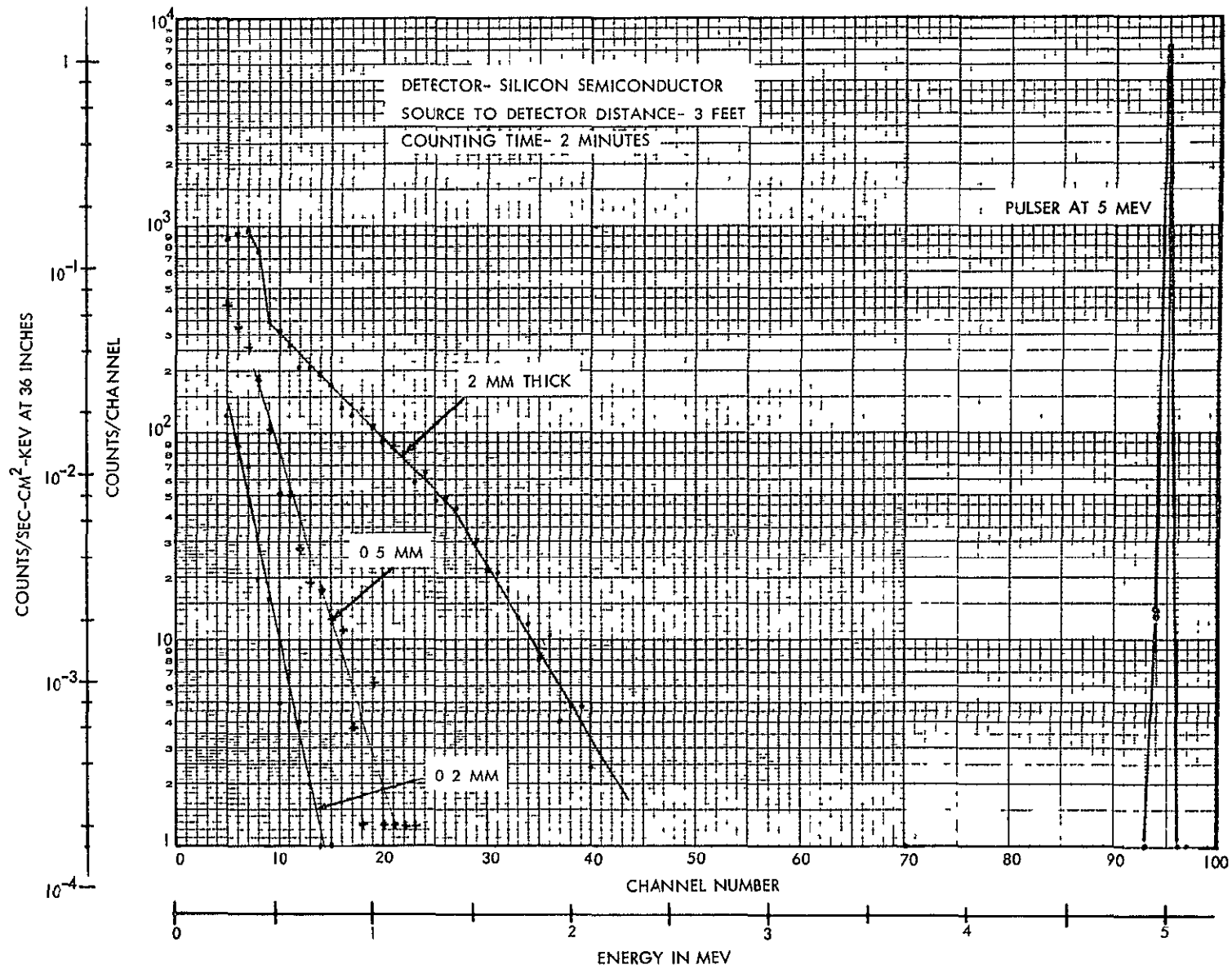
FIGURE 5.5-2   RESPONSE OF SEMICONDUCTOR DETECTORS TO SNAP-27 FUEL CAPSULE RADIATION
ENERGY RANGE 0 TO 5 Mev

Data obtained with the 5 cm^2 area, 3 mm thick NASA/Goodard detector are given in Figures 5.5-3 and 5.5-4 for energy ranges 0 to 5 Mev and 0-10 Mev, respectively.

Spectra showing the effects of several absorber materials are given in Figure 5.5-5.

Absorption plots obtained with the 2 mm thick detector with lead, aluminum and polyethylene absorbers are given in Figure 5.5-6.

Figure 5.5-7 shows the detector response as a function of detector orientation in relation to the fuel capsule.

5.6   CsI Scintillator

Four CsI scintillators were selected for testing with the SNAP-27 fuel capsule. These scintillators were as follows:

o   Harshaw detector type 6S8-X, 1.5" dia x 1.5" thick CsI (Na). This is an integrally mounted scintillator and photomultiplier assembly designed for general lab use.

o   Harshaw 1 cm thick x 1.5 inch dia.

o   Harshaw 3 mm thick x 1.5 inch dia.

o   Harshaw 1 mm thick x 1.5 inch dia.

The 1 cm, 3mm, and 1 mm thick crystals were mounted in Harshaw type H mounts with a 0.001" thick aluminum front window and were operated with RCA 6199 photomultiplier tubes. The scintillators were coupled to the multiplier tubes using silicon grease. The tube bases were of standard Harshaw manufacture which use 470K ohm resistors for the dynode string with .001 µf capacitors for pulse shaping between dynodes 9 and 10 and the anode.

The PM tube output was connected to a Harshaw NA11 RC clipped amplifier and the amplifier was connected directly to a pulse height analyzer. High voltage power for the photomultiplier tubes was provided by Fluke 408A or Fluke 412A d.c. power supplies.
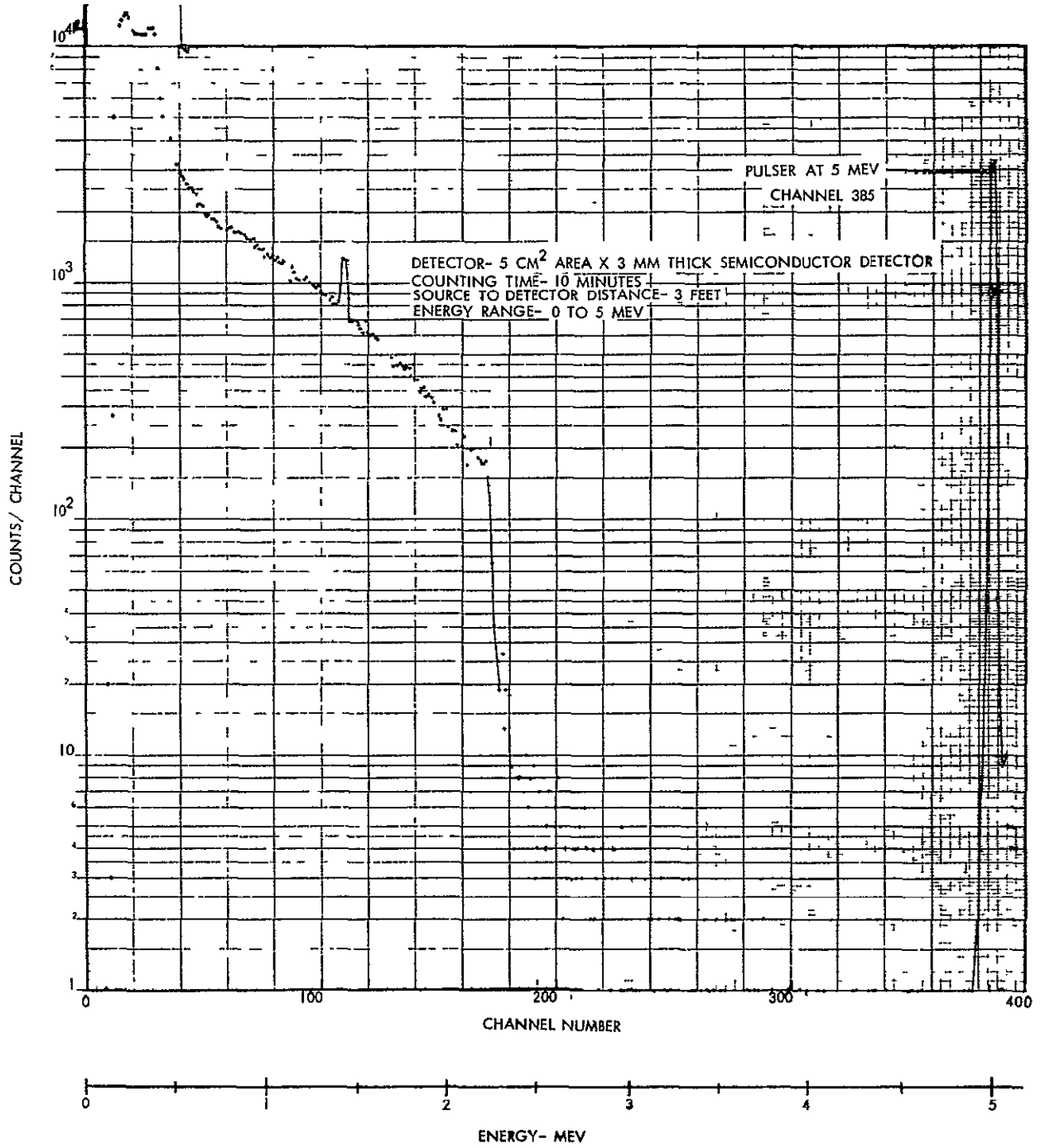
FIGURE 5.5-3   SNAP-27 HEAT SOURCE SPECTRA TAKEN WITH 5cm^2 AREA
x 3mm THICK SEMICONDUCTOR RADIATION DETECTOR
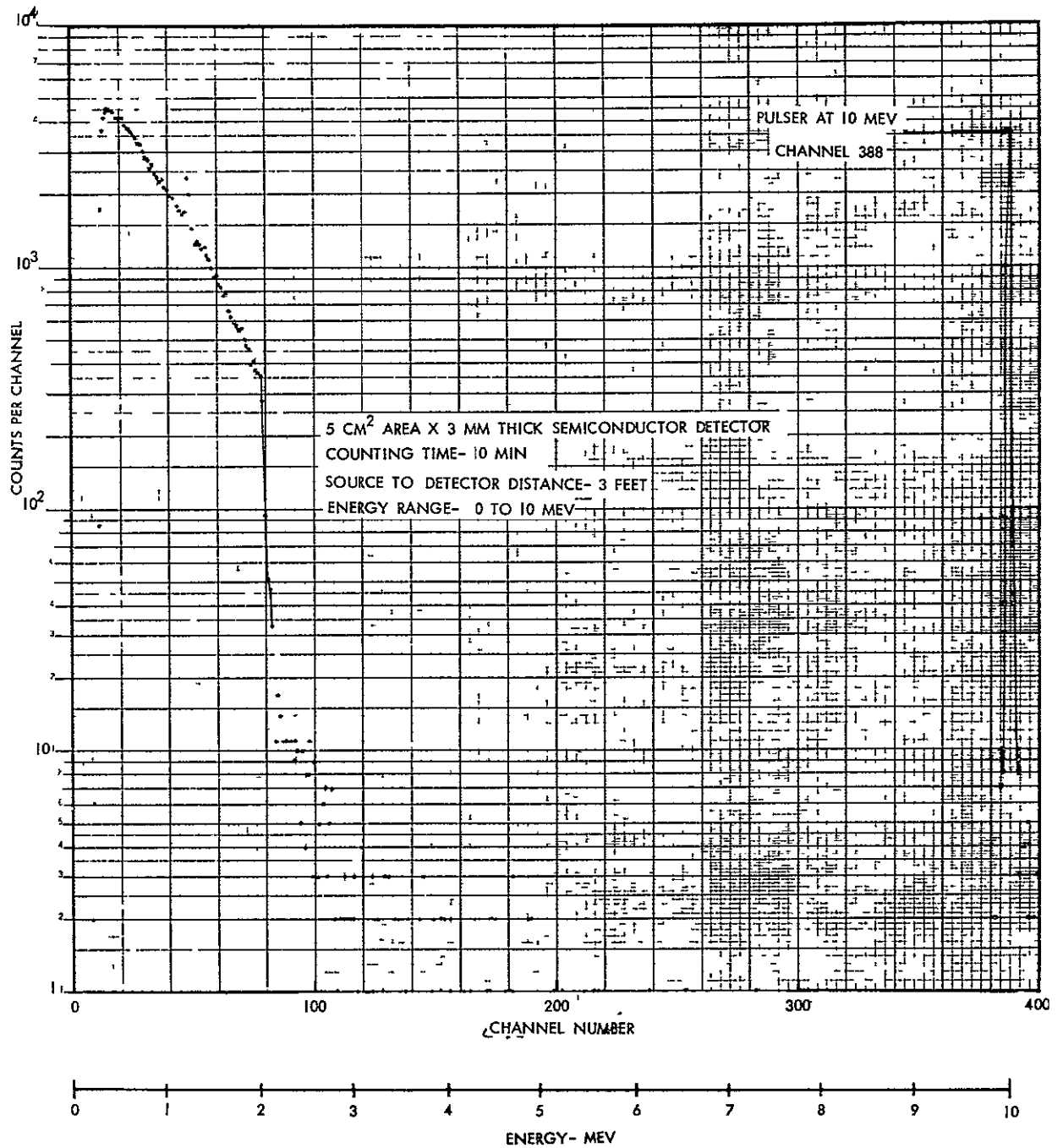
FIGURE 5.5-4 SNAP-27 HEAT SOURCE SPECTRA TAKEN WITH 5cm² AREA
x 3mm THICK SEMICONDUCTOR RADIATION DETECTOR
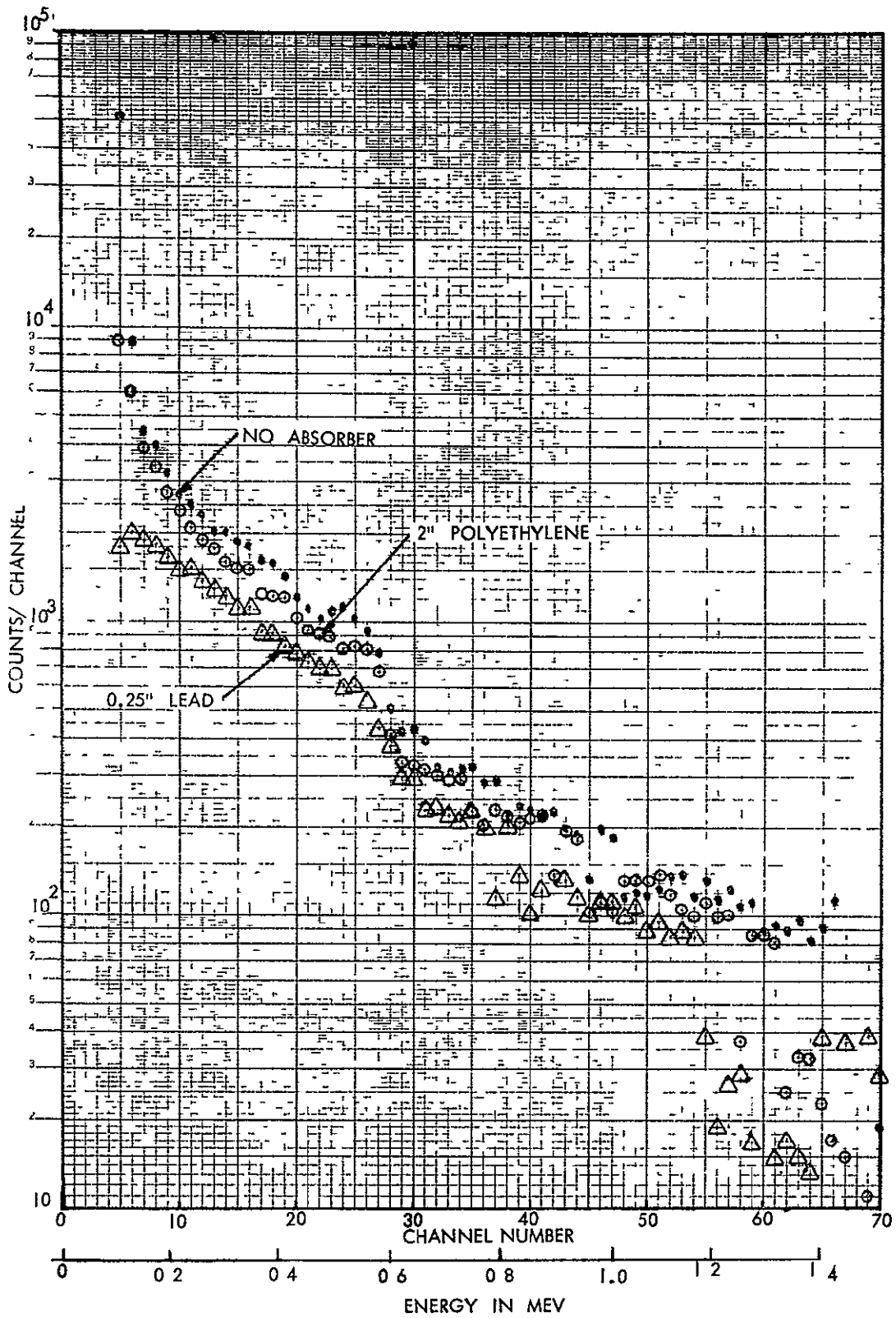
FIGURE 5.5-5   EFFECTS ON ABSORBERS ON
SEMICONDUCTOR DETECTOR SPECTRAL RESPONSE
TO SNAP-27 FUEL CAPSULE RADIATION
2 mm THICK X .8 cm^2 AREA
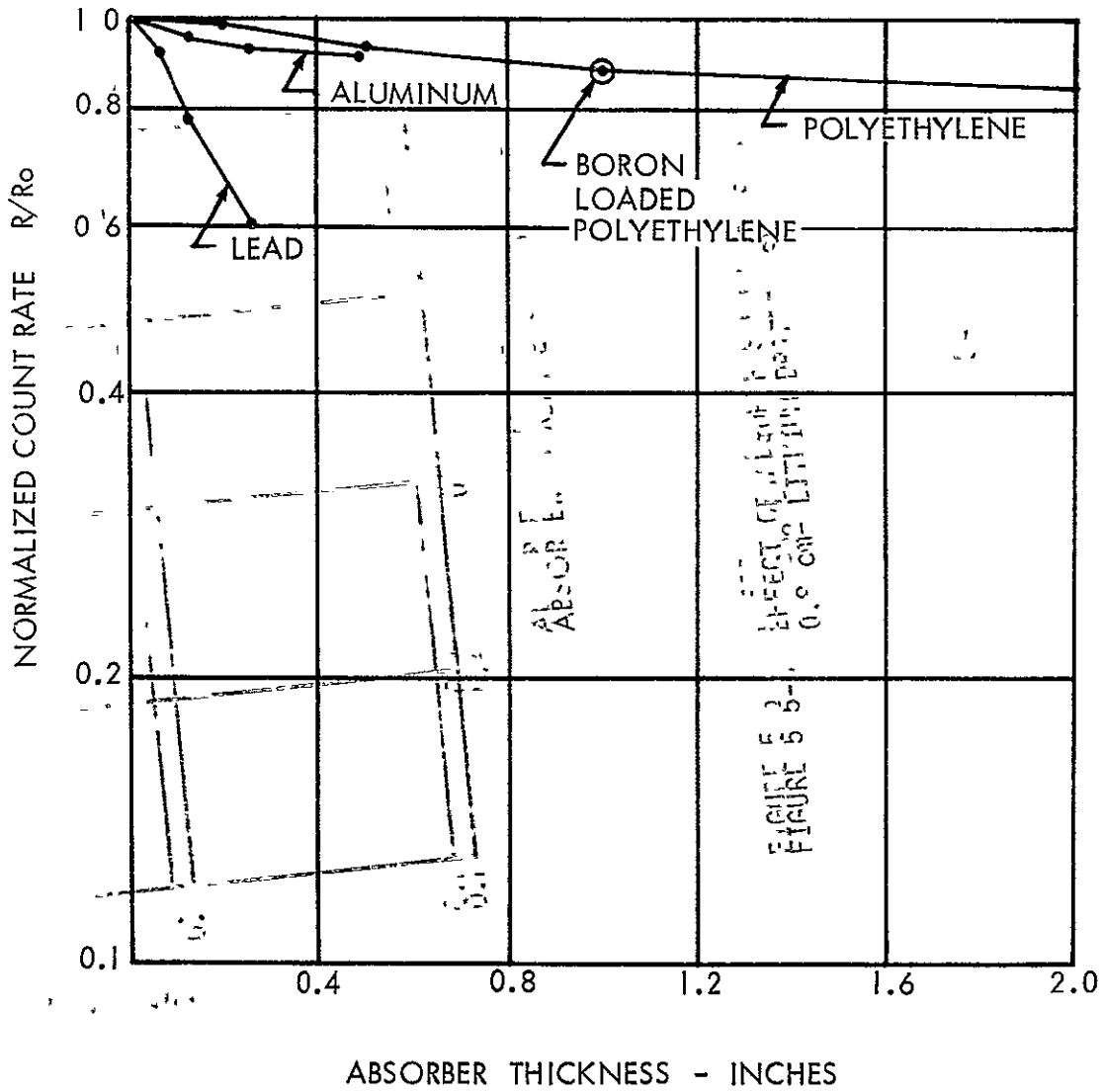
FIGURE 5.5-6   EFFECT OF ABSORBERS ON COUNTS DETECTED BY A 2 mm X
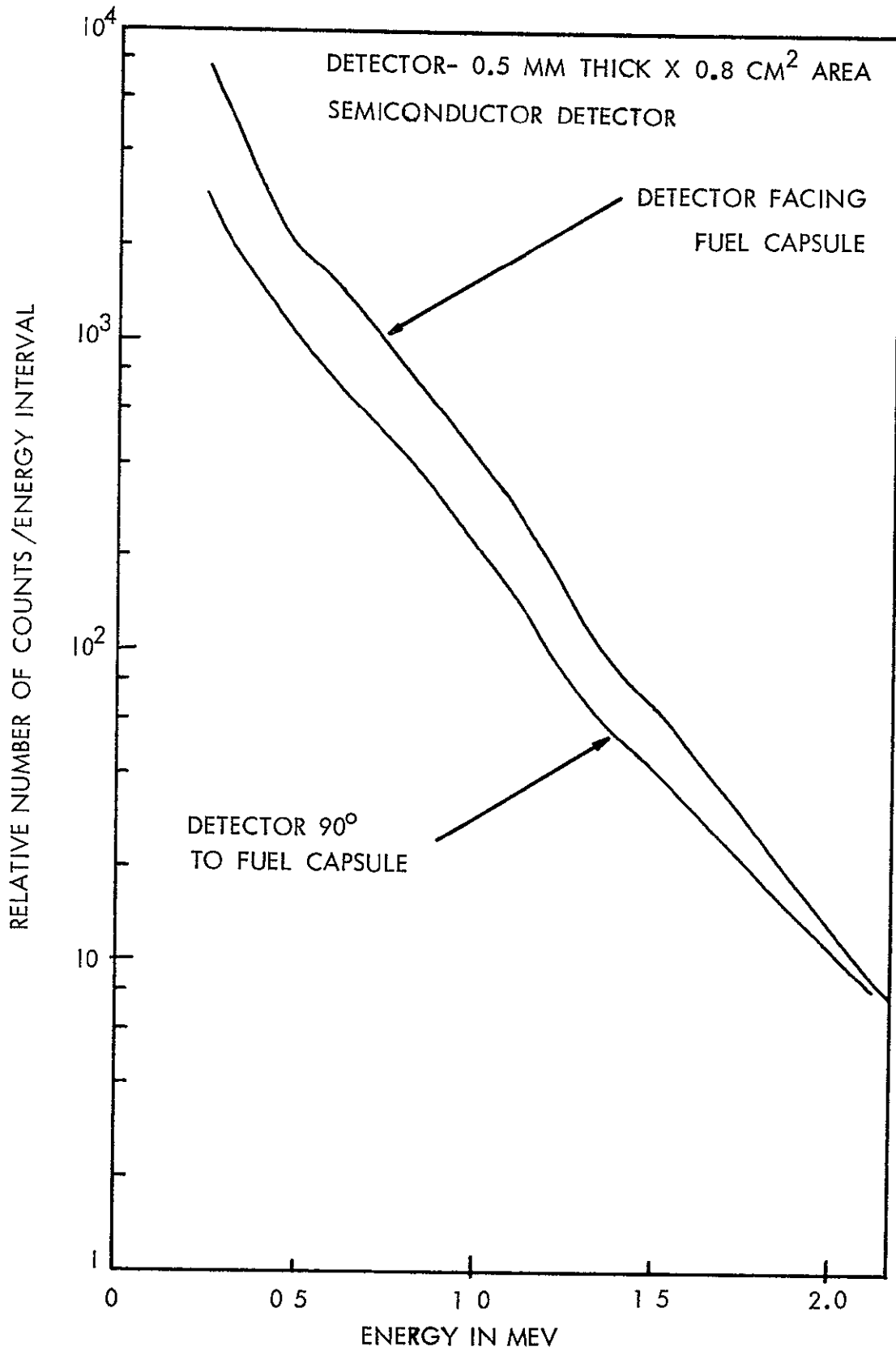0.8 cm^2 LITHIUM DRIFTED SEMICONDUCTOR DETECTOR

FIGURE 5 5-7   SEMICONDUCTOR DETECTOR RESPONSE AS A FUNCTION OF DETECTOR
ORIENTATION IN RESPECT TO THE FUEL CAPSULE

The SNAP-27 fuel capsule spectra obtained with CsI scintillators of four thicknesses are shown in Figure 5.6-1.

Spectra showing the effect of several absorbers are illustrated in Figure 5.6-2.

The effect of detector orientation in relation to the heat source for a 3 mm thick detector is given in Figure 5.6-3.

5.7   Plastic Scintillators

Four plastic scintillators, 1.5 inch diameter and 3 cm, 1 cm, 3 mm, and 1 mm thick, were selected for tests with the SNAP-27 fuel capsule. The scintillators were machined from 2"-diameter Pilot B (Pilot Chemicals Division, New England Nuclear Corporation, Watertown, Massachusetts) scintillator stock, polished by hand to have glossy surfaces, and coupled to RCA 6199 photomultiplier tube using silicon grease. The photomultiplier tube scintillator assembly was attached to Harshaw 1-1/2 inch tube bases, and the entire assembly covered with a thin (~.005") and light-tight stainless steel case. The photomultiplier tube output was connected to a Harshaw NA-11 amplifier, and the amplifier output was connected to a pulse height analyzer. Power for the photomultiplier tubes was provided by Fluke Model 408A d.c. power supply.

The plastic scintillator spectral response to the SNAP-27 fuel capsule radiation is shown in Figures 5.7-1 and 5.7-2 for two energy ranges

Since it was difficult to obtain energy calibration for the thin scintillators (1 and 3 mm thick) due to their very poor energy resolution, the energy calibration was performed using Co^{60} and Cs^{137} sources on the 3 mm thick detector only. Tests on other size detectors to obtain Figures 5.7-1 and 5.7-2 were performed using the same photomultiplier tube, amplifiers, and other electronics, being careful not to disturb the photomultiplier tube orientation when scintillators were changed.
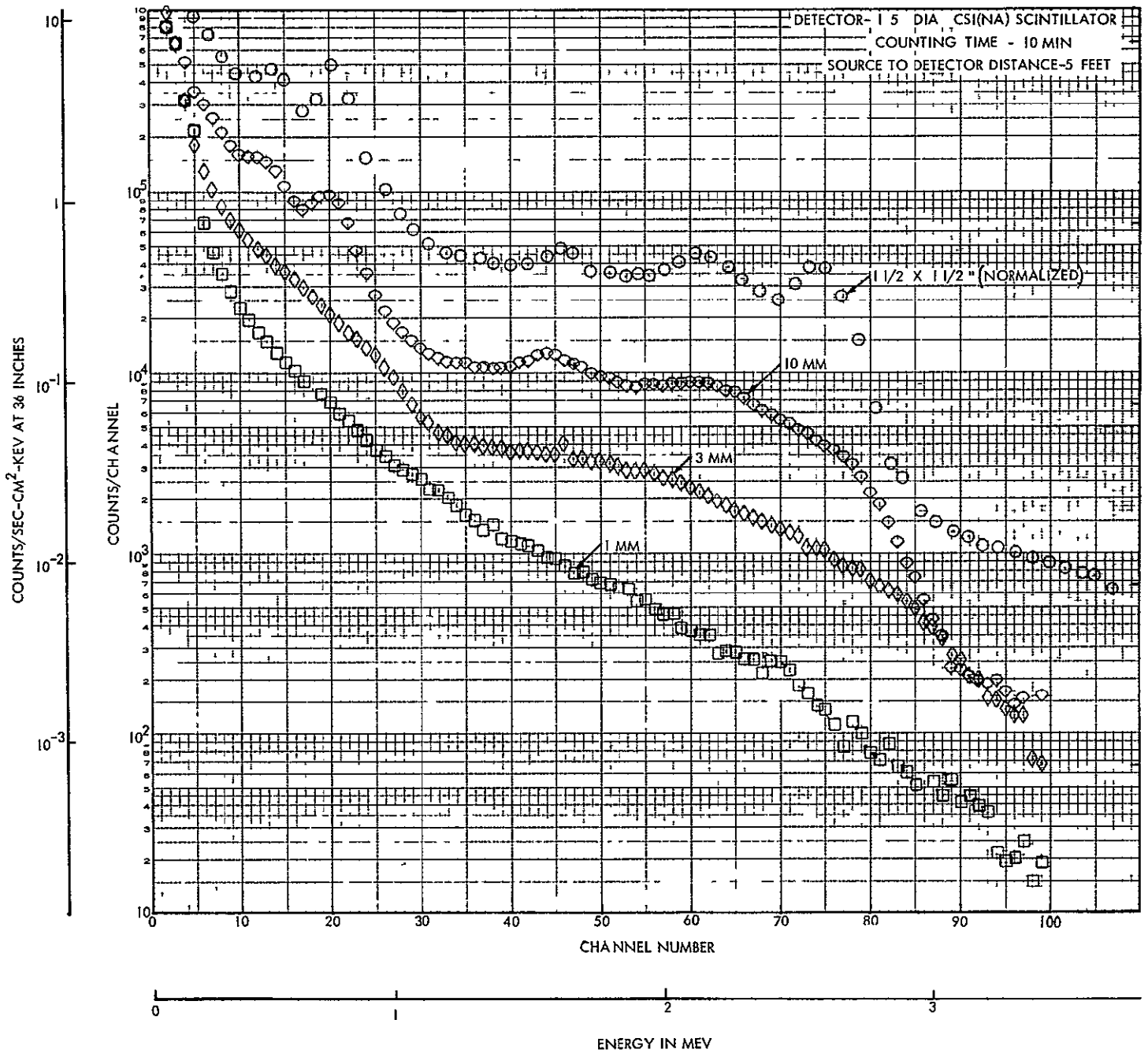
FIGURE 5.6-1   RESPONSE OF CsI DETECTORS
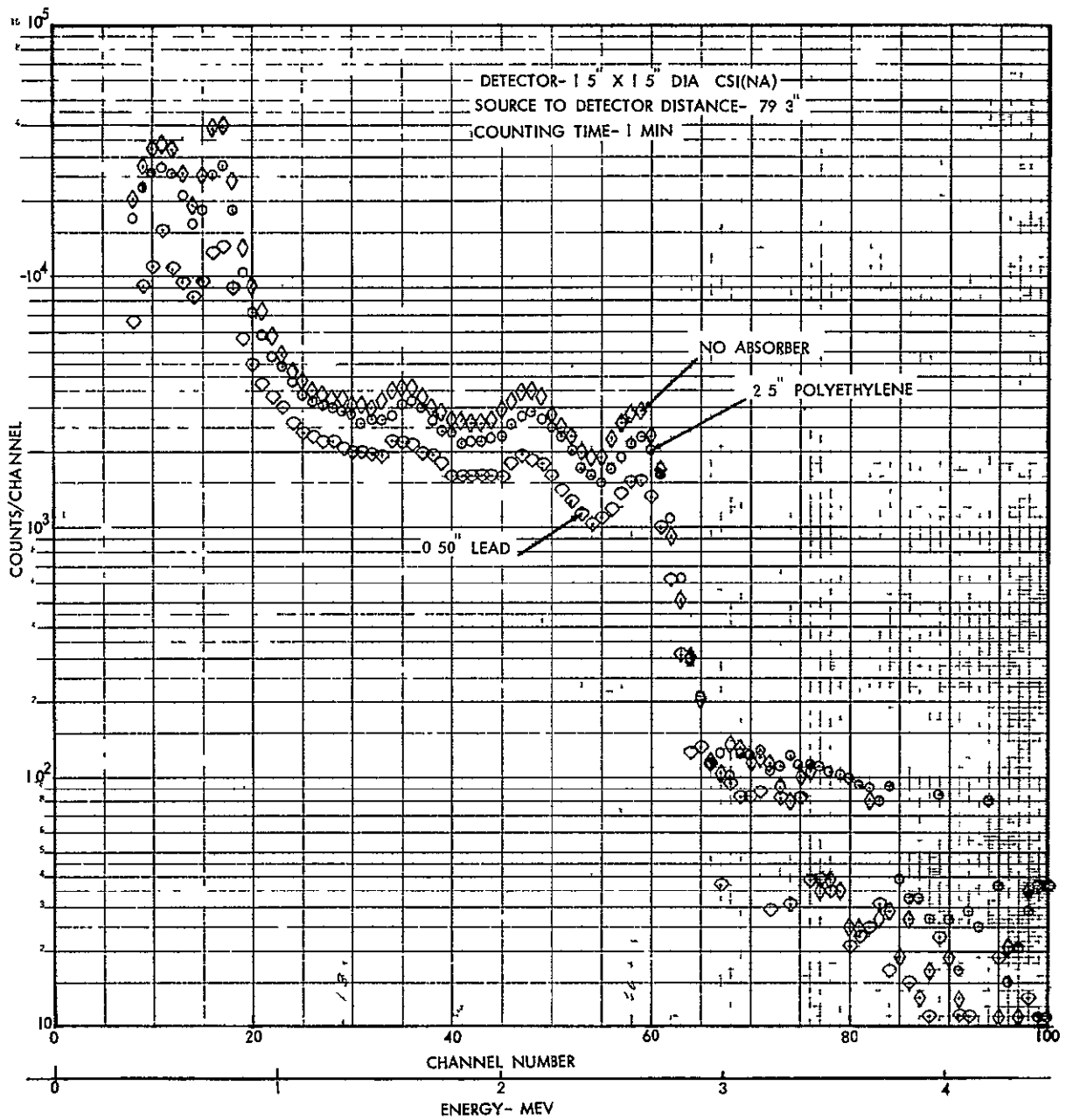TO SNAP-27 FUEL CAPSULE RADIATION

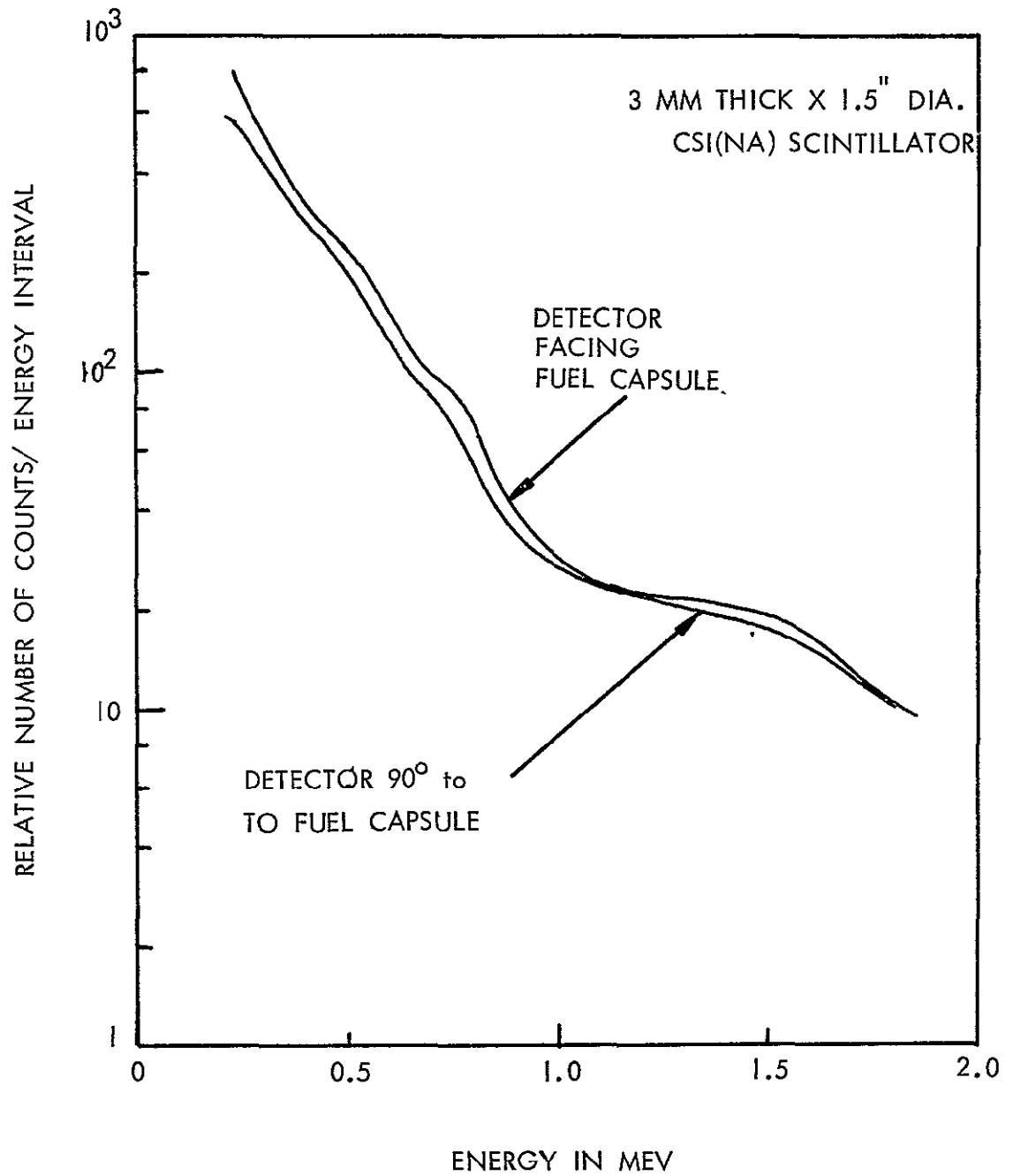FIGURE 5.6-2 EFFECT OF ABSORBERS ON SNAP-27
FUEL CAPSULE RADIATION

FIGURE 5.6-3 CsI DETECTOR RESPONSE AS A FUNCTION OF
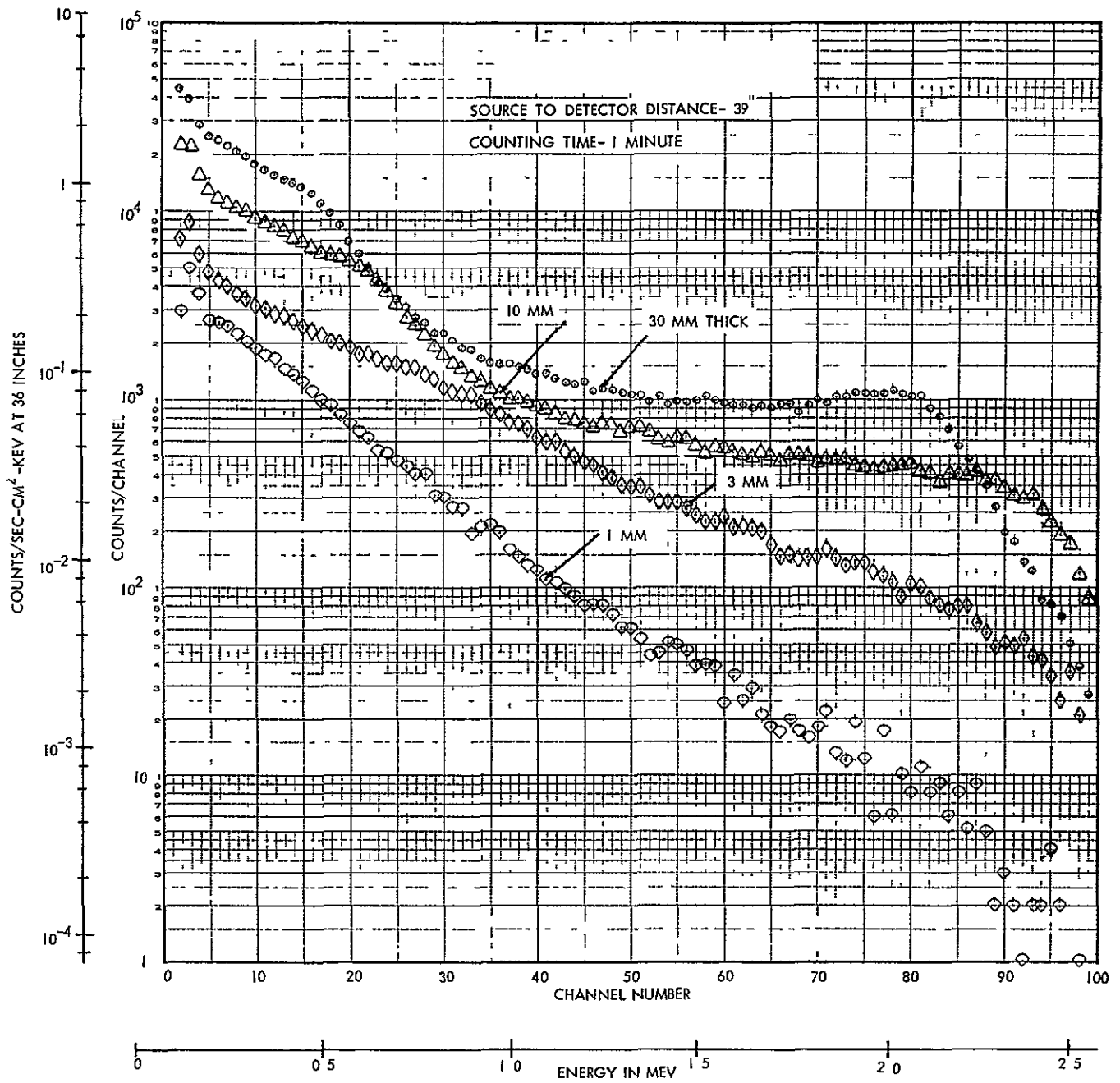DETECTOR ORIENTATION IN RESPECT TO THE FUEL CAPSULE

FIGURE 5.7-1 SPECTRAL RESPONSE OF PLASTIC SCINTILLATORS
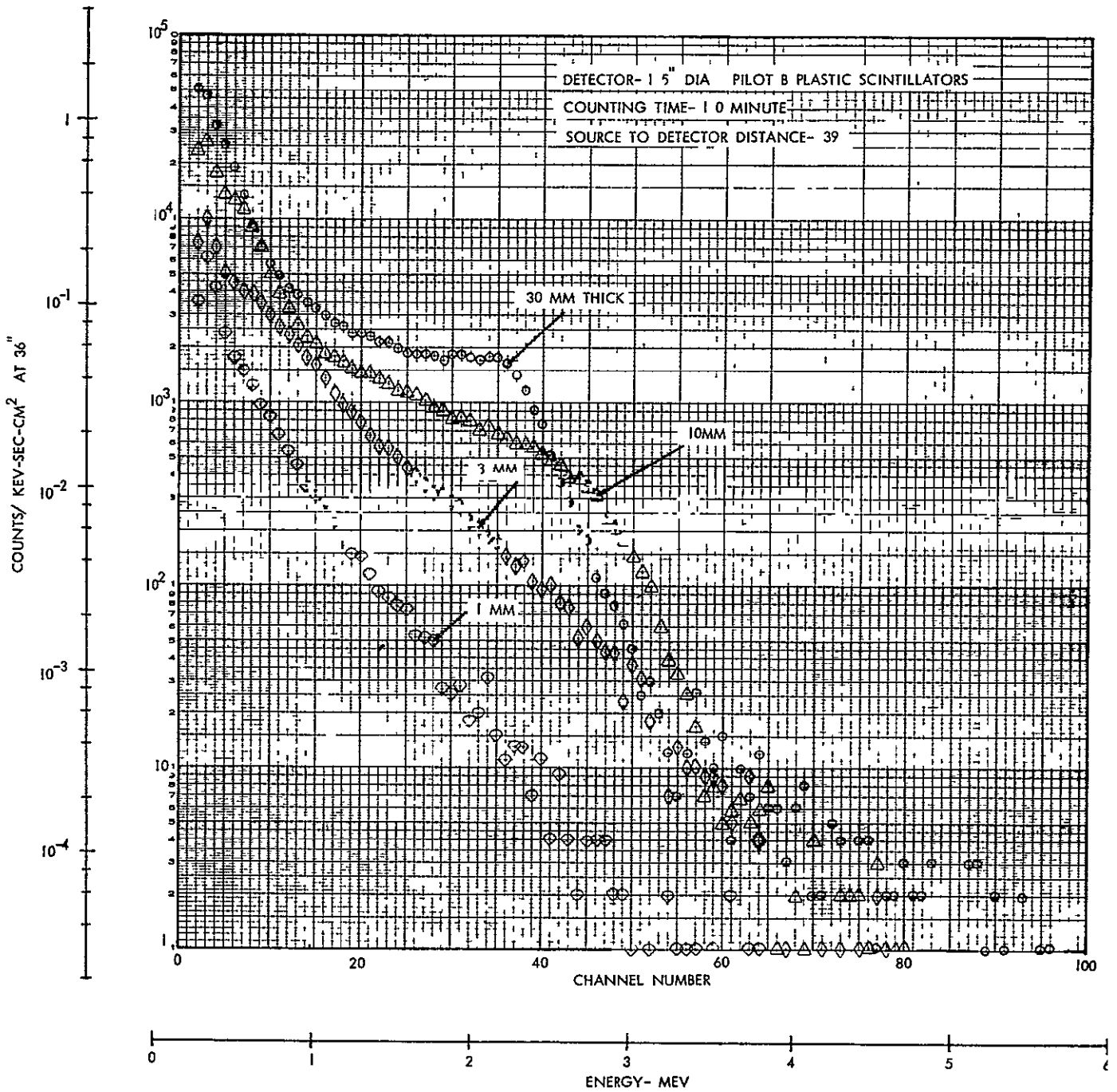TO SNAP-27 FUEL CAPSULE RADIATION ENERGY RANGE 0 TO 2 5 Mev

FIGURE 5.7-2 SPECTRAL RESPONSE OF PLASTIC SCINTILLATORS
TO SNAP-27 FUEL CAPSULE RADIATION ENERGY RANGE 0 TO 6 Mev

At the end of the test, which took less than one hour to complete, the system gain was checked by mounting the 3 cm thick scintillator and repeating the calibration with Co^{60} and Cs^{137} sources. The gain was found to be the same as at the beginning of the test within less than 2 percent. Absorption data, effects of detector orientation with respect to the heat source, and count rate as a function of distance from the fuel capsule measurements were obtained at a later time. The energy calibration for these tests was obtained by comparing the data to spectra of Figures 5.7-1 and 5.7-2. Absorption spectra taken with several absorbers are shown in Figure 5.7-3. Absorption plots for lead, aluminum, and polyethylene absorbers for several energy ranges are given in Figure 5.7-4. No significant change in the detected spectra as a function of detector orientation in relation to the heat source was observed.

5.8 NaI Scintillators

Two NaI scintillator detectors were used to perform measurements with the fuel capsule. The detectors were Harshaw Model 6S8-X, 1.5 x 1.5 inch NaI (Tl) and Harshaw Model 5S30 K/Q, 1-1/4" diameter x 0.030" thick NaI (Tl). Both detectors were standard laboratory type detectors and were operated with the same equipment as CsI and plastic scintillators described in Section 5.6.

The purpose of using NaI scintillators to measure the SNAP-27 heat source radiation was not because these detectors are frequently used in spacecraft instrumentation. In fact, NaI crystals are quite fragile and, therefore, are difficult to use outside the laboratory environment. However, they provide the best energy resolution that is available with scintillation detectors. Also, radiation detection efficiencies of NaI detectors are well documented so it becomes relatively easy to convert from the radiation response obtained with a NaI crystal to the actual radiation spectra and flux emitted by the SNAP-27 fuel capsule. Spectral response to the SNAP-27 heat source radiation obtained with two detectors; 1.5 x 1.5 and a .030 inch thick x 1.25" dia crystals are given in Figures 5.8-1 through 5.8-3 in several energy ranges.
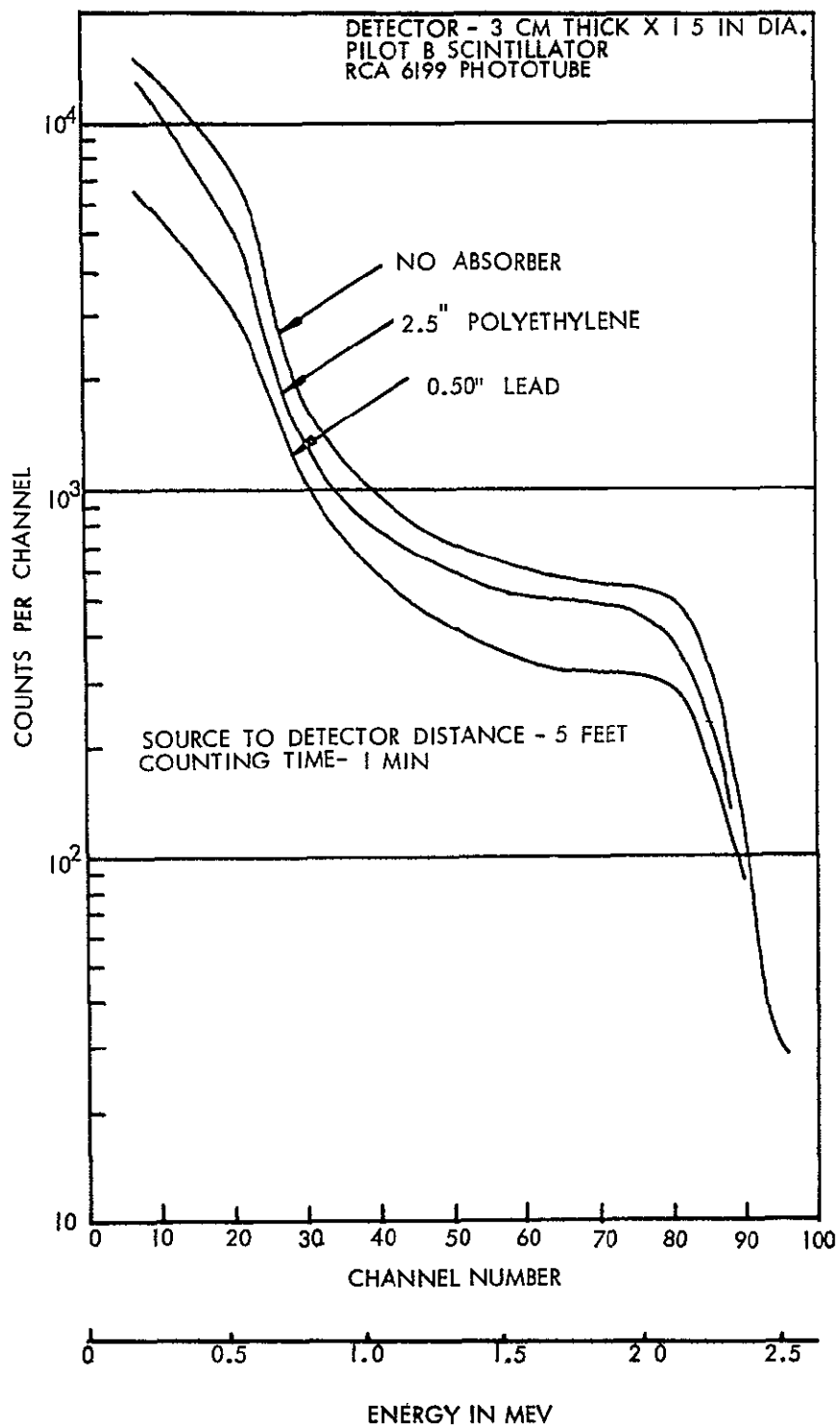
FIGURE 5.7-3 EFFECTS OF ABSORBERS ON SPECTRAL RESPONSE
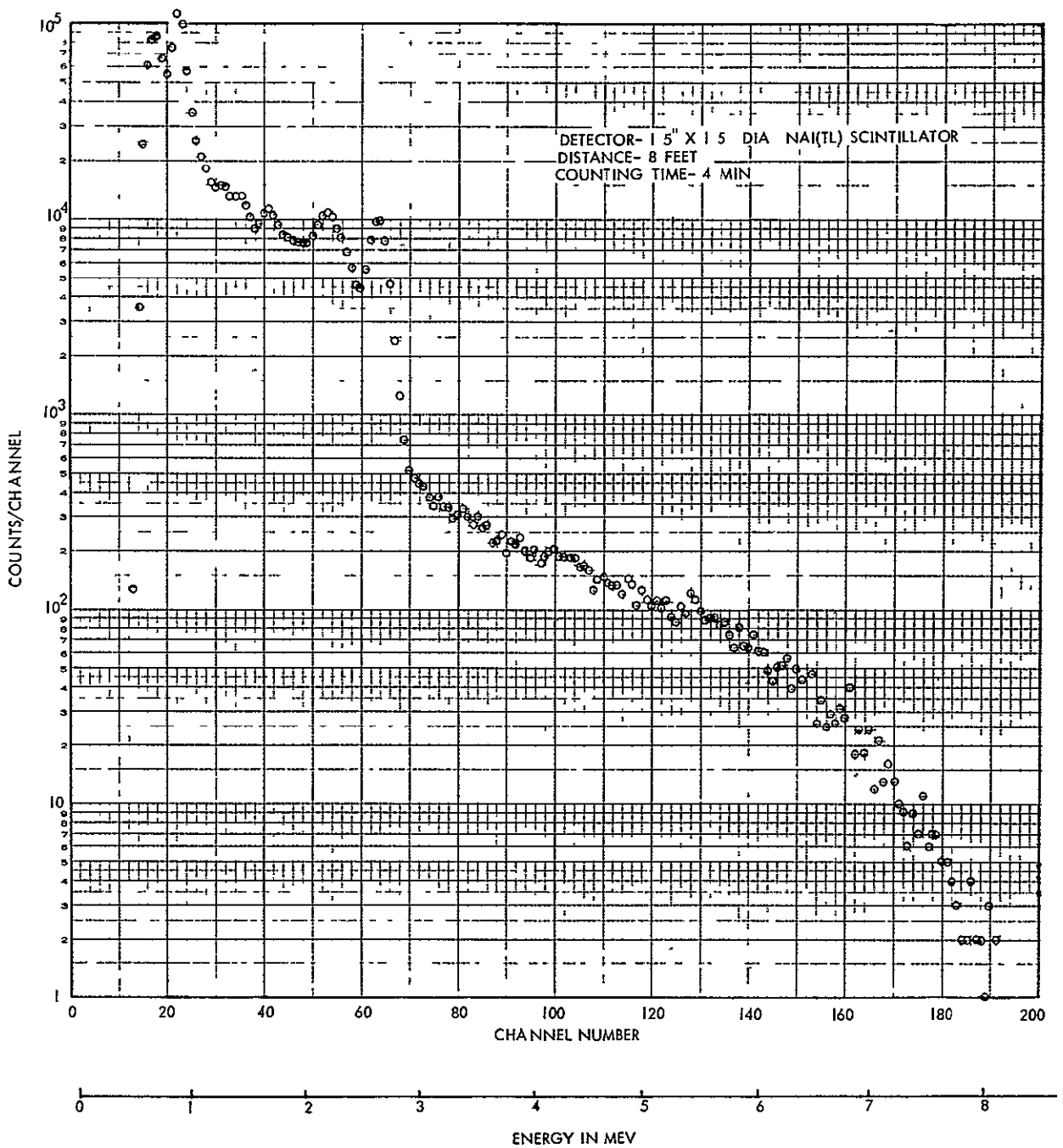OF PLASTIC SCINTILLATORS TO SNAP-27 FUEL CAPSULE RADIATION

FIGURE 5.8-1   RESPONSE OF NaI DETECTORS TO SNAP-27 FUEL CAPSULE RADIATION
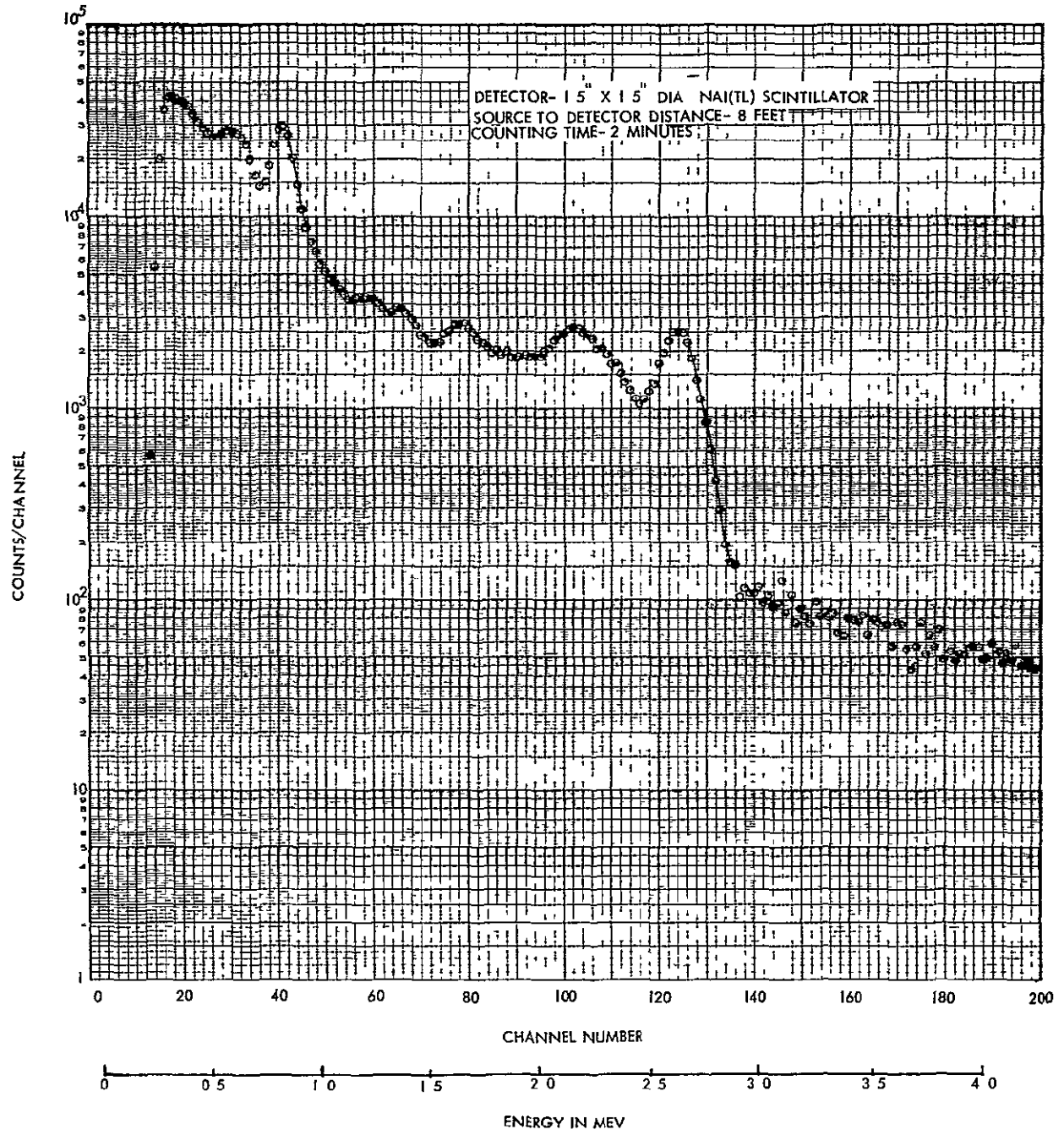ENERGY RANGE 0 TO 8 Mev

5-38

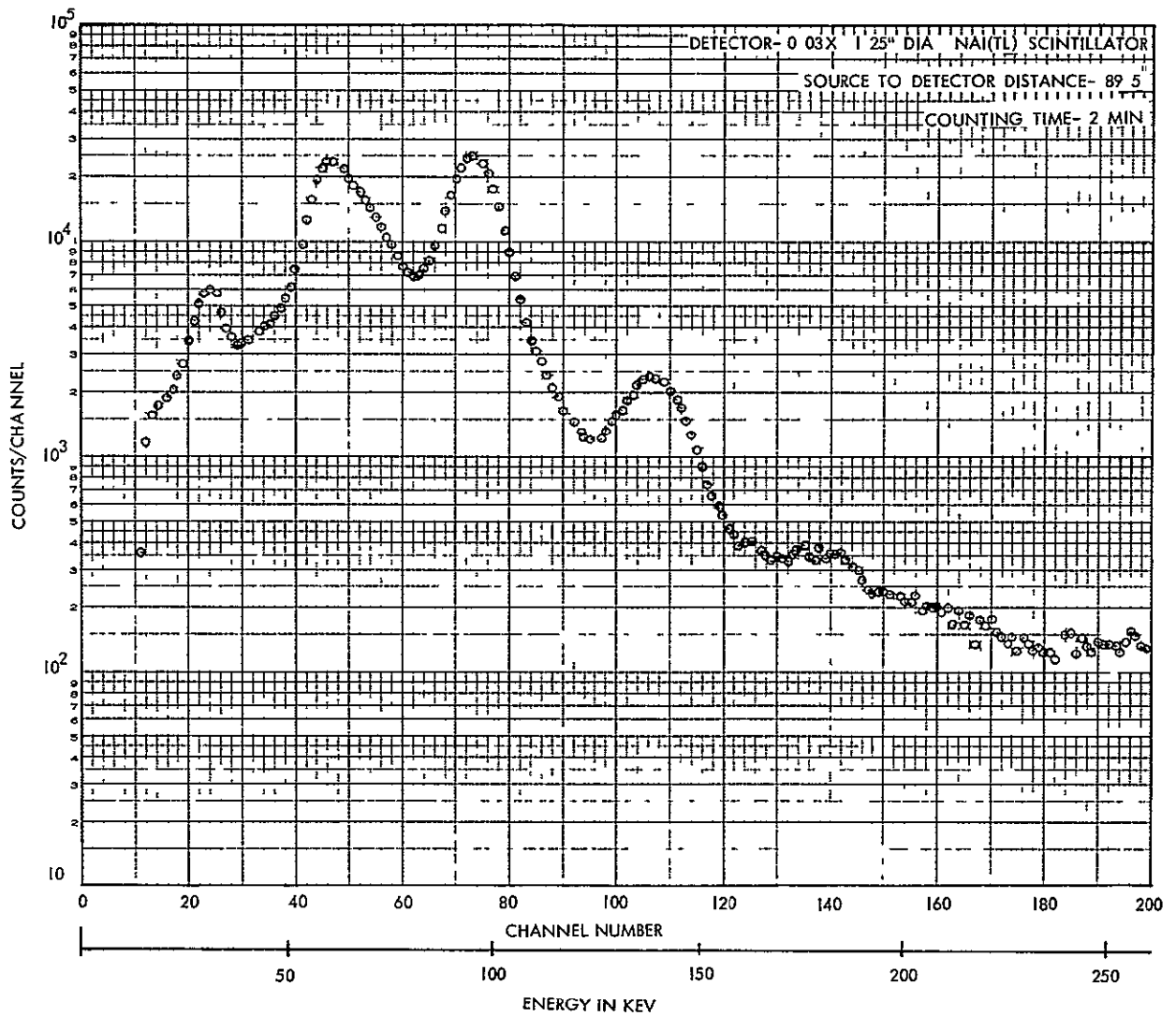DETECTOR- 1 5" X 1 5" DIA NAI(TL) SCINTILLATOR
SOURCE TO DETECTOR DISTANCE- 8 FEET
COUNTING TIME- 2 MINUTES

COUNTS/CHANNEL

CHANNEL NUMBER

ENERGY IN MEV

FIGURE 5.8-2 RESPONSE OF NaI DETECTORS TO SNAP-27 FUEL CAPSULE RADIATION
ENERGY RANGE 0 TO 4.0 Mev

FIGURE 5.8-3 RESPONSE OF NaI DETECTORS TO SNAP-27 FUEL CAPSULE RADIATION
ENERGY RANGE 0 TO 250 Mev

The spectra of the SNAP-27 fuel capsule obtained with the 1-1/2 x 1-1/2" NaI scintillator using various absorbers are given in Figure 5.3-1. The same data taken with the 0.03" thick NaI scintillator are given in Figure 5.8-4.

5.9   Cherenkov Detectors

Four different thickness Cherenkov radiation detectors were selected for tests with the SNAP-27 fuel capsule. They were 3 cm, 1 cm, 3 mm and 1 mm thick and all were 1-1/2 inch diameter. The crystals were machined out of Lucite, polished by hand to have glossy surfaces and coupled to RCA 6199 photomultiplier tube using silicon grease. Since no provisions existed to calibrate the individual tube gains, all tests with the Cherenkov detector were performed using the same photomultiplier tube and electronics. In the beginning of the test the tube gain was measured using a Pilot B scintillator and Co^{60} source, then the Pilot B plastic scintillator removed, and Cherenkov detectors were coupled to the PM tube one at a time, and measurements of the fuel capsule radiation were made. At the end of the test, which took less than one hour to perform, the tube gain was checked using the same Pilot B scintillator and Co^{60} source and was found to be the same within less than 2 percent. The results are shown in Figure 5.9-1. Since no provisions existed to obtain an absolute energy calibration of the Cherenkov detectors, the data are presented relative to Cherenkov radiation produced by Co^{60} radiation.

5.10   Phototubes

Gamma radiation interacts directly with the cathode and dynodes of phototubes and thus contributes unwanted noise counts. To evaluate this effect, two phototubes (RCA 6199 and RCA 4440) without scintillation crystals were exposed to the radiation source.

The phototube signal was shaped by a Hamner NA-11 amplifier and passed to a multichannel pulse height analyzer. For calibration, a 10 mm CsI (Na) crystal was attached to each tube and Co^{57} and Bi^{207} spectra were taken. Then the crystal was removed and the spectral
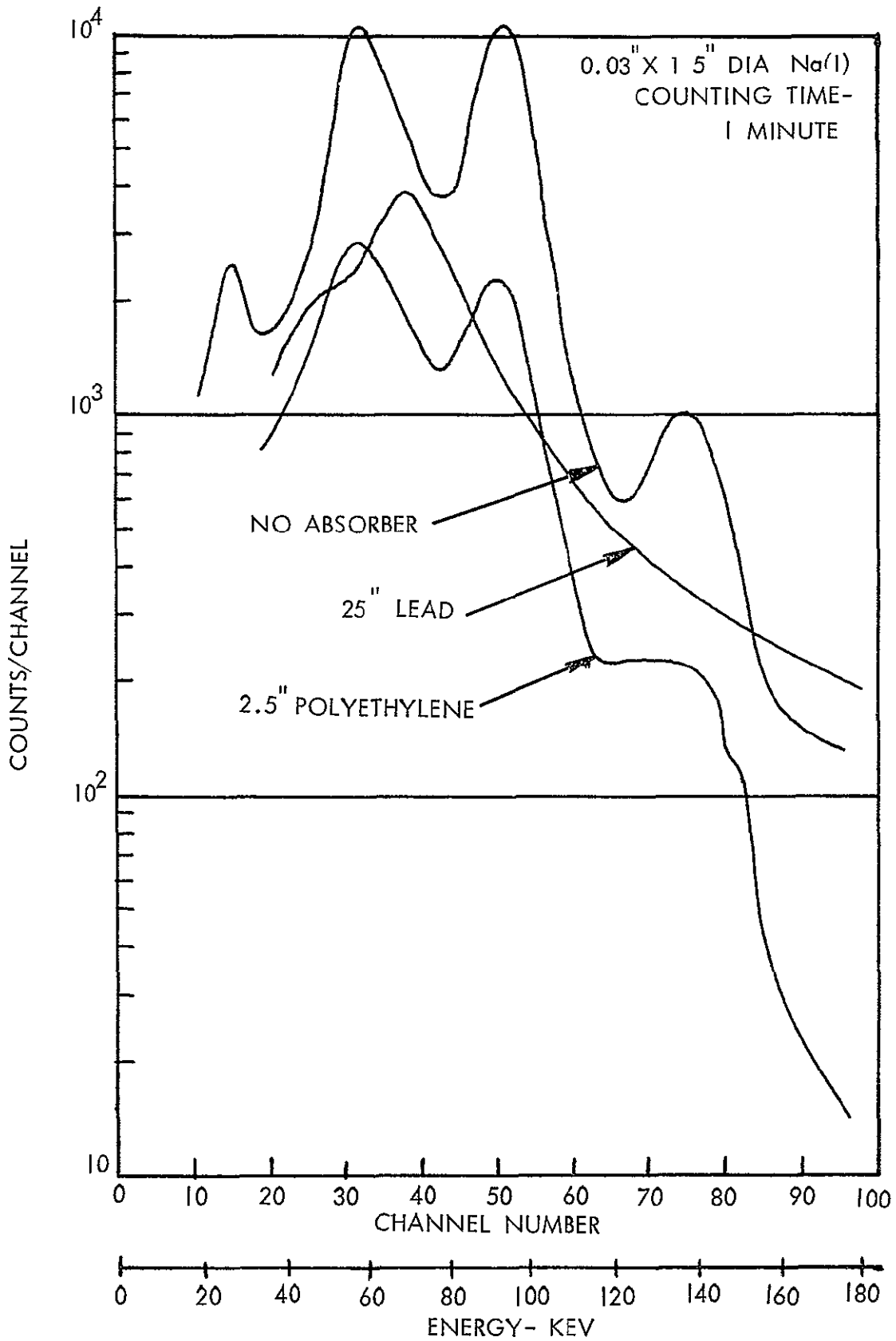
FIGURE 5 8-4   EFFECT OF ABSORBERS ON SPECTRAL RESPONSE OF
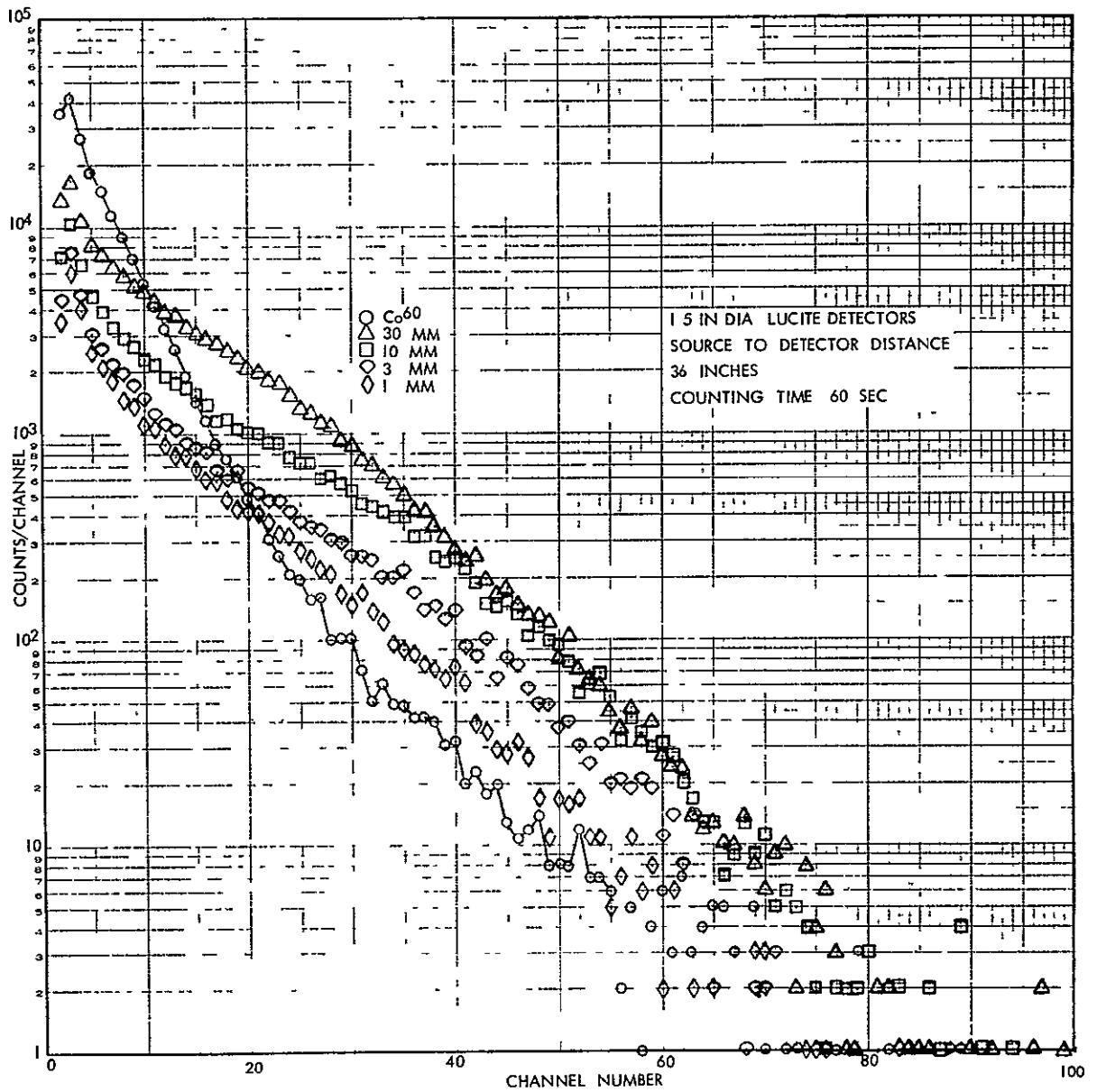0.03" x 1.5" DIA NaI SCINTILLATOR TO SNAP-27 FUEL CAPSULE RADIATION

FIGURE 5.9-1 RESPONSE OF CHERENKOV DETECTORS
TO SNAP-27 FUEL CAPSULE RADIATION

response of the bare phototube was measured. To provide a basis for comparison with CsI (Na) and other scintillators, the results are presented in terms of energy equivalent for CsI (Na).

Figures 5.10-1 and 5.10-2 show the spectral response of the RCA 6199 and RCA 4440 phototubes at 1 foot from the SNAP-27 fuel capsule.

5.11   Geiger Tube Experiments

Radiation response measurements were performed using the EON 7302 and EON 6213 Geiger-Mueller tubes. The purpose of the measurements was to produce plots of the Geiger-Mueller tube responses as a function of distance and as a function of attenuation through lead, aluminum, and polyethylene.

The Geiger-Mueller tubes were powered by a Fluke Model 412A high voltage power supply. The signals were passed through a decoupling capacitor to a laboratory counter. The long axis of the detector was oriented at right angles to the fuel capsule axis. Count rates were taken at various distances between the fuel capsule and the Geiger tubes from 1 to 8 feet. Count rates never exceeded 400 cps and, therefore, dead time effects were negligible. Total counts were maintained above 2200 counts to achieve standard deviations of $\pm$ 2% or better.

The source-to-detector distance, R, was adjusted to 2 feet and absorbers of aluminum, lead, polyethylene, and boron-loaded polyethylene were positioned between source and detector. Thickness ranges of 0 to 2 inches for lead, 0 to 1-1/2 inches for aluminum, and 0 to 3 inches for polyethylene were used. Count rates did not exceed 120 cps and total counts exceeded 2200 counts as described in the last paragraph.

Figures 5.11-1 and 5.11-2 are plots of the response of the EON 7302 and EON 6213, respectively, to the SNAP-27 fuel capsule as a function of $1/R^2$ where R is distance in feet from the capsule to the Geiger-Mueller tube.

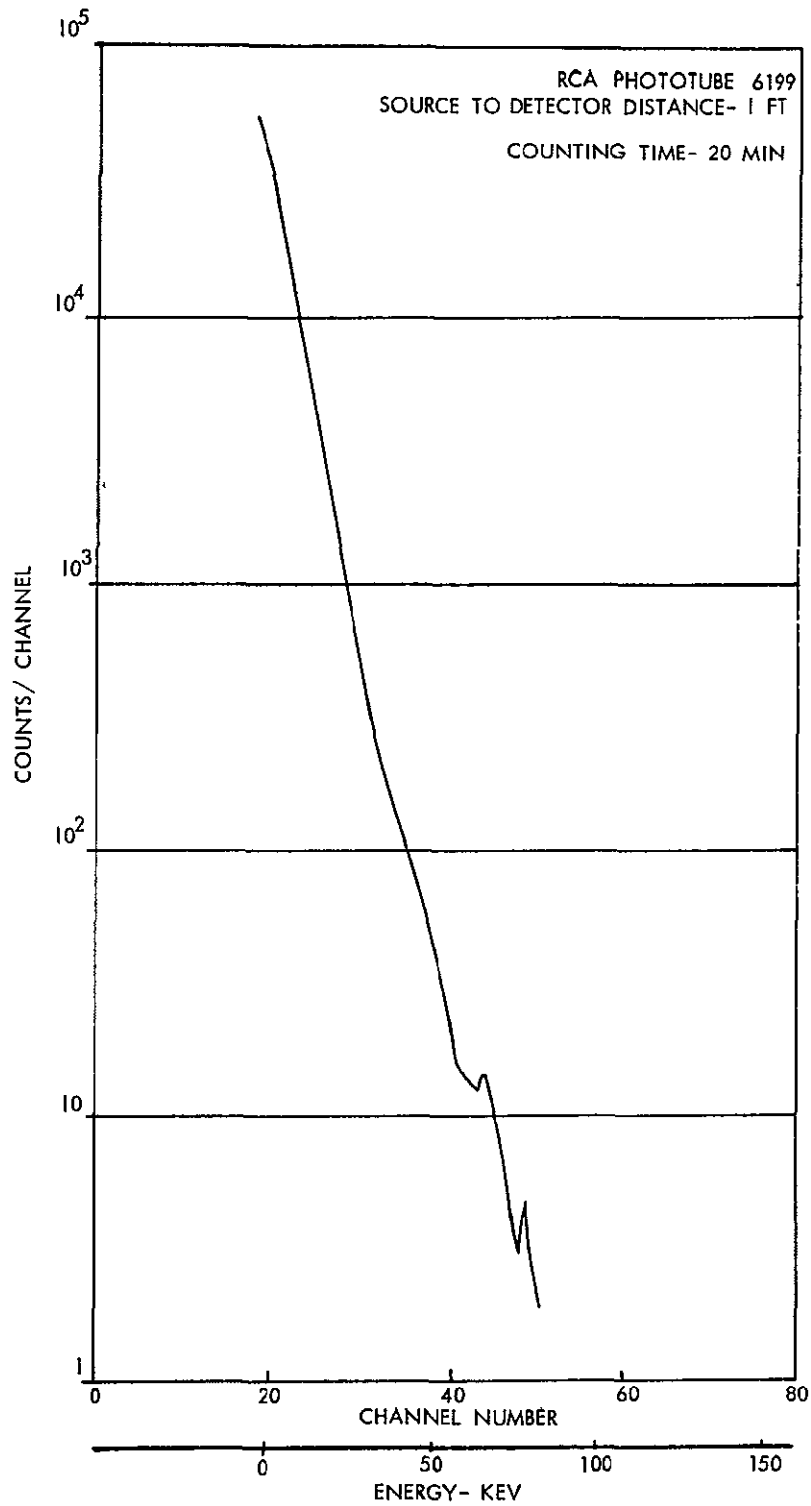Figure 5.11-3 gives the effects of absorbers in reducing the count rate for both tubes tested.

FIGURE 5.10-1   RESPONSE OF BARE RCA 6199 PHOTOTUBE TO SNAP-27
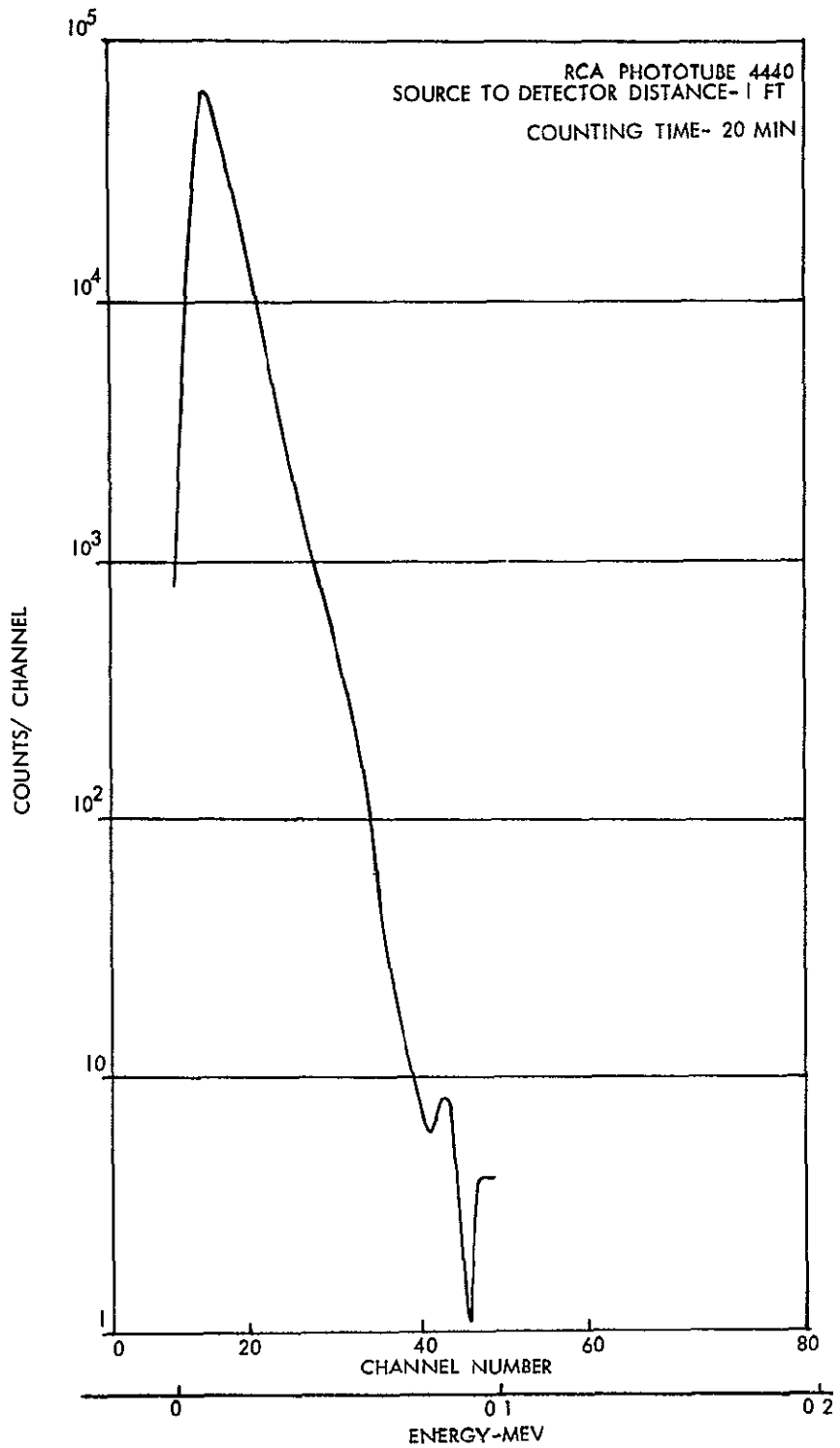'FUEL CAPSULE RADIATION

FIGURE 5.10-2   RESPONSE OF BARE RCA 4440 PHOTOTUBE TO SNAP-27
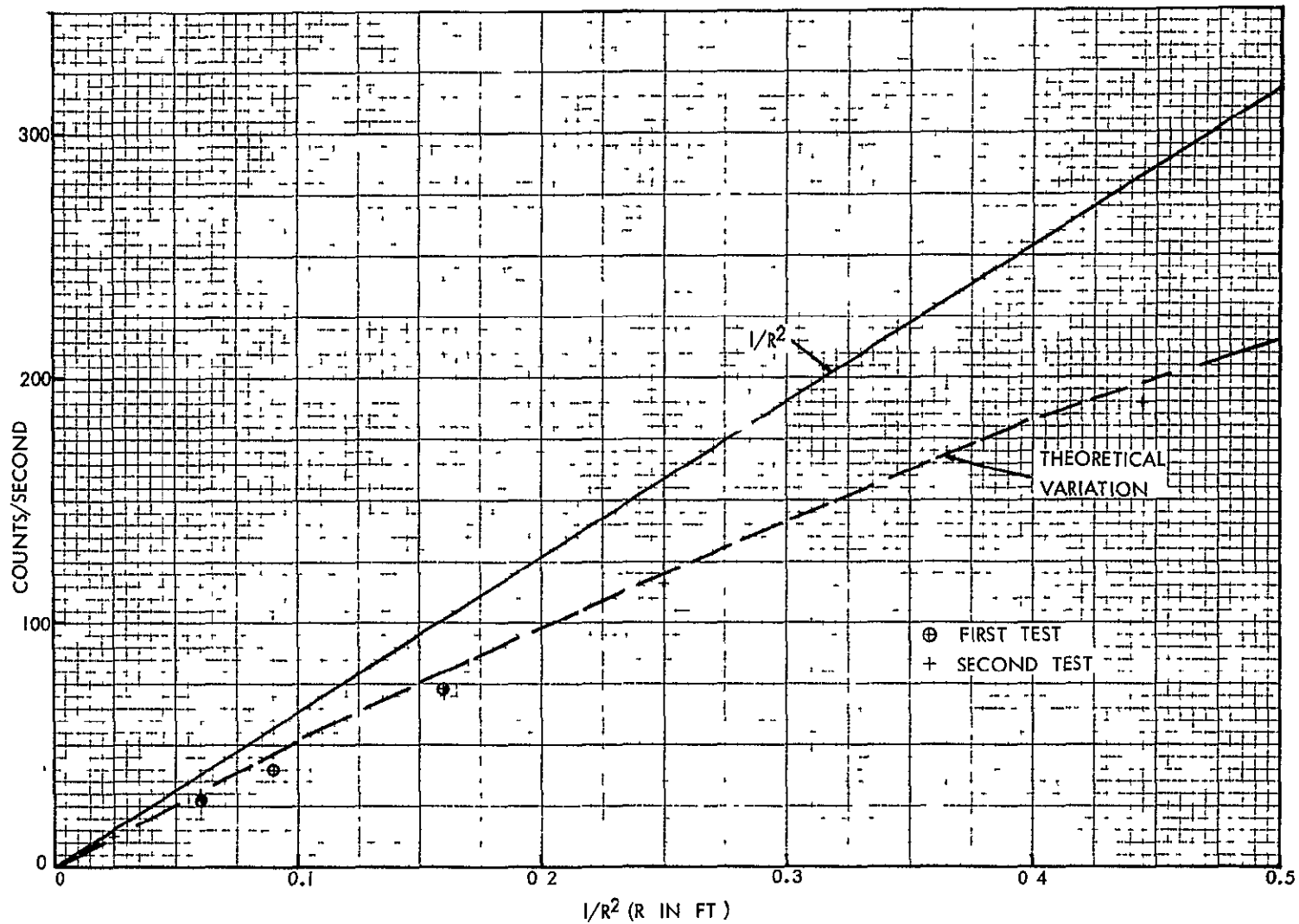FUEL CAPSULE RADIATION

FIGURE 5.11-1 EON 7302 TUBE COUNT RATE AS A FUNCTION OF
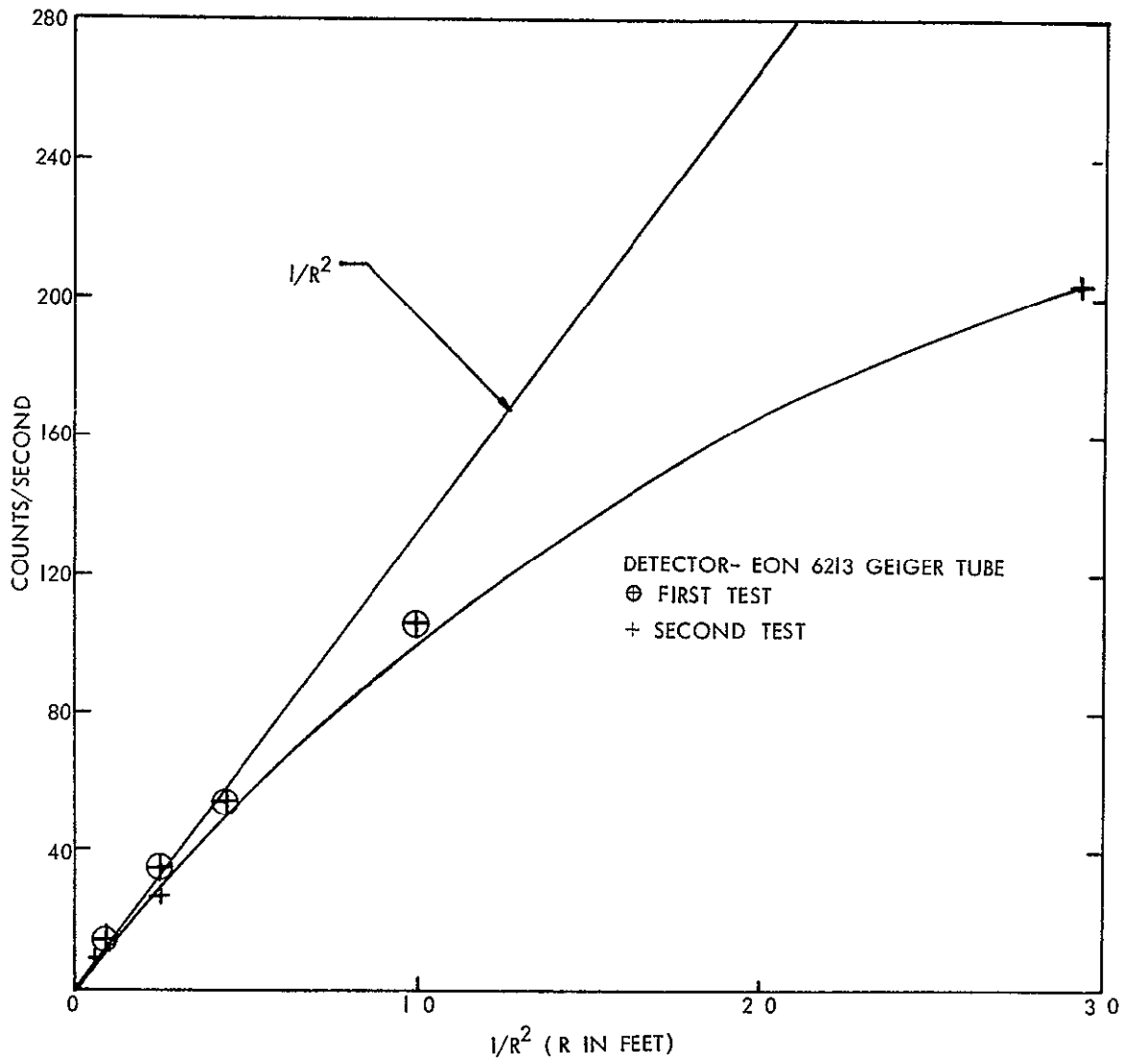DISTANCE FROM THE SNAP-27 HEAT SOURCE

FIGURE 5.11-2 EON 6213 TUBE COUNT RATE AS A FUNCTION OF
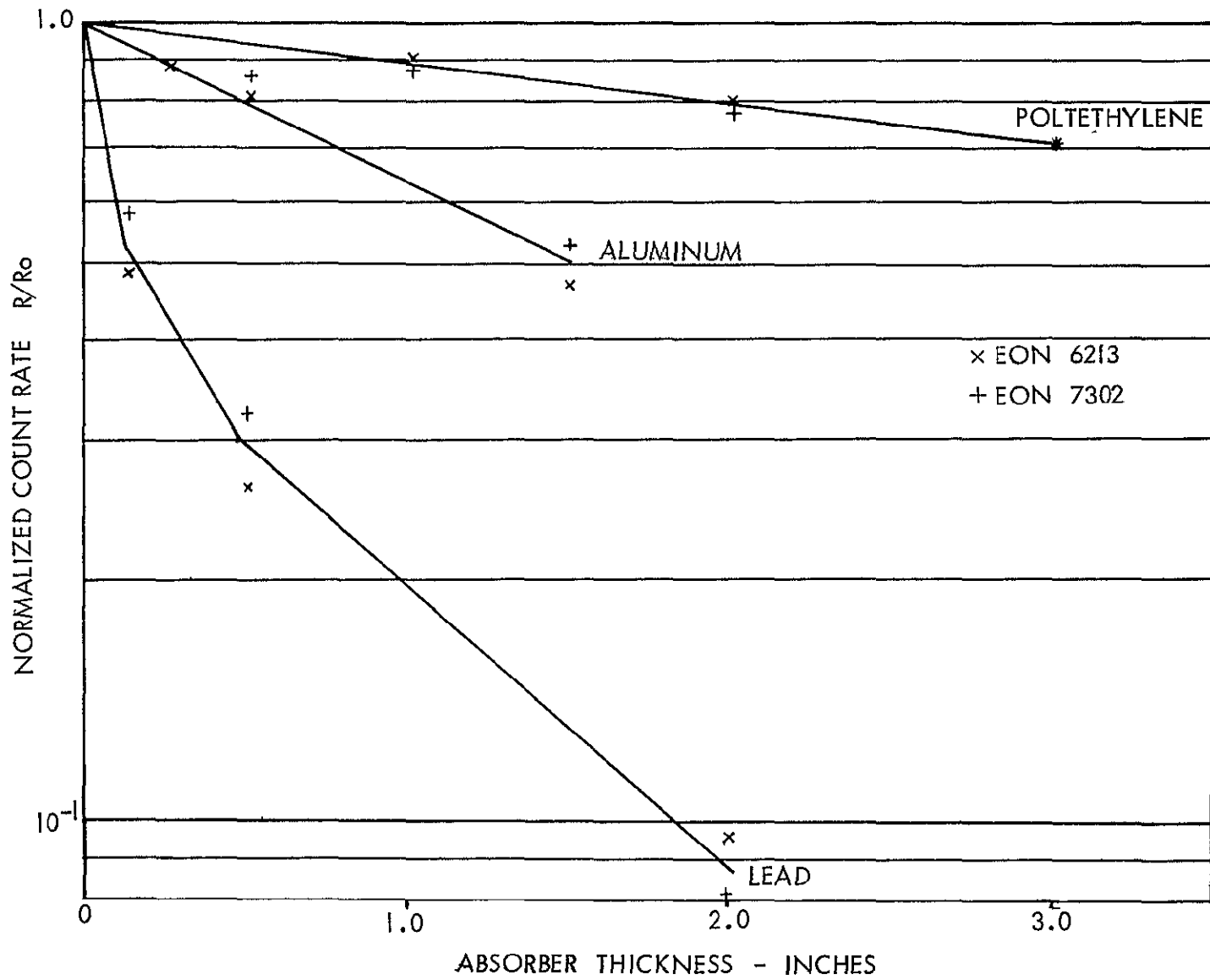DISTANCE FROM THE SNAP-27 HEAT SOURCE

FIGURE 5.11-3 GEIGER TUBE COUNT RATE AS A FUNCTION OF
ABSORBER THICKNESS

If the RTG were a point source, the response would follow the straight line indicated on the plot. Since the RTG is more like a line source, it follows the function:

$$C_R = \frac{2C_0}{R\left(R + \frac{h}{2}\right)}$$

Where C_R is the count rate at the distance R, C_0 is an equivalent zero distance count rate, and h is the source length. For purposes of curve fitting, C_0 may be calculated by substitution of experimental values of R and C_R.

The shape of the curve relating distance to count rate for the EON 6213, shown in Figure 5.11-2, is very similar to the curve obtained with EON 7302 except for the magnitude of the count rates.

5.12   Proportional Tube

The purpose of this experiment was to measure the response of a representative proportional tube to the SNAP-27 fuel capsule radiation. A Harshaw G-15 proportional tube was operated at 2500 volts with a Tennelec TC-130 preamplifier and Tennelec TC-200 amplifier system which was coupled to a multichannel pulse height analyzer. A special adapter with a decoupling capacitor and load resistor was made to adapt the proportional counter to the TC-130 amplifier.

The detector was placed 4 feet from the SNAP-27 fuel capsule with its cylindrical axis parallel to the capsule axis. Spectra from the SNAP-27 fuel capsule were taken at 0-16, 0-100, and 0-300 kev full scale. These data are given in Figures 5.12-1, 5.12-2 and 5.12-3.

Figure 5.12-4 shows the effect of Pb, Al, and polyethylene absorbers on count rates in the energy range 0 to 100 kev.

FIGURE 5.12-1 SPECTRAL RESPONSE OF HARSHAW G-15
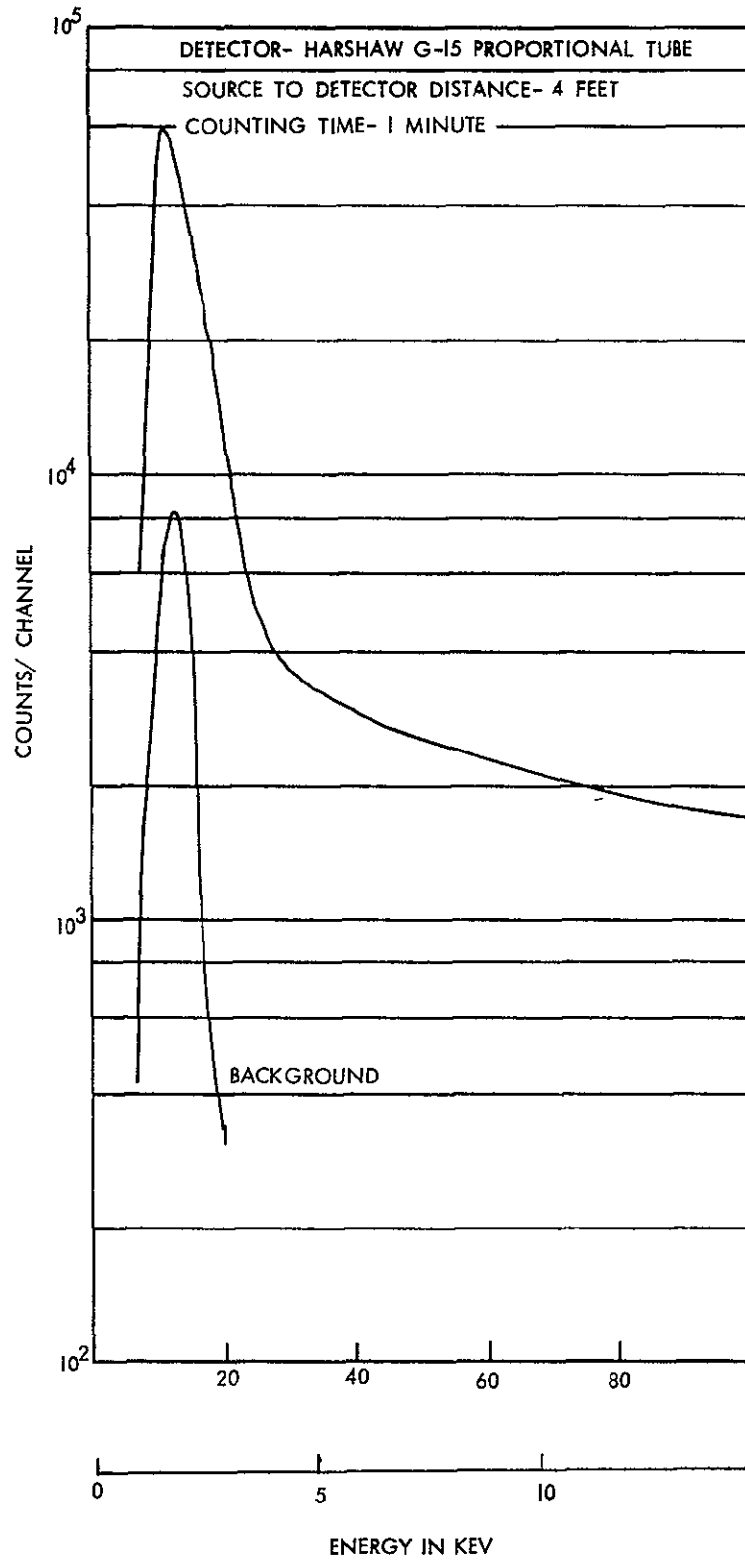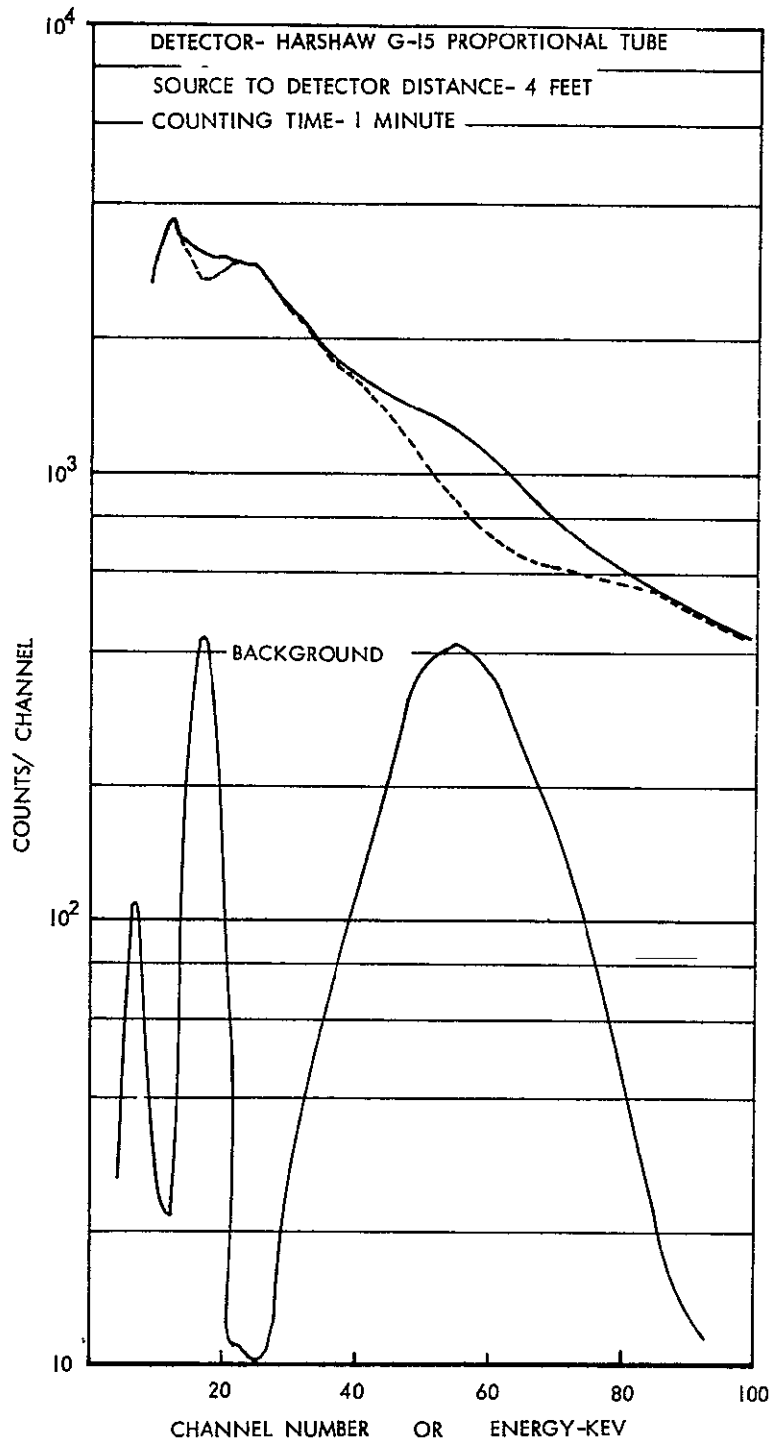PROPORTIONAL TUBE TO SNAP-27 FUEL CAPSULE RADIATION

FIGURE 5.12-2   SPECTRAL RESPONSE OF HARSHAW G-15
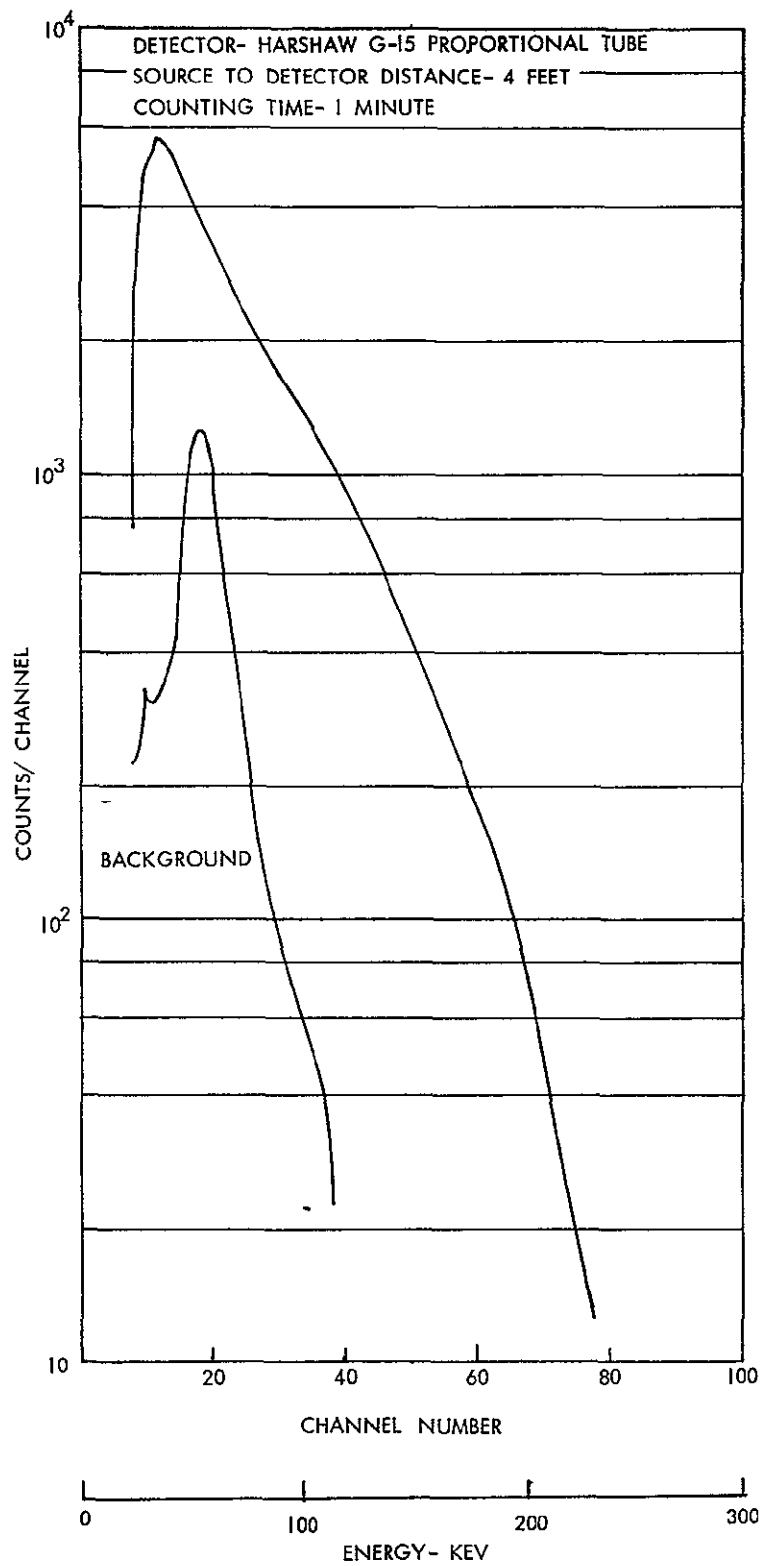PROPORTIONAL COUNTER TO SNAP-27 FUEL CAPSULE RADIATION

FIGURE 5.12-3   SPECTRAL RESPONSE OF HARSHAW G-15
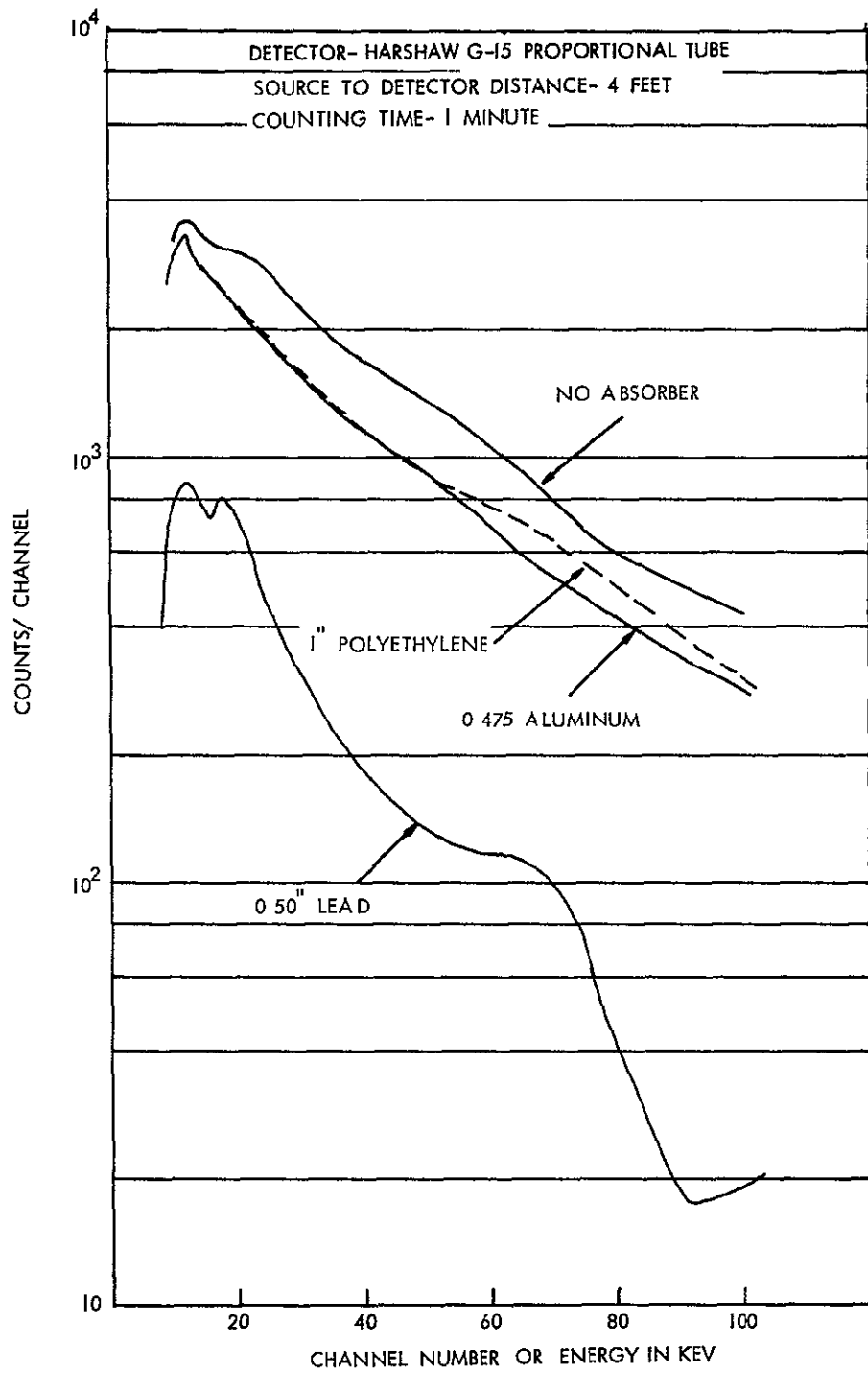PROPORTIONAL TUBE TO SNAP-27 FUEL CAPSULE RADIATION

FIGURE 5.12-4 EFFECT OF ABSORBERS ON SPECTRAL RESPONSE OF
HARSHAW G-15 PROPORTIONAL TUBE TO SNAP-27 FUEL CAPSULE RADIATION

5.13   Channeltrons

A Bendix CEM 4028 channeltron* was used to measure its response to the SNAP-27 fuel capsule radiation. The purpose of the measurements was to determine the response as a function of distance and absorber thickness. In order to provide a vacuum operating environment, the channeltron was sealed inside a glass cylinder and pumped down by a diffusion pump to 5×10^{-5} torr. The channeltron was operated in the saturated mode. The electrical set up used for the tests is shown in Figure 5.13-1.

In order to determine the proper operating voltage, differential pulse height spectra were taken with a Co^{60} source at various high voltages. Spectra obtained with a 3700 volt bias as illustrated in Figure 5.13-2. The saturation peak of Figure 5.13-2 is not as well defined for the Co^{60} source as it would be for a charged particle incident on the funnel. The charged particles produce photo-electrons from the funnel only, whereas the Co^{60} gammas produce photo-electrons from along the entire length of the channeltron.

The channeltron funnel was oriented to point parallel to the fuel capsule cylindrical axis and count rates were recorded as a function of distance and absorber thickness.

Figure 5.13-3 is a plot of the channeltron response to the fuel capsule radiation attenuated by Pb, Al, and polyethylene. Measurements with boron-loaded polyethylene showed no significant change from data obtained with polyethylene.

Figure 5.13-4 gives the channeltron count rate as a function of distance R from the fuel capsule.

---

* A channeltron of the type being used for the Pioneer F/G U.V. experiment was provided by Dr. D. L. Judge of the University of Southern California.
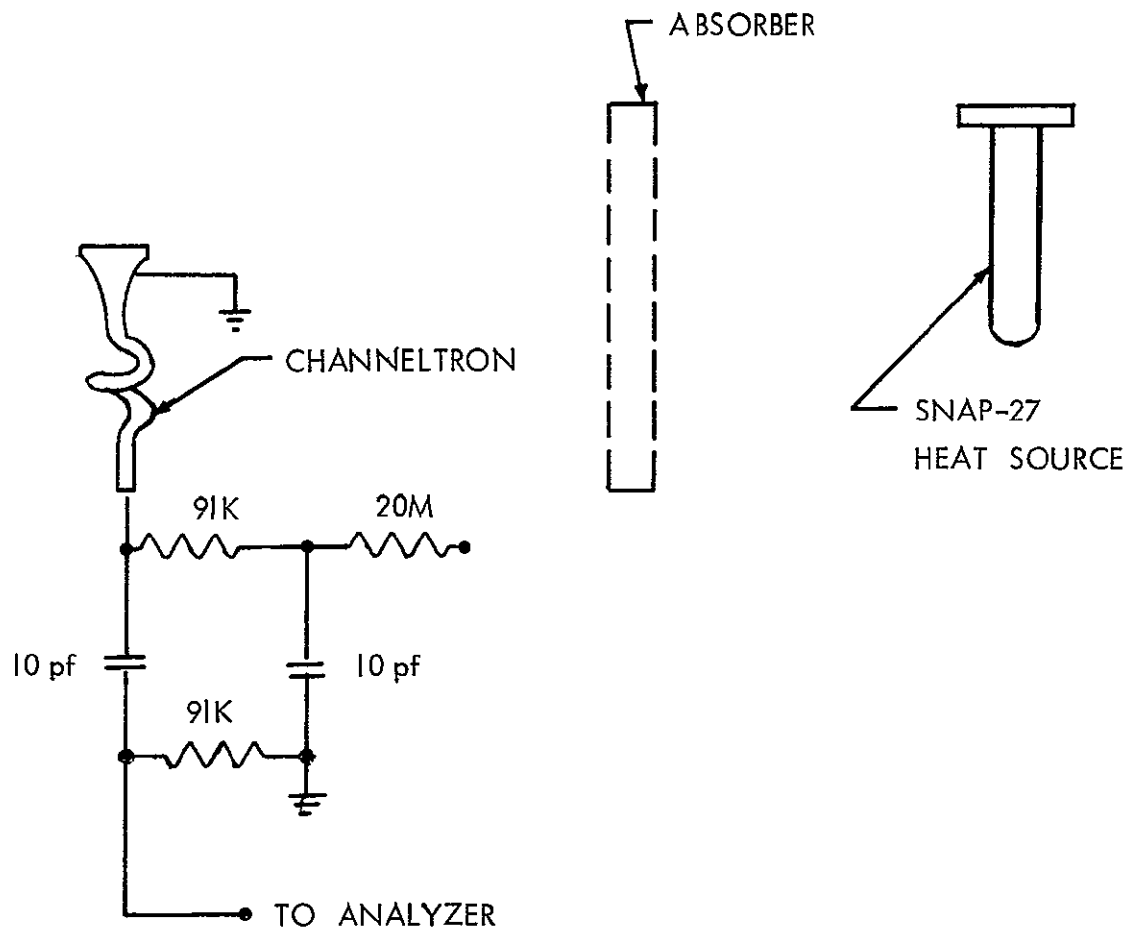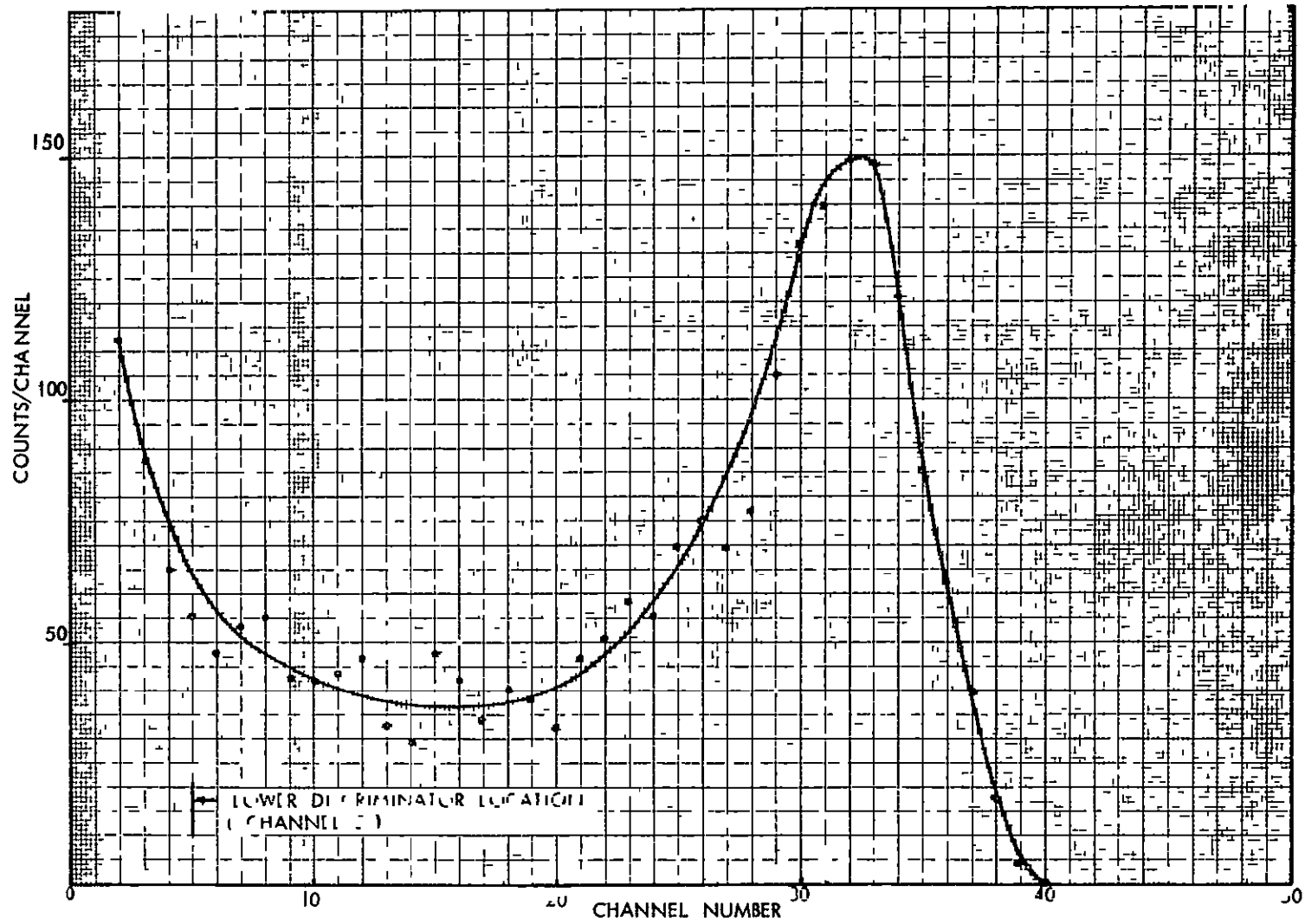
FIGURE 5.13-1 EXPERIMENTAL SETUP BENDIX CEM 4028 CHANNELTRON

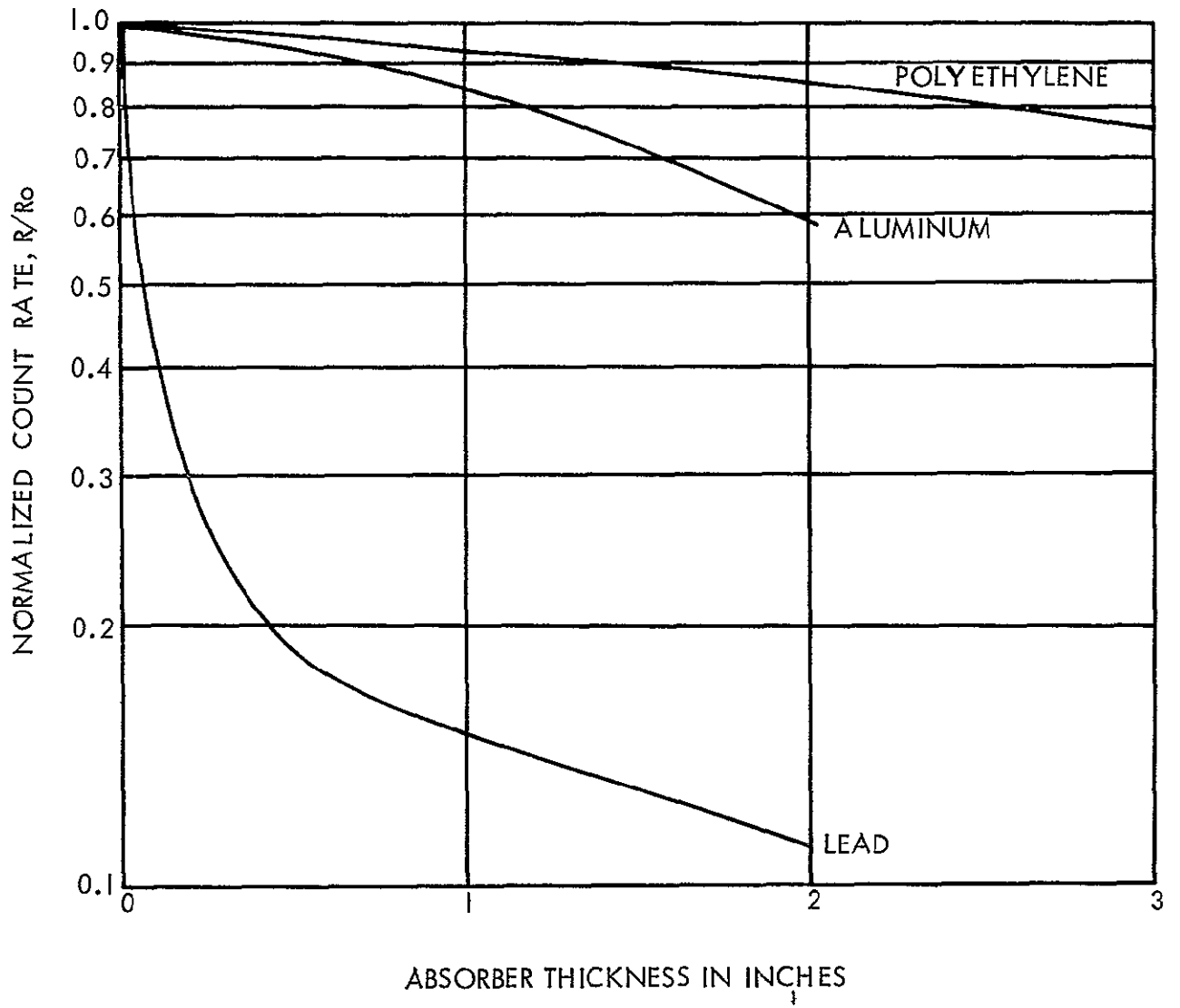FIGURE 5.13-2   RESPONSE OF 4028 CHANNELTRON TO Co^{60} GAMMA RADIATION

FIGURE 5.13-3 EFFECT OF ABSORBERS ON RESPONSE OF 4028
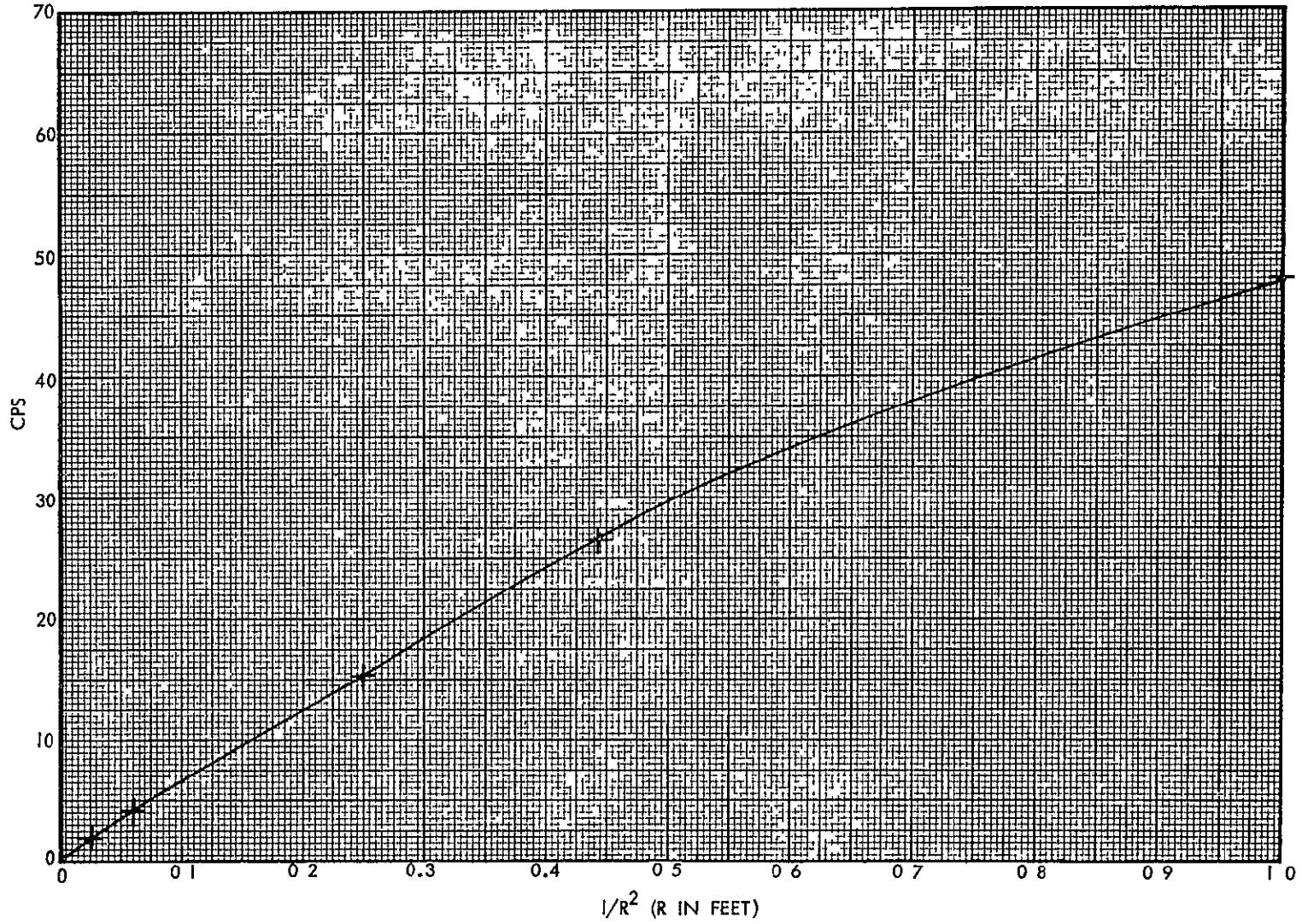CHANNELTRON TO SNAP-27 FUEL CAPSULE RADIATION

FIGURE 5.13-4 COUNT RATE AS A FUNCTION OF DISTANCE FROM SNAP-27 HEAT SOURCE FOR
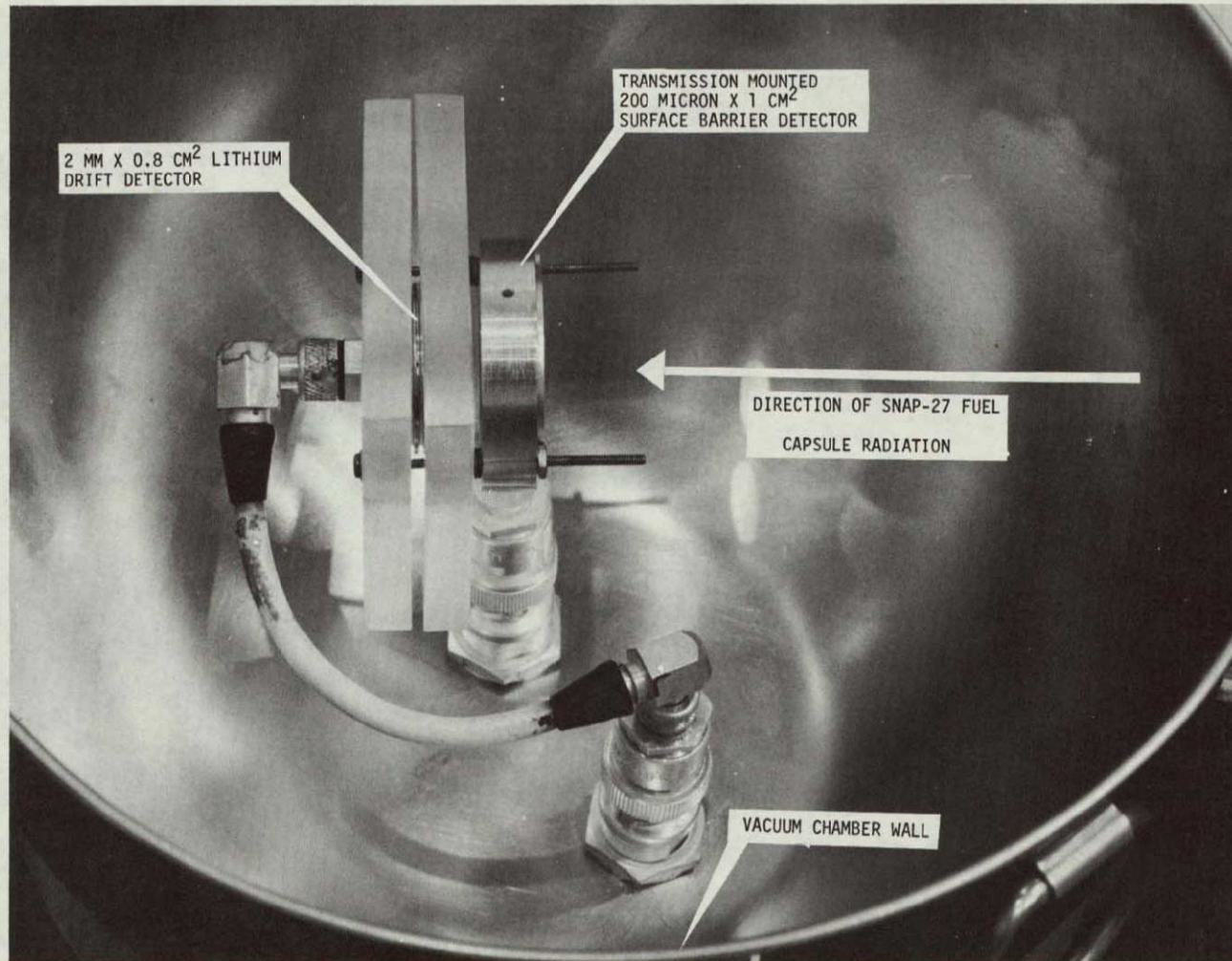CEM 4028 CHANNELTRON

5.14 Semiconductor Telescope

To provide a measure of the interference of the fuel capsule radiation with detectors operated in a coincidence telescope configuration, a test unit was built consisting of two semiconductor detectors as illustrated in Figure 5.14-1. A 200 μ x 1.0 cm^2 surface barrier semiconductor detector in a transmission mount was placed adjacent to a 2000 μ x 0.8 cm^2 lithium drifted detector. The two detectors were 0.47 cm apart and were operated in coincidence to detect charged particles sufficiently energetic to penetrate the thin detector and also leave charge in the thick detector. The entire detector assembly was mounted in a vacuum chamber to reduce air scattering of Compton electrons.

Figure 5.14-2 is a block diagram of the electronics used for the coincidence measurements. The transmission mounted detector signals were amplified by a low-noise charge-sensitive preamplifier and amplifier system and passed through a single channel analyzer to provide a gating pulse to a Hamner NA-11 gate. The 2000 micron detector signals were amplified and routed to the input of the gate. The resolving time was set at one microsecond. The gated output was analyzed by a multi-channel analyzer.

A bismuth-207 conversion electron calibration source was used with the transmission-mounted detector to obtain an energy calibration for setting the single channel analyzer threshold level to 96 kev. The SNAP-27 fuel capsule was located at a distance of 1 foot and spectra were taken in the no-coincidence, anticoincidence and coincidence modes in the energy range of 0 to 2.8 kev. The accidental coincidence rate was measured to be 0.5 counts per second over this energy range by placing a 3.2 mm Al plate between the two detectors to prevent the Compton electrons of energy less than 2 Mev from passing through both detectors simultaneously. The measured accidental coincidence rate was in good agreement with the calculated value of 0.8 counts per second

2 MM X 0.8 CM^2 LITHIUM DRIFT DETECTOR

TRANSMISSION MOUNTED 200 MICRON X 1 CM^2 SURFACE BARRIER DETECTOR

DIRECTION OF SNAP-27 FUEL CAPSULE RADIATION

VACUUM CHAMBER WALL

!NOT REPRODUCIBLE

FIGURE 5.14-1   PHOTOGRAPH OF SEMICONDUCTOR DETECTOR TELESCOPE

LOCATION OF SNAP-27 FUEL CAPSULE

LOCATION OF Bi^{207} CALIBRATION SOURCE

200μ SURFACE BARRIER

2000μ Li DRIFT

ORTEC
PREAMPL.

ORTEC
MAINAMPL.

HAMNER
NA-11
AMPLIFIER

HAMNER
NA-19
DELAY
AMPL.

TENNELEC
PREAMPL.

TENNELEC
MAINAMPL.

HAMNER
NA-11
AMPLIFIER

HAMNER
NC-11
SINGLE
CHANNEL
ANALYZER

HAMNER NG-11

GATE   GATED
              AMPLIFIER
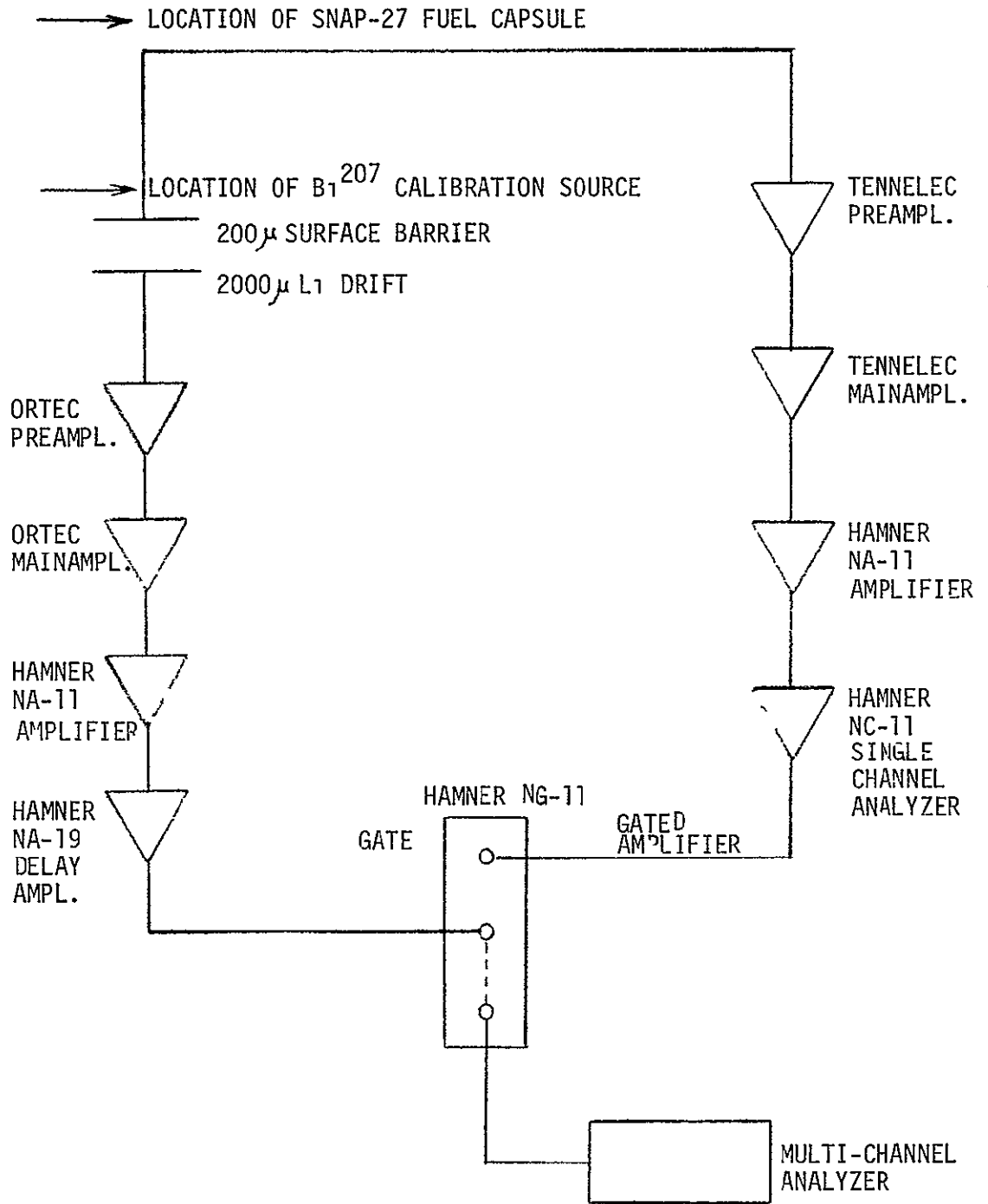
MULTI-CHANNEL
ANALYZER

FIGURE 5.14-2.   BLOCK DIAGRAM-ELECTRONICS FOR SEMICONDUCTOR
TELESCOPE

The results of the measurements with the SNAP-27 fuel capsule are presented in Figure 5.14-3. The no-coincidence count rate over the range from 0 to 2.8 kev was 776 cps, the anticoincidence rate was 736 cps, the coincidence rate was 43 cps, and the accidental coincidence rate was 0.5 cps. The coincidence spectrum represents the SNAP-27 fuel capsule radiation interference that would be superimposed on the spectrum of coincidence charged particles detected by the semiconductor telescope operated with the described parameters of geometry, resolving time, and gating threshold energy.

5.15   Phoswich

A plastic scintillator (Pilot B) and a CsI crystal sandwich was obtained for testing with the SNAP-27 fuel capsule. However, no data were taken with this detector. Attempts to instrument the phoswich resulted in excessive attenuation of the fast component of the signal (from the plastic scintillator) due to capacitance in the tube base and transmission lines to the electronics. As a result, the separation between the fast and slow rise time pulses was quite poor (approximately 20 db) giving poor resolution and excessive coincidence counts. It became obvious that the effort required to obtain a satisfactory phoswich would require improving the frequency response characteristics of the electronics which was not feasible to perform within the scope of the current program.
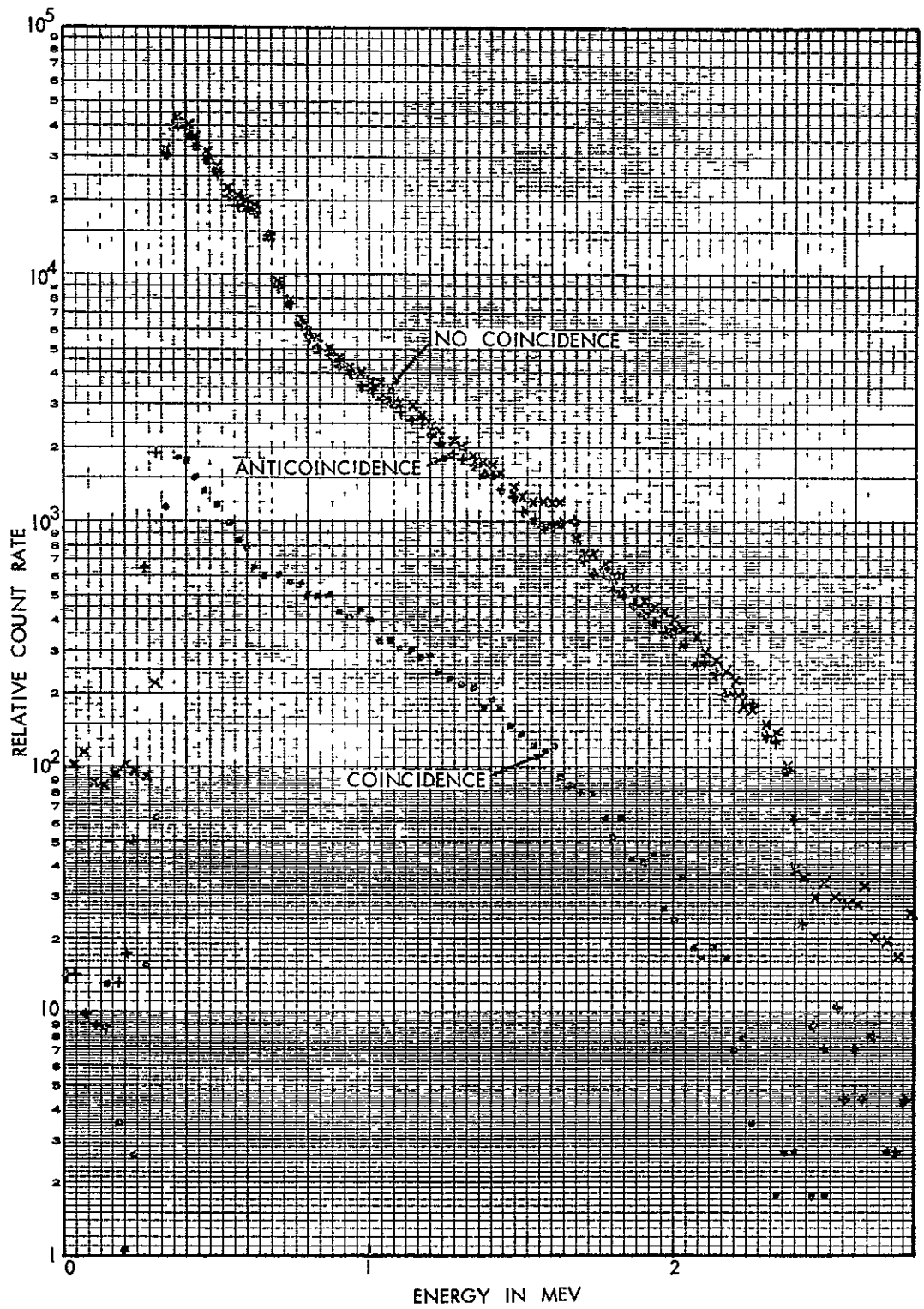
FIGURE 5.14-3   SNAP-27 FUEL CAPSULE RADIATION SPECTRA MEASUREMENTS
WITH SEMICONDUCTOR DETECTOR TELESCOPE

6. CONCLUSIONS AND RECOMMENDATIONS

The data presented in this report provide a starting point for assessing RTG heat source/science instrument interactions. The RTG background radiation flux and spectra that are superimposed on each radiation-sensitive detector have been presented along with the effectiveness of various absorber materials in reducing these radiation levels and modifying the spectra. The extent of the RTG radiation interference will, of course, depend on the function and objectives of each detector. The data can also be used to scale to other RTG power levels and/or separation distances and the information presented in Section 4 can be used to determine the effects of plutonium fuel form age on the resultant RTG radiation spectrum. As was mentioned earlier, the radiation-sensitive elements included in this program were only the detector elements that, on a theoretical basis, were assessed to be most sensitive to the RTG radiation and also were frequently used in spacecraft instrumentation. There were many other sensors in spacecraft that may also be significantly affected by the RTG heat source, and some of these are scheduled for detailed experimental study in Phase II of this program. However, from the results of this Phase I effort, several important conclusions and recommendations for further testing may be drawn.

- The preliminary analysis performed during Phase I revealed that for RTG-to-instrument distances on the order of 8 feet (roughly the configuration presently planned for Pioneer F/G) in general the scientific objectives will not be significantly impaired. However, some shielding (on the order of 1-5 pounds) will be required for the more sensitive radiation detection instruments to reduce the RTG radiation to an acceptable level.

- Most of the radiation measurements carried out during Phase I were conducted with the detector facing the capsule broadside, i.e., perpendicular to the longitudinal axis of the capsule However, as illustrated in Figure 5.4-1 both the gamma ray flux and its spectral distribution are very significantly

affected by the heat source orientation relative to the detectors. Methods for applying these data for different RTG orientation angles should be developed.

- The radiation levels with the capsule facing the detector end-on were as much as a factor of ten lower than with the broadside orientation. The predicted differences were on the order of a factor of two. These results suggest that the heat source orientation relative to the detectors could be an important consideration in determining the spacecraft design and in locating the most sensitive detectors.

- The absorption tests made with polyethylene and boron-loaded polyethylene demonstrated that thermalization and absorption of neutrons from the RTG heat source appeared to have very little effect on reducing the detected radiation. However, measurements performed with a neutron probe showed that a significant reduction in neutron flux actually did occur when the polyethylene shields were placed in front of the fuel capsule. This indicates that the neutrons emitted from the Pu^{238} fuel do not add significantly to the RTG radiation background for the detectors tested in this program.

- The limited work performed with the semiconductor detector telescope indicates that there are a significant number of coincidence counts generated by the RTG radiation. Therefore, an anticoincidence shield could probably be employed to reduce the RTG background. Of course, the efficiency of such a system is sensitive to the type and physical configuration of the detectors used and also electronic parameters such as coincidence gating speeds and locations of level descriminators. Clearly, additional work is required in this area to adequately determine the potential of this method in reducing the detected RTG background.

● The utility and applicability of the program is increased
by close coordination with spacecraft science experimenters,
particularly those involved in Pioneer F/G. This was not
completely implemented during Phase I of the program because
the detectors were selected and testing had commenced before
the selection of Pioneer F/G flight instruments. Toward the
end of the program, however, contacts were made with several
of the experimenters on the Pioneer F/G Program and three
experimenters provided their detectors for testing with the
RTG heat source. Valuable information was obtained from
discussions with the experimenters on the details of their
instrument design, method of operation, and scientific
objectives. During Phase II of the program, close liaison
should be maintained with the Pioneer F/G experimenters and
they should be invited to participate in the test program at
TRW.

A P P E N D I X

SNAP-27 Heat Source Assembly No. 4

Fuel Characteristics and Processing

Report

TABLE 1

FOURTH CAPSULE FUEL DATA
(First Liner)

Capsule No.	Lot	Batch	Stoichiometry w/o	Isotopic Ratio w/o	Pu-236 ppm	Other w/o	Total w/o	Silicon w/o	Iron w/o	47-50 μ	250-262 μ	262-280 μ	Apparent Density GMS/CC	Crush Strength GMS	Melting Temp. °C	Fines w/ox10⁻⁴	Watts	Date Meas'd.
4	341		2.00	80.03	0.94	<0.17	<0.97	0.14	0.57	0	0	0	9.61	235	2310			
		A														<0.8	80.431	3-5-68
		B														<0.32	74.690	3-5-68
		C														<0.5	80.341	3-5-68
		D														.0.058	72.591	3-5-68
		E														<0.3	81.043	3-5-68
	360		2.00	80.23	0.89	<0.14	<0.72	0.29	0.23	0	0	0	9.82	270	2290			
		A														0.61	70.945	2-22-68
		B														4.1	76.984	2-22-68
		C														0.43	73.128	2-22-68
		D														7.6	82.841	2-22-68
		E														1.9	78.067	2-22-68
		F														1.6	76.786	2-22-68

A-2

TABLE 2

FOURTH CAPSULE FUEL DATA
(Second Liner)

A-3

Capsule No.	Lot	Batch	Stoichi- ometry w/o	Isotopic Ratio w/o	Impurities Actinides Pu-236 ppm	Other w/o	Cation Total w/o	Silicon w/o	Iron w/o	Size Range 47-50 μ Part. %	250-262 μ Part. %	262-280 μ Part. %	Apparent Density GMS/CC	Crush Strength GMS	Melting Temp. °C	Fines w/ox10⁻⁴	Thermal Output Watts	Date Meas'd
4		106	2.00	79.66	1.6	0.07	0.20	0.04	0.08	0·	0	0	10.33	294	2300	0.018	76.209	6-15-67
		133	2.00	80.72	1.3	0.10	0.88	0.04	0.17	0	0	0	10.29	429	2165	0.89	89.159	10-27-67
		144	2.00	80.22	0.9	0.13	1.23	0.05	0.37	0	0	0	10.45	273	2185	1.2	89.203	11-7-67
		146	2.00	80.27	0.8	<0.11	1.14	0.03	0.52	0	0	0	10.25	313	2115	3.3	80.919	11-1-67
		156	2.00	80.66	0.79	<0.20	<0.92	0.07	0.49	0	0	0	10.24	239	2355	0.94	76.584	5-1-68
	307		2.00	79.11	0.82	<0.30	<1.29	0.30	0.36	0	0	0	9.92	201	2190			
		A														3.0	83.434	4-25-68
		B														0.087	92.807	4-25-68
		C														3.4	92.192	4-26-68
		D														0.087	94.036	4-26-68
		E														0.34	92.423	4-29-68
	346	C	2.00	80.20	1.13	<0.17	<0.53	0.29	0.15	0	0	0	10.06	251	2315	0.82	77.539	5-1-68
	360		2.00	80.23	0.89	<0.14	<0.72	0.29	0.23	0	0	0	9.82	270	2290			
		A														0.61	70.945	2-22-68
		B														4.1	76.984	2-22-68
		C														0.43	73.128	2-22-68
		D														7.6	82.841	2-22-68
		E														1.9	78.007	2-22-68
		F														1.6	76.786	2-22-68

TABLE 3

MICROSPHERE FABRICATION DATES
(SNAP-27 Fuel Capsule #4)

Lot #341 - Batches A thru E consist of a mixture of the following
eight batches:

SP-2 - 11/12/66 to 11/17/66   77 - 2/14/67 to 2/15/67
57   - 11/19/66 to 11/29/66   79 - 2/17/67 to 2/17/67
58R3 - 10/30/66 to 12/2/66   81R - 2/21/67 to 2/23/67
76R - 2/8/67 to 2/14/67   82R - 2/22/67 to 2/23/67

Lot #360 - Batches A thru F consist of a mixture of the following
eight batches:

40   - 10/22/66 to 10/24/66   51R - 11/10/66 to 11/11/66
43   - 10/26/66 to 10/27/66   53R - 11/14/66 to 11/17/66
44   - 10/27/66   68 - 1/6/67 to 1/11/67
46   - 10/28/66 to 11/1/66   72 - 1/31/67 to 2/1/67

Lot #307 - Batches A thru E consist of a mixture of the following
ten batches:

60-1 - 4/66   60-13 - 7/66
   3 - 4/66   17 - 7/66
   6 - 4/66   18 - 7/66
   8 - 4/66   19 - 7/66
  11 - 4/66   21 - 8/66

Lot #346 - Batch C consists of a mixture of the following
nine batches:

37S - 10/16/66 to 10/24/66   49R - 11/5/66 to 11/8/66
39SR - 10/22/66 to 10/26/66   50R2 - 11/8/66 to 11/10/66
45R - 10/28/66 to 10/31/66   56   - 11/23/66 to 11/29/66
47   - 10/27/66 to 11/3/66   67   - 1/11/67
48S - 11/4/66 to 11/11/66

Batches   106 - 5/11/67   146 - 10/26/67
            133 - 10/67   156 - 3/18/68
            144 - 10/26/67

TABLE 4

CONTRIBUTION OF FUEL BATCHES AND LOTS TO CAPSULE WATTAGE AND WEIGHT
(SNAP-27 Fuel Capsule #4)

Liner	Lot or Batch	% of Total Thermal Output	Fuel Contribution Watts	Grams
First	Lot 341	52.3	387.10	988.47
	Lot 360	47.7	353.05	896.33
		100.0	740.15	1884.80
Second	Lot 307	59.68	443.87	1154.05
	Lot 360	13.86	103.10	261.68
	Lot 346	10.43	77.49	196.77
	Batch 106	0.39	2.90	7.3
	Batch 133	0.61	4.47	11.19
	Batch 144	1.21	9.00	22.83
	Batch 146	8.52	63.39	160.50
	Batch 156	5.31	39.50	99.09
		100.0	743.72	1913.41